Politecnico di Milano
School of Industrial and Information Engineering
Master of Science in Mathematical Engineering

Numerical analysis for a model of faults in an elastic medium: direct and inverse algorithms

Advisor: Prof. Paola F. ANTONIETTI
Co-Advisor: Prof. Elena BERETTA

Candidate:
Sara Francesca Pichierri Matr. 899850

Academic Year 2019–2020

A zia Angelina

Acknowledgments

Ringrazio di cuore la prof. Antonietti, relatrice di questo progetto di tesi, per avermi sostenuto in ogni momento di difficoltà e per essere stata sempre presente nonostante l'emergenza sanitaria. La ringrazio anche per tutti i sorrisi che le sue bimbe mi hanno donato durante le chiamate Skype.
Ringrazio la prof. Beretta per essere stata una correlatrice costantemente disponibile, per il suo grandissimo apporto di conoscenze e di esperienza, per la sua pazienza e la precisione dimostratemi durante tutto il periodo di stesura.
Al termine di questo lungo percorso, faticoso, pieno di soddisfazioni ma anche di delusioni, il mio ringraziamento più grande va alla mia famiglia, a Fausto, a mamma e a papà. Il mio alloro oggi è il vostro, perchè mi avete accompagnato durante tutto il mio percorso educativo, con supporto morale e materiale e fiduciosi che le mie scelte sarebbero state giuste. Grazie perchè siete stati il mio porto sicuro, le braccia che mi hanno sempre donato conforto anche quando le mie scelte non erano giuste. Grazie per aver gioito con me e più di me per i successi e i traguardi che ho raggiunto. Grazie mamma e papà perché avete saputo vivere i vostri figli come potenziale e non come proprietà.
Ringrazio anche tutto il resto della mia famiglia, i miei nonni, i miei zii e i miei cugini, che hanno sempre saputo donarmi illimitato affetto, stima e fiducia, nonostante i chilometri di lontananza.
Un ringraziamento sincero va alle mie amiche di sempre, a Eleonora, a Veronica e a Stefania. Descrivere a parole il bene immenso che vi voglio è difficile, siamo cresciute insieme e conoscete meglio di chiunque altro le mie debolezze e i miei punti di forza. Grazie per essere state più che sorelle, il mio pilastro e il mio punto di riferimento. La nostra amicizia non teme nè distanze nè tempo.
Grazie ai miei compagni del liceo, con i quali ho mantenuto un meraviglioso rapporto di amicizia. Grazie a Francesca, Agnese, Maria Chiara e a quei cuoricini di Marco, Antonio, Piergiorgio e Ivano. Sono felice di condividere con voi questo traguardo del mio percorso di istruzione, perchè ne siete stati una parte fondamentale.
Infine, come non ringraziare la mia seconda e numerosissima famiglia, quella del Martinitt, il campus che ha reso la mia esperienza universitaria indimenticabile. In particolare un grazie alla mia amica Alessandra: siamo arrivate insieme a Milano dalla lontana Puglia e da allora non ci siamo più separate. Grazie per essere stata la persona più vicina a me in questi ultimi sei anni, grazie per le serate insieme, sia quelle in discoteca, sia quelle sul divano a vedere serie TV. Grazie per avermi ascoltata e supportata in ogni situazione e per essere stata la spalla su cui piangere nelle giornate più difficili.

Grazie anche a Emanuele, Fabio T., Gandi, Chiara, Lorenzo, Federico, Anita, Mimmo, Peppe, Christian, Tigre, PM, Perrino, Stefano, Ettore, Vizz, Peluso, Silvia, Cristina, Marta, Scintilla, Riccardo, Andrea C., Fabio R., Polipino, Valerio, Dario S., Dario Z. e tanti tanti tanti altri. Nominarvi tutti sarebbe davvero impossibile, ma sappiate che ognuno di voi, nel momento in cui ha messo piede al Martinitt, ha contribuito a creare ricordi e momenti che saranno sempre scolpiti nel mio cuore.

Abstract

The thesis deals with the analysis and implementation of numerical algorithms for fault reconstruction in geophysical applications. We represent a portion of the Earth's crust as a bounded elastic body with a buried fault surface, along which slip occurs. A discontinuous Galerkin method is analyzed for the direct problem, presenting both theoretical and numerical results. In the second part of the work, we establish uniqueness for the problem of determining simultaneously the fault surface and the slip field from boundary measurements and we prove a theoretical stability estimate. Finally, we propose a reconstruction algorithm and we confirm its efficiency with numerical tests.

Contents

List of Figures

List of Tables

Introduction

Inverse boundary value problems appear every time we want to determine internal properties of a medium (e.g. conduction, stiffness, density) from observations on its boundary. Such problems lie at the heart of scientific progress and technological development and have applications in medical imaging, nondestructive testing of materials, seismology, underground prospection to mention but a few.
The mathematical modelling of the *forward problem*, that is of the data formation process, is based on partial differential equations (PDEs) or systems of PDEs.
The *inverse problem* then consists in reconstructing the unknown parameters or sources in the PDE from boundary measurements of the solution of the PDE itself. In general, these parameter estimation problems are highly nonlinear and ill-posed in the sense of Hadamard (cf. [1]): small errors in the data may cause incontrollable variations in the unknowns. This feature makes an analysis of these instabilities crucial, in order to get reliable reconstructions. In view of the many applications, this leads to the search of appropriate methods to contain such instability. One way is by introducing mathematically suitable but physically relevant, a-priori assumptions on the unknown parameters so that one can mitigate the ill-posedeness, for example restricting the class of admissible parameters to a subset of a finite dimensional space.

Here, we consider the two dimensional version of an *inverse problem* with applications in geophysics related to a model of buried faults in the Earth crust, see for instance [2], [3] and [4], and we analyze the slip conditions between different subduction zones, as in Figure 1. More precisely, the physics of our problem is modeled using the equations of elastodynamics, which have been massively investigated due to their capability to simulate seismic scenarios. The *forward problem* consists in finding the elastic displacement in the Earth's crust induced by the slip along the fault, while the *inverse problem* consists in determining the fault and the slip on the fault from measurements of the surface displacement, see [5], [6] and [7] . An accurate solution of the *inverse problem*

has become more and more important in order to anticipate and possibly prevent the damages of large earthquakes.

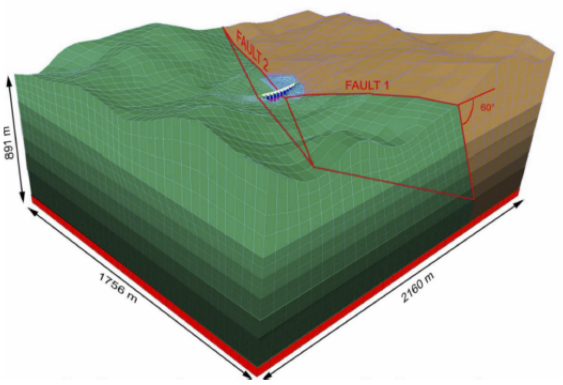

Figure 1: Example of subduction zones. Image taken from [8].

One fundamental step towards the solution of the *inverse problem* is the generation of accurate synthetic data from the forward model that are as close as possible to the "true" data. For this reason, in this thesis we start studying the static equations of the linear elasticity system in its $forward$ form. An important definition to be introduced in the context of problems with faults is certainly the one of transmission conditions at subdomain interfaces, which allow to reformulate a boundary value problem in a multi-domain formulation. There are several heterogeneous domain decomposition methods that can be developed within this context (cf. [9] and [10]). To discretize the elasticity equations supplemented with the interface conditions, different numerical schemes like Finite Differences, Finite Elements or Spectral Element Methods (SEM) can be exploited. In particular SEM (see [11]) are based on high-order Lagrangian interpolants and are well suited for parallel computations, that are mandatory for three-dimensional problems. On the other hand, they can lead to a large computational effort. For this reason, nowadays it is preferable to use discontinuous Galerkin (DG) methods which combine the features of the finite element and the finite volume framework. DG methods received considerable interest for hyperbolic, elliptic and parabolic problems arising from a wide range of applications, in electrodynamics, elastodynamics, fluid mechanics and plasma physics, see [12] and [13].

Figure 2: Piecewise continuous functional spaces.

Discontinuous Galerkin methods were first proposed and analyzed in the early 1970s. However jump penalization in the modern sense were developed gradually and thanks to the earlier influential contribution of Babuška, J.-L. Lions, Joachim Nitsche and Miloš Zlámal, see for instance [14], [15], [16] and [17]. Like the Continuous Galerkin (CG method), the DG method is a finite element method formulated relative to a weak formulation of a particular model system. Unlike traditional continuous schemes that are conforming, the DG method works over a trial space of functions that are only piecewise continuous, as in Figure 2, and thus often comprise more inclusive functional spaces. Moreover DG methods have the advantage to be locally conservative, stable and of high-order accuracy. They are suitable for irregular meshes with hanging nodes (see Figure 3) and approximations that have polynomials of different degree in different elements. DG methods are proved to be particularly well suited also for dealing with cracks phenomena, which is our case of interest. Indeed, unlike the continuous formulation, the interior-penalty discontinuous Galerkin method allows to incorporate the transmission conditions directly in the semi-discrete scheme, cf. [18].
Such interface problems, yielding discontinuous solutions across the interface, can be naturally analyzed in the DG setting simply by modifying the interior penalty DG numerical fluxes accordingly and without alterating the order of accuracy of the method as explained in this work.

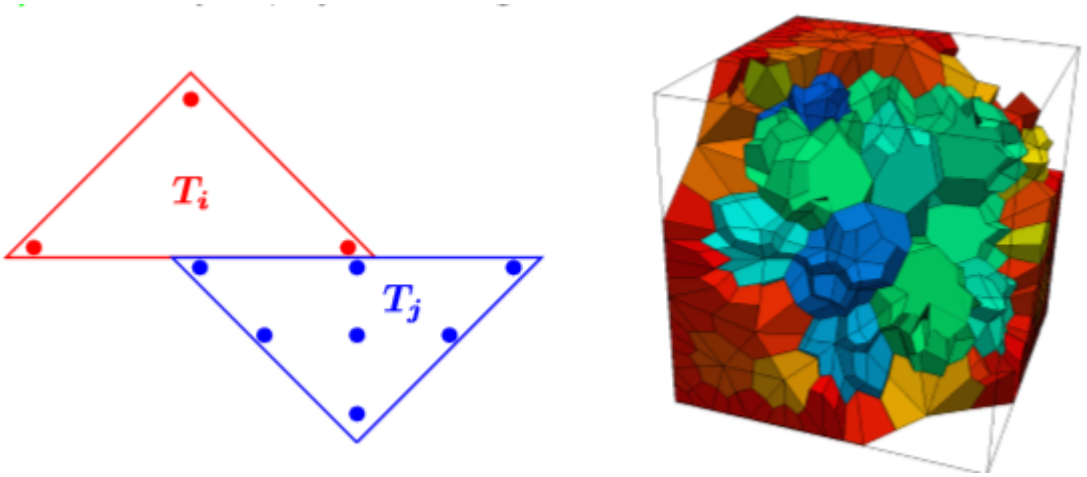

Figure 3: Non-conforming and irregular meshes.

The thesis is organized as follows: in Chapter 1 we present the *forward* elastostatic model applied to homogeneous domains without a crack. We study the well-posedness of the weak formulation for the continuous problem and we explain in details how the numerical scheme is derived. Then, we prove that the solution approximated with the DG method converges to the "true" solution and we show an *a-priori* error estimate, that is confirmed by the numerical experiments.
In Chapter 2 we present the system of PDEs for the linear elasticity model applied to heterogeneous domains with a crack. We report some results about the existence and uniqueness of the solution for the interface problem, according to the regularity of the slip field on the fault. Then, we slightly modify the DG method in order to treat the interface conditions, we study the well-posedness of the new scheme and we develop a theoretical error analysis confirmed by the numerical results.
In Chapter 3 we introduce the *inverse problem*, we study its uniqueness property and we prove a Lipschitz stability under suitable assumptions on the fault and on the slip field. Finally, we propose a reconstruction algorithm for the determination of the unknown parameters and we report some verification tests.

Chapter 1

The elastostatic problem

1.1 The mathematical model

We introduce the mathematical model for the elastostatic problem in an open bounded domain $\Omega \subset \mathbb{R}^2$, with Lipschitz boundary $\partial\Omega$ and outward normal unit vector $\mathbf{n}$. The boundary is assumed to be composed of two portions: $\Gamma_D \neq \emptyset$, which is closed and where the displacement vector $\mathbf{u}$ is prescribed, and Γ_N where an external load applies. We assume that Γ_D and Γ_N are disjoint, i.e. $\Gamma_D \cap \Gamma_N = \emptyset$ and that $\partial\Omega = \Gamma_D \cup \Gamma_N$. On the Dirichlet boundary Γ_D the medium is rigidly fixed in the space and on Γ_N we prescribe surface tractions.
The problem reads as follows: find the medium displacement $\mathbf{u} : \Omega \to \mathbb{R}^2$ such that

$$\begin{aligned} -\nabla \cdot \underline{\sigma}(\mathbf{u}) &= \mathbf{f} \quad \text{in } \Omega, \\ \underline{\sigma}(\mathbf{u}) - \mathbf{D}\underline{\epsilon}(\mathbf{u}) &= \mathbf{0} \quad \text{in } \Omega, \\ \mathbf{u} &= \mathbf{g}_D \quad \text{on } \Gamma_D, \\ \underline{\sigma}(\mathbf{u})\mathbf{n} &= \mathbf{g}_N \quad \text{on } \Gamma_N, \end{aligned} \tag{1.1}$$

where $\mathbf{f} \in \mathbf{L}^2(\Omega)$ is a given source term, $\mathbf{g}_D \in \mathbf{H}^{\frac{1}{2}}(\Gamma_D)$, $\mathbf{g}_N \in \mathbf{H}^{-\frac{1}{2}}(\Gamma_N)$ are the Dirichlet and the Neumann boundary conditions, respectively.
We have employed the standard notation for the Sobolev spaces, see [19]. More precisely, given the standard space $L^2(\Omega)$, $H^m(\Omega)$, $m \geq 0$, we set by $\mathbf{L}^2(\Omega) = [L^2(\Omega)]^2$, $\mathbf{H}^m(\Omega) = [H^m(\Omega)]^2$ and $\mathcal{L}^2(\Omega) = [L^2(\Omega)]^{2\times 2}_{\text{sym}}$, $\mathcal{H}^m(\Omega) = [H^m(\Omega)]^{2\times 2}_{\text{sym}}$ their vectorial and tensorial counterpart, respectively. Each space is endowed with its usual norm, see [20].

Note that with $\nabla \cdot \underline{a}$ we represent the divergence of an arbitrary tensor $\underline{a}$ in 2 dimensions, i.e.

$$(\nabla \cdot \underline{a})_i = \sum_{j=1}^{2} \frac{\partial \underline{a}_{ij}}{\partial x_j}.$$

The second equation in (1.1) is the Hooke's constitutive law that relates the strain tensor

$$\underline{\epsilon}(\mathbf{u}) = \frac{1}{2}(\nabla \mathbf{u} + \nabla \mathbf{u}^T), \tag{1.2}$$

to the stress tensor $\underline{\sigma}$ through the 4^{th} order stiffness tensor $\mathbf{D}$, defined as follows:

$$\mathbf{D}\underline{\epsilon}(\mathbf{u}) = 2\mu\underline{\epsilon} + \lambda \text{tr}(\underline{\epsilon})\underline{I}, \tag{1.3}$$

where λ and μ are the first and second Lamé parameters, respectively, and where we suppose that $\lambda, \mu \in L^\infty(\Omega)$. However, an equivalent description (see [21]) can be obtained with the coefficients' pair made of the Young modulus (E) and the Poisson ratio (ν):

$$\lambda = \frac{\nu E}{(1-2\mu)(1+\mu)}, \qquad \mu = \frac{E}{2(1+\nu)}.$$

In the definition (1.3), "tr$(\cdot)$" is the trace operator, $\underline{I} \in \mathbb{R}^{2\times 2}$ is the identity tensor and $\mathbf{D}$ is symmetric, strictly convex and uniformly bounded over Ω, i.e.

$$\exists\ D_0, D_1 \text{ such that } : 0 < D_0 \sum_{i,j} X_{ij}^2 \leq \sum_{i,j,k,l} X_{ij} D_{ijkl} X_{kl} \leq D_1 \sum_{i,j} X_{ij}^2 \tag{1.4}$$

for any 2×2 symmetric matrix $\underline{X} \neq \underline{0}$.

In the case of a homogeneous and isotropic material, the assumption of strictly convexity on $\mathbf{D}$ turns into the following conditions on the Lamè coefficients:

$$\mu > 0, \qquad \lambda + \mu > 0,$$

or, equivalently, into a condition on the Young modulus and on the Poisson ratio, namely:

$$E > 0, \qquad -1 < \nu < \frac{1}{2}.$$

From now on, we will make use of the following notation:

$$a \cdot b = ab \quad a, b \in \mathbb{R},$$

$$\mathbf{a} \cdot \mathbf{b} = \sum_{i=1}^{2} a_i b_i \quad \mathbf{a}, \mathbf{b} \in \mathbb{R}^2,$$

$$\underline{a} : \underline{b} = \sum_{i,j=1}^{2} a_{ij} b_{ij} \quad \underline{a}, \underline{b} \in \mathbb{R}^{2\times 2}.$$

1.1.1 The weak formulation

In order to write the weak formulation of the elastostatic problem (1.1), we suppose without loss of generality homogeneous Dirichlet boundary conditions. Multiplying the first equation in (1.1) by a smooth enough test function $\mathbf{v}$ and integrating over Ω we get:

$$\int_\Omega -(\nabla \cdot \underline{\sigma}(\mathbf{u})) \cdot \mathbf{v} \, \mathrm{d}\mathbf{x} = \int_\Omega \mathbf{f} \cdot \mathbf{v} \, \mathrm{d}\mathbf{x}.$$

Now, using the Green's formula and the boundary conditions, we have :

$$\begin{aligned} \int_\Omega -(\nabla \cdot \underline{\sigma}(\mathbf{u})) \cdot \mathbf{v} \, \mathrm{d}\mathbf{x} &= \int_\Omega \underline{\sigma}(\mathbf{u}) : \underline{\epsilon}(\mathbf{v}) \, \mathrm{d}\mathbf{x} \; - \int_{\partial\Omega} (\underline{\sigma}(\mathbf{u})\mathbf{n}) \cdot \mathbf{v} \, \mathrm{d}\mathbf{s} = \\ &= \int_\Omega \underline{\sigma}(\mathbf{u}) : \underline{\epsilon}(\mathbf{v}) \, \mathrm{d}\mathbf{x} \; - \int_{\Gamma_D} (\underline{\sigma}(\mathbf{u})\mathbf{n}) \cdot \mathbf{v} \, \mathrm{d}\mathbf{s} - \int_{\Gamma_N} (\underline{\sigma}(\mathbf{u})\mathbf{n}) \cdot \mathbf{v} \, \mathrm{d}\mathbf{s} \end{aligned}$$

We can employ the Neumann boundary conditions and it follows:

$$\int_\Omega \underline{\sigma}(\mathbf{u}) : \underline{\epsilon}(\mathbf{v}) \, \mathrm{d}\mathbf{x} - \int_{\Gamma_D} (\underline{\sigma}(\mathbf{u})\mathbf{n}) \cdot \mathbf{v} \, \mathrm{d}\mathbf{s} = \int_\Omega \mathbf{f} \cdot \mathbf{v} \, \mathrm{d}\mathbf{x} + \langle \mathbf{g}_N, \mathbf{v} \rangle_{\Gamma_N}.$$

where we indicate with $\langle \cdot, \cdot \rangle_{\Gamma_N}$ the duality pairing on $\mathbf{H}^{-\frac{1}{2}}(\Gamma_N)$. Imposing that $\mathbf{v} = 0$ on Γ_D, the second integral on the left-hand side cancels.
We define the Sobolev space (cf. [19]):

$$\mathbf{H}^1_{0,\Gamma_D}(\Omega) = \{\mathbf{u} \in \mathbf{H}^1(\Omega) : \mathbf{u} = 0 \text{ on } \Gamma_D\}.$$

The variational formulation reads: find $\mathbf{u} \in \mathbf{H}^1_{0,\Gamma_D}(\Omega)$ such that

$$B(\mathbf{u}, \mathbf{v}) = F(\mathbf{v}) \qquad \forall \; \mathbf{v} \in \mathbf{H}^1_{0,\Gamma_D}(\Omega), \tag{1.5}$$

where the bilinear form $B(\cdot, \cdot) : \mathbf{H}^1_{0,\Gamma_D}(\Omega) \text{ x } \mathbf{H}^1_{0,\Gamma_D}(\Omega) \to \mathbb{R}$ is defined as:

$$B(\mathbf{u}, \mathbf{v}) = \int_\Omega \underline{\sigma}(\mathbf{u}) : \underline{\epsilon}(\mathbf{v}) \, \mathrm{d}\mathbf{x},$$

and the linear functional $F(\cdot) : \mathbf{H}^1_{0,\Gamma_D}(\Omega) \to \mathbb{R}$ is given by:

$$F(\mathbf{v}) = \int_\Omega \mathbf{f} \cdot \mathbf{v} \, \mathrm{d}\mathbf{x} + \langle \mathbf{g}_N, \mathbf{v} \rangle_{\Gamma_N} \quad \forall \ \mathbf{v} \in \mathbf{H}^1_{0,\Gamma_D}(\Omega).$$

From now on we will endow the space $\mathbf{H}^1_{0,\Gamma_D}(\Omega)$ with the following norm:

$$||\mathbf{v}||_{\mathbf{H}^1_{0,\Gamma_D}(\Omega)} = ||\nabla \mathbf{v}||_{\mathcal{L}^2(\Omega)} \quad \forall \ \mathbf{v} \in \mathbf{H}^1_{0,\Gamma_D}(\Omega). \tag{1.6}$$

Notice that this is a norm in $\mathbf{H}^1_{0,\Gamma_D}(\Omega)$ thanks to the following Lemma (cf. Teorema 8.2 in [22]):

Lemma 1. *(Poincarè inequality). Let Ω be a bounded Lipschitz domain. If $\boldsymbol{u} \in \boldsymbol{H}^1_{0,\Gamma_D}(\Omega)$, then there exists a constant C_P such that:*

$$||\boldsymbol{u}||_{\boldsymbol{L}^2(\Omega)} \leq C_P ||\nabla \boldsymbol{u}||_{\mathcal{L}^2(\Omega)}.$$

Problem (1.5) is well posed and admits a unique solution. The details will be presented in the next section.

1.1.2 Existence and uniqueness of the weak solution

Theorem 1. *Let $\boldsymbol{f} \in \boldsymbol{L}^2(\Omega)$ be a given source term and let $\boldsymbol{g}_N \in \boldsymbol{H}^{-\frac{1}{2}}(\Gamma_N)$, then there exists a unique solution $\boldsymbol{u} \in \boldsymbol{H}^1_{0,\Gamma_D}(\Omega)$ which satisfies problem* (1.5)*.*

Proof. To simplify the notation, we define $\mathbf{V} := \mathbf{H}^1_{0,\Gamma_D}(\Omega)$. The proof of Theorem 1 follows directly from Lax-Milgram theorem (see [23]). More precisely (1.5) is well posed provided that the following properties are satisfied:

- $B(\cdot, \cdot)$ is continuous over $\mathbf{V} \times \mathbf{V}$, i.e.

  $$\exists \ M > 0 \text{ such that } |B(\mathbf{u}, \mathbf{v})| \leq M ||\mathbf{u}||_{\mathbf{V}} \ ||\mathbf{v}||_{\mathbf{V}},$$

  where the norm is the one defined in (1.6).

- $B(\cdot, \cdot)$ is $\mathbf{V}$-coercive, i.e.

  $$\exists \ \alpha > 0 \text{ such that } |B(\mathbf{u}, \mathbf{u})| \geq \alpha ||\mathbf{u}||^2_{\mathbf{V}}.$$

- The linear functional $F(\cdot)$ is continuous over $\mathbf{V}$, i.e.

$$\exists\ \gamma > 0 \text{ such that } |F(\mathbf{u})| \leq \gamma ||\mathbf{u}||_{\mathbf{V}}.$$

We start by proving the continuity of $B(\cdot,\cdot)$, exploiting the assumptions on $\mathbf{D}$ (strong convexity and uniform boundedness) and the *Poincarè inequality* of Lemma 1:

$$\int_\Omega \sigma_{ij}(\mathbf{u})\epsilon_{ij}(\mathbf{v})\ \mathrm{d}\mathbf{x} = \int_\Omega \sum_{k,l=1}^{2} D_{ijkl}\epsilon_{kl}(\mathbf{u})\epsilon_{ij}(\mathbf{v})\ \mathrm{d}\mathbf{x} \leq C\int_\Omega \sum_{k,l=1}^{2} \epsilon_{kl}(\mathbf{u})\epsilon_{kl}(\mathbf{v})\ \mathrm{d}\mathbf{x}$$

$$\leq C||\underline{\epsilon}(\mathbf{u})||_{\mathcal{L}^2(\Omega)}||\underline{\epsilon}(\mathbf{v})||_{\mathcal{L}^2(\Omega)} \leq C||\nabla\mathbf{u}||_{\mathcal{L}^2(\Omega)}||\nabla\mathbf{v}||_{\mathcal{L}^2(\Omega)} = C||\mathbf{u}||_{\mathbf{V}}||\mathbf{v}||_{\mathbf{V}}.$$

We next show the coercivity of $B(\cdot,\cdot)$:

$$B(\mathbf{u},\mathbf{u}) = \int_\Omega \underline{\sigma}(\mathbf{u}) : \underline{\epsilon}(\mathbf{u})\ \mathrm{d}\mathbf{x} = \int_\Omega \mathbf{D}\underline{\epsilon}(\mathbf{u}) : \underline{\epsilon}(\mathbf{u})\ \mathrm{d}\mathbf{x} \geq D_0\int_\Omega \underline{\epsilon}(\mathbf{u}) : \underline{\epsilon}(\mathbf{u})\ \mathrm{d}\mathbf{x} \geq$$

$$\geq D_0\beta||\mathbf{u}||^2_{\mathbf{V}} = \alpha||\mathbf{u}||^2_{\mathbf{V}},$$

where we have used the strict convexity of the stiffness tensor $\mathbf{D}$ and the following *Korn's inequality* (see [24]):

$$\exists\ \beta > 0 \text{ such that } \int_\Omega \underline{\epsilon}(\mathbf{u}) : \underline{\epsilon}(\mathbf{u})\ \mathrm{d}\mathbf{x} \geq \beta||\mathbf{u}||^2_{\mathbf{V}} \quad \forall\ \mathbf{u} \in \mathbf{V}.$$

Finally, the continuity of the linear functional $F(\cdot)$ follows directly from its definition, the hypothesis of regularity on the source $\mathbf{f}$ and the data $\mathbf{g}_N$ and using the *Cauchy-Schwarz inequality* (cf. [25]):

$$|F(\mathbf{v})| \leq \int_\Omega |\mathbf{f}\cdot\mathbf{v}|\ \mathrm{d}\mathbf{x} + |\langle \mathbf{g}_N, \mathbf{v}\rangle|_{\Gamma_N} \leq \gamma||\mathbf{v}||_{\mathbf{V}}.$$

□

Note that, even if it is not a necessary hypothesis of Theorem 1, it can be proved by simple algebraic manipulations that the bilinear form $B(\cdot,\cdot)$ is also symmetric:

$$\int_\Omega \underline{\sigma}(\mathbf{u}) : \underline{\epsilon}(\mathbf{v})\ \mathrm{d}\mathbf{x} = \int_\Omega \sum_{i,j=1}^{2} \sigma_{ij}(\mathbf{u})\epsilon_{ij}(\mathbf{v})\ \mathrm{d}\mathbf{x}$$

$$= \int_\Omega \sum_{i,j=1}^{2} \Big(\lambda(\nabla\cdot\mathbf{u})\delta_{ij}\epsilon_{ij}(\mathbf{v}) + 2\mu\epsilon_{ij}(\mathbf{u})\epsilon_{ij}(\mathbf{v})\Big)\ \mathrm{d}\mathbf{x} = \int_\Omega \sum_{i,j=1}^{2} \Big(\lambda(\nabla\cdot\mathbf{u})\epsilon_{ii}(\mathbf{v}) + 2\mu\epsilon_{ij}(\mathbf{u})\epsilon_{ij}(\mathbf{v})\Big)\ \mathrm{d}\mathbf{x}$$

$$= \int_\Omega \sum_{i,j=1}^{2} \Big(\lambda\epsilon_{ii}(\mathbf{u})(\nabla\cdot\mathbf{v}) + 2\mu\epsilon_{ij}(\mathbf{u})\epsilon_{ij}(\mathbf{v})\Big)\, \mathrm{d}\mathbf{x} = \int_\Omega \sum_{i,j=1}^{2} \Big(\lambda(\nabla\cdot\mathbf{v})\delta_{ij}\epsilon_{ij}(\mathbf{u}) + 2\mu\epsilon_{ij}(\mathbf{v})\epsilon_{ij}(\mathbf{u})\Big)\, \mathrm{d}\mathbf{x}$$

$$= \int_\Omega \underline{\sigma}(\mathbf{v}) : \underline{\epsilon}(\mathbf{u})\ \mathrm{d}\mathbf{x}.$$

1.2 Discrete approximation

1.2.1 Mesh partitions and finite element spaces

To analyze the discrete approximation, we consider a family $\{\mathcal{T}_h, 0 < h \leq 1\}$ of shape-regular partitions of Ω into non-overlapping triangles $\mathcal{K}$, such that $\overline{\Omega} = \cup_{\mathcal{K}\in\mathcal{T}_h}\overline{\mathcal{K}}$.
For a given mesh $\mathcal{T}_h$, as the one shown in Figure 1.1, we define the granularity $h = \max_{\mathcal{K}\in\mathcal{T}_h} h_\mathcal{K}$ with $h_\mathcal{K} = \mathrm{diam}(\mathcal{K})$.

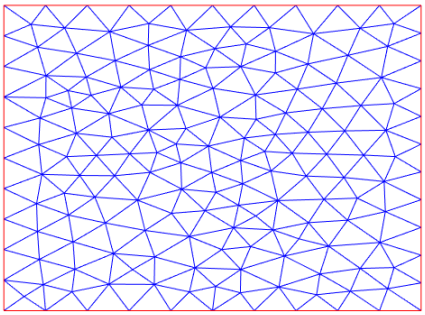

Figure 1.1: Example of a shape regular triangular discretization of a rectangular domain.

We collect all the interior faces γ in $\mathcal{F}_I$. Here a face $\gamma \in \mathcal{F}_I$ is defined in such a way that there exists two adjacent elements of $\mathcal{T}_h$: $\mathcal{K}^+$, $\mathcal{K}^-$, such that $\gamma = \partial\mathcal{K}^+ \cap \partial\mathcal{K}^-$. Similarly we gather all the faces belonging to the Dirichlet and Neumann boundary γ in $\mathcal{F}_D$ and $\mathcal{F}_N$, respectively: $\mathcal{F}_D = \{\gamma : \exists\ \mathcal{K}$ such that $\gamma \subseteq \partial\mathcal{K} \cap \Gamma_D\}$ and $\mathcal{F}_N = \{\gamma : \exists\ \mathcal{K}$ such that $\gamma \subseteq \partial\mathcal{K} \cap \Gamma_N\}$. Implicit in this definition there is the assumption that the mesh respects the decomposition of the boundary $\partial\Omega$; i.e., any face γ belongs exactly either to $\mathcal{F}_D$ or $\mathcal{F}_N$.

For an integer $s \geq 1$, we define the *Broken* Sobolev spaces:

$$H^s(\mathcal{T}_h) = \{v \in L^2(\Omega) : v|_\mathcal{K} \in H^s(\mathcal{K}) \quad \forall\ \mathcal{K} \in \mathcal{T}_h\},$$

and the *broken* norms:

$$||v||^2_{H^s(\mathcal{T}_h)} = \sum_{\mathcal{K}\in\mathcal{T}_h} ||v||^2_{H^s(\mathcal{K})},$$

$$||v||^2_{L^2(\mathcal{F}_i)} = \sum_{\gamma\in\mathcal{F}_i} ||v||^2_{L^2(\gamma)}, \quad i = \{I, D, N\}.$$

We will use the following notation for their vectorial and tensorial counterpart in two dimensions:

$$\mathbf{H}^s(\mathcal{T}_h), ||\cdot||_{\mathbf{H}^s(\mathcal{T}_h)}, ||\cdot||_{\mathbf{L}^2(\mathcal{F}_i)}, \quad \mathcal{H}^s(\mathcal{T}_h), ||\cdot||_{\mathcal{H}^s(\mathcal{T}_h)}, ||\cdot||_{\mathcal{L}^2(\mathcal{F}_i)}, \quad i = \{I, D, N\}.$$

For an integer $r \geq 1$, the discontinuous finite dimensional space is given by:

$$V_h^r = \{v_h \in L^2(\Omega) : v_h|_{\mathcal{K}} \in \mathbb{P}^r(\mathcal{K}) \quad \forall\, \mathcal{K} \in \mathcal{T}_h\},$$

where $\mathbb{P}^r(\mathcal{K})$ is the space of polynomials of total degree r defined on $\mathcal{K}$. We set $\mathbf{V}_h^r = [V_h^r]^2$ and $\mathcal{V}_h^r = [V_h^r]^{2\times 2}_{\text{sym}}$.

1.2.2 Trace operators

In order to deal with piecewise discontinuous functions we need suitable trace operators. Let $\gamma \in \mathcal{F}_I$ be an interior face shared by two elements $\mathcal{K}^+$ and $\mathcal{K}^-$ of $\mathcal{T}_h$, and let $\mathbf{n}^+$, $\mathbf{n}^-$ be the unit normal vectors on γ pointing outward $\mathcal{K}^+$ and $\mathcal{K}^-$, respectively (see Figure 1.2). On γ we define the *average* and the *jump* operators for regular enough vector-valued and tensor-valued functions $\mathbf{v}$ and $\underline{\sigma}$ as:

$$\begin{aligned} \{\mathbf{v}\} &= \frac{1}{2}(\mathbf{v}^+ + \mathbf{v}^-), \\ [\![\mathbf{v}]\!] &= \mathbf{v}^+ \otimes \mathbf{n}^+ + \mathbf{v}^- \otimes \mathbf{n}^-, \\ \{\underline{\sigma}\} &= \frac{1}{2}(\underline{\sigma}^+ + \underline{\sigma}^-), \\ [\![\underline{\sigma}]\!] &= \underline{\sigma}^+\mathbf{n}^+ + \underline{\sigma}^-\mathbf{n}^-, \end{aligned} \tag{1.7}$$

respectively, where $\mathbf{v} \otimes \mathbf{n} = (\mathbf{v}\mathbf{n}^T + \mathbf{n}\mathbf{v}^T)/2$.
Note that the jump operator is defined using normal unit vectors and thus transforming a vector-valued into a tensor-valued function and viceversa. In the numerical scheme, this definition is preferable to the most common one " $[\![\mathbf{v}]\!] = \mathbf{v}^+ - \mathbf{v}^-$ " because it involves a sum instead of a difference and we can exploit its commutative property.

In particular, it allows the operator to be independent on the numbering of the elements ($\mathcal{K}^+$ and $\mathcal{K}^-$) when implementing the code.
Analogously, if an edge is on the boundary of the domain, $\gamma \in \mathcal{F}_D \cup \mathcal{F}_N$, we set:

$$\begin{aligned} \{\mathbf{v}\} &= \mathbf{v}^+, \\ [\![\mathbf{v}]\!] &= \mathbf{v}^+ \otimes \mathbf{n}, \\ \{\underline{\sigma}\} &= \underline{\sigma}^+, \\ [\![\underline{\sigma}]\!] &= \underline{\sigma}^+ \mathbf{n}. \end{aligned} \tag{1.8}$$

1.2.3 Discontinuous Galerkin finite element method

In this section we derive the variational formulation for DG methods, supposing the following assumptions: Ω is a bounded convex polygon in $\mathbb{R}^2$ and the Cauchy stress tensor is strictly convex, uniformly bounded as in (1.4) and Lipschitz continuous on Ω. For example, if the Lamè parameters are constant, we can write:

$$\begin{pmatrix} \sigma_{11} \\ \sigma_{22} \\ \sigma_{12} \end{pmatrix} = \begin{pmatrix} \lambda + 2\mu & \lambda & 0 \\ \lambda & \lambda + 2\mu & 0 \\ 0 & 0 & \mu \end{pmatrix} \begin{pmatrix} \epsilon_{11} \\ \epsilon_{22} \\ \epsilon_{12} \end{pmatrix}. \tag{1.9}$$

Moreover, without loss of generality, we suppose homogeneous Dirichlet and Neumann conditions. It is always possible to treat the most general case exploiting the linearity of the problem (cf. [26]).
Note that we are assuming Ω and $\mathbf{D}$ to be sufficiently regular so that we posses the following regularity: $\mathbf{u} \in \mathbf{H}^m(\Omega)$, for some $m \geq 2$ and $\underline{\sigma} \in \mathcal{H}^m(\Omega)$, for some $m \geq 1$, since we will need to write the trace of the Cauchy tensor average and we will make use of a duality argument for the error analysis. However, it is also possible to show similar results, relaxing some of these hypotheses and using different technical tools. We will analyze it in detail in Chapter 3, when discussing the interface problem.
We multiply the first equation in (1.1) by a test function $\mathbf{v} \in \mathbf{V}_h^r$, integrate over a generic $\mathcal{K} \in \mathcal{T}_h$, integrate by parts as in the variational formulation (1.5) and sum over every $\mathcal{K} \in \mathcal{T}_h$, to obtain:

$$\sum_{\mathcal{K} \in \mathcal{T}_h} \int_{\mathcal{K}} \underline{\sigma}(\mathbf{u}) : \underline{\epsilon}(\mathbf{v}) \, \mathrm{d}\mathbf{x} - \sum_{\mathcal{K} \in \mathcal{T}_h} \int_{\partial \mathcal{K}} (\underline{\sigma}(\mathbf{u})\mathbf{n}) \cdot \mathbf{v} \, \mathrm{d}\mathbf{x} = \sum_{\mathcal{K} \in \mathcal{T}_h} \int_{\mathcal{K}} \mathbf{f} \cdot \mathbf{v} \, \mathrm{d}\mathbf{x}. \tag{1.10}$$

Note that the integrals are computed on each triangle of the mesh; in particular, this means that in the second sum on the left in equation (1.10), the integrals over faces are calculated twice for those elements that share an edge (see Figure 1.2), each one with its respective normal vector $\mathbf{n}^+$ and $\mathbf{n}^-$.

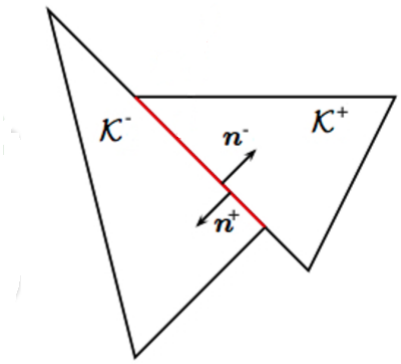

Figure 1.2: Example of two adjacent elements.

In other words, we can also rewrite this term as a sum over the internal and the Dirichlet boundary faces; it turns out that:

$$\sum_{\mathcal{K}\in\mathcal{T}_h}\int_{\partial\mathcal{K}}(\underline{\sigma}(\mathbf{u})\mathbf{n})\cdot\mathbf{v}\,\mathrm{d}\mathbf{x}=\sum_{\gamma\in\mathcal{F}_I}\int_\gamma\Big((\underline{\sigma}(\mathbf{u})^+\mathbf{n}^+)\cdot\mathbf{v}^+ + (\underline{\sigma}(\mathbf{u})^-\mathbf{n}^-)\cdot\mathbf{v}^-\Big)\,\mathrm{d}\mathbf{s}+\sum_{\gamma\in\mathcal{F}_D}\int_\gamma(\underline{\sigma}(\mathbf{u})\mathbf{n})\cdot\mathbf{v}\,\mathrm{d}\mathbf{s}.$$

Then using only the definition of the average and jump operators as in (1.7) and (1.8), we get:

$$\sum_{\gamma\in\mathcal{F}_I}\int_\gamma\Big((\underline{\sigma}(\mathbf{u})^+\mathbf{n}^+)\cdot\mathbf{v}^+ + (\underline{\sigma}(\mathbf{u})^-\mathbf{n}^-)\cdot\mathbf{v}^-\Big)\,\mathrm{d}\mathbf{s}+\sum_{\gamma\in\mathcal{F}_D}\int_\gamma(\underline{\sigma}(\mathbf{u})\mathbf{n})\cdot\mathbf{v}\,\mathrm{d}\mathbf{s}=$$

$$=\sum_{\gamma\in\mathcal{F}_I\cup\mathcal{F}_D}\int_\gamma\{\underline{\sigma}(\mathbf{u})\}:[\![\mathbf{v}]\!]\,\mathrm{d}\mathbf{s}+\sum_{\gamma\in\mathcal{F}_I}\int_\gamma[\![\underline{\sigma}(\mathbf{u})]\!]\cdot\{\mathbf{v}\}\,\mathrm{d}\mathbf{s}. \tag{1.11}$$

The proof of the *magic formula* (1.11) is postponed below, see Section 1.2.4.

Since we are supposing that the solution $\mathbf{u}\in\mathbf{H}^2(\Omega)$, the second integral of (1.11) is null because the term $[\![\underline{\sigma}(\mathbf{u})]\!]$ is zero. We remind the reader that we are still deriving a discrete scheme for the elastostatic problem (1.1) without a crack, in which we assume that both the solution and the stress are continuous through all the interior elements of the mesh. This implies that we can also add extra integrals containing the null term $[\![\mathbf{u}]\!]$,

without modifying the problem we want to solve.
For example, we can add the term " $\int_\gamma [\![\mathbf{u}]\!] : \{\underline{\sigma}(\mathbf{v})\}\ \mathrm{d}\mathbf{s}$ " in the sum over the edges in order to maintain the symmetric form of the original problem.
Moreover, it can be proved that a null integral of the form " $\int_\gamma \eta [\![\mathbf{u}]\!] : [\![\mathbf{v}]\!]\ \mathrm{d}\mathbf{s}$ " ensures the stability of the numerical method, without altering the symmetry. Generally speaking, η is a stabilization function, that might depend on the discretization of the domain. We introduce the following definition for the *penalization* parameter $\eta \in L^\infty(\mathcal{F}_I \cup \mathcal{F}_D)$:

$$\eta|_\gamma = \alpha \overline{\mathbf{D}} \frac{r^2}{h} \qquad \forall \gamma \in \mathcal{F}_I \cup \mathcal{F}_D, \tag{1.12}$$

where α is a positive constant to be properly chosen, h is the size of the mesh, r is the polynomial degree and $\overline{\mathbf{D}} = (|\mathbf{D}^{\frac{1}{2}}|_2^2)^{\frac{1}{2}}$ with $|\cdot|_2$ is the operator norm induced by the l^2-norm on $\mathbb{R}^2$.
Even without a rigorous proof, that can be found in [27], we can morally understand how the parameter η entails a stabilization of the method, as it "penalizes" the jump of the continuous solution. Having an increasingly refined mesh, i.e. $h \to 0$, η increases forcing the jump of $\mathbf{u}$ to become close to zero. This is also the reason why the method is called **interior-penalty** discontinuous Galerkin, cf. [28] and [29].

We obtain the following bilinear form:

$$\begin{aligned} A(\mathbf{u},\mathbf{v}) = &\sum_{\mathcal{K}\in\mathcal{T}_h} \int_{\mathcal{K}} \underline{\sigma}(\mathbf{u}) : \underline{\epsilon}(\mathbf{v})\ \mathrm{d}\mathbf{x} \ - \sum_{\gamma\in\mathcal{F}_I\cup\mathcal{F}_D} \int_\gamma \{\underline{\sigma}(\mathbf{u})\} : [\![\mathbf{v}]\!]\ \mathrm{d}\mathbf{s} \\ &- \sum_{\gamma\in\mathcal{F}_I\cup\mathcal{F}_D} \int_\gamma [\![\mathbf{u}]\!] : \{\underline{\sigma}(\mathbf{v})\}\ \mathrm{d}\mathbf{s} \ + \sum_{\gamma\in\mathcal{F}_I\cup\mathcal{F}_D} \int_\gamma \eta [\![\mathbf{u}]\!] : [\![\mathbf{v}]\!]\ \mathrm{d}\mathbf{s}. \end{aligned} \tag{1.13}$$

Recalling the definition (1.8) of the jump and average operators on a boundary face, we define:

$$F(\mathbf{v}) = \sum_{\mathcal{K}\in\mathcal{T}_h} \int_{\mathcal{K}} \mathbf{f}\cdot\mathbf{v}\ \mathrm{d}\mathbf{x}. \tag{1.14}$$

Finally, the discrete problem reads as follows (cf. [30] and [31]): find $\mathbf{u}_h \in \mathbf{V}_h^r$ such that:

$$A(\mathbf{u}_h,\mathbf{v}_h) = F(\mathbf{v}_h) \qquad \forall\ \mathbf{v}_h \in \mathbf{V}_h^r. \tag{1.15}$$

When non-homogeneous Dirichlet and Neumann conditions are considered, the bilinear

form $A(\cdot,\cdot)$ does not change, whereas the functional $F(\cdot)$ becomes:

$$F(\mathbf{v}) = \sum_{\mathcal{K}\in\mathcal{T}_h} \int_{\mathcal{K}} \mathbf{f}\cdot\mathbf{v}\ \mathrm{d}\mathbf{x} - \sum_{\gamma\in\mathcal{F}_D} \int_{\gamma} \mathbf{g}_D\cdot(\underline{\sigma}(\mathbf{v})\mathbf{n} - \eta\mathbf{v})\ \mathrm{d}\mathbf{s}\ + \sum_{\gamma\in\mathcal{F}_N} \langle \mathbf{g}_N, \mathbf{v}\rangle_{\gamma}. \tag{1.16}$$

1.2.4 Proof of the *magic formula*

We present an excursus to demonstrate the *magic formula* that we used to derive the discontinuous Galerkin method.
We report the formula and then we show with some manipulations that the term on the right hand side (rhs) is equal to the one on the left (lhs):

$$\sum_{\gamma\in\mathcal{F}_I} \int_{\gamma} \Big((\underline{\sigma}(\mathbf{u})^{+}\mathbf{n}^{+})\cdot\mathbf{v}^{+} + (\underline{\sigma}(\mathbf{u})^{-}\mathbf{n}^{-})\cdot\mathbf{v}^{-} \Big)\ \mathrm{d}\mathbf{s} + \sum_{\gamma\in\mathcal{F}_D} \int_{\gamma} (\underline{\sigma}(\mathbf{u})\mathbf{n})\cdot\mathbf{v}\ \mathrm{d}\mathbf{s} =$$

$$= \sum_{\gamma\in\mathcal{F}_I\cup\mathcal{F}_D} \int_{\gamma} \{\underline{\sigma}(\mathbf{u})\} : [\![\mathbf{v}]\!]\ \mathrm{d}\mathbf{s} + \sum_{\gamma\in\mathcal{F}_I} \int_{\gamma} [\![\underline{\sigma}(\mathbf{u})]\!]\cdot\{\mathbf{v}\}\ \mathrm{d}\mathbf{s}.$$

Proof. First, separating the integrals over the internal and the Dirichlet faces and using the definition of the jump and the average operators for a boundary edge, we can rewrite the rhs as:

$$\sum_{\gamma\in\mathcal{F}_I} \int_{\gamma} \Big(\{\underline{\sigma}(\mathbf{u})\} : [\![\mathbf{v}]\!] + [\![\underline{\sigma}(\mathbf{u})]\!]\cdot\{\mathbf{v}\} \Big)\ \mathrm{d}\mathbf{s} + \sum_{\gamma\in\mathcal{F}_D} \int_{\gamma} (\underline{\sigma}(\mathbf{u})\mathbf{n})\cdot\mathbf{v}\ \mathrm{d}\mathbf{s}.$$

Thus, we want to prove that:

$$\sum_{\gamma\in\mathcal{F}_I} \int_{\gamma} \Big((\underline{\sigma}(\mathbf{u})^{+}\mathbf{n}^{+})\cdot\mathbf{v}^{+} + (\underline{\sigma}(\mathbf{u})^{-}\mathbf{n}^{-})\cdot\mathbf{v}^{-} \Big)\ \mathrm{d}\mathbf{s} + \sum_{\gamma\in\mathcal{F}_D} \int_{\gamma} (\underline{\sigma}(\mathbf{u})\mathbf{n})\cdot\mathbf{v}\ \mathrm{d}\mathbf{s} =$$

$$\sum_{\gamma\in\mathcal{F}_I} \int_{\gamma} \Big(\{\underline{\sigma}(\mathbf{u})\} : [\![\mathbf{v}]\!] + [\![\underline{\sigma}(\mathbf{u})]\!]\cdot\{\mathbf{v}\} \Big)\ \mathrm{d}\mathbf{s} + \sum_{\gamma\in\mathcal{F}_D} \int_{\gamma} (\underline{\sigma}(\mathbf{u})\mathbf{n})\cdot\mathbf{v}\ \mathrm{d}\mathbf{s}.$$

This implies that we are only left to prove the following statement for any $\gamma\in\mathcal{F}_I$:

$$\int_{\gamma} \Big((\underline{\sigma}(\mathbf{u})^{+}\mathbf{n}^{+})\cdot\mathbf{v}^{+} + (\underline{\sigma}(\mathbf{u})^{-}\mathbf{n}^{-})\cdot\mathbf{v}^{-} \Big)\ \mathrm{d}\mathbf{s} = \int_{\gamma} \Big(\{\underline{\sigma}(\mathbf{u})\} : [\![\mathbf{v}]\!] + [\![\underline{\sigma}(\mathbf{u})]\!]\cdot\{\mathbf{v}\} \Big)\ \mathrm{d}\mathbf{s}.$$

We will show that the rhs is equal to the lhs above, using the definitions of jump and average and the fact that $\mathbf{n}^+ = -\mathbf{n}^-$:

$$\int_\gamma \left(\{\underline{\sigma}(\mathbf{u})\} : [\![\mathbf{v}]\!] + [\![\underline{\sigma}(\mathbf{u})]\!] \cdot \{\mathbf{v}\} \right) \mathrm{d}\mathbf{s} =$$

$$\int_\gamma \left(\frac{\underline{\sigma}(\mathbf{u})^+ + \underline{\sigma}(\mathbf{u})^-}{2} \right) : (\mathbf{v}^+ \otimes \mathbf{n}^+ + \mathbf{v}^- \otimes \mathbf{n}^-) \, \mathrm{d}\mathbf{s} + \int_\gamma (\underline{\sigma}(\mathbf{u})^+ \mathbf{n}^+ + \underline{\sigma}(\mathbf{u})^- \mathbf{n}^-) \cdot (\frac{\mathbf{v}^+ + \mathbf{v}^-}{2}) \, \mathrm{d}\mathbf{s} =$$

$$\int_\gamma \left(\frac{\underline{\sigma}(\mathbf{u})^+ + \underline{\sigma}(\mathbf{u})^-}{2} \right) : \left((\mathbf{v}^+ - \mathbf{v}^-) \otimes \mathbf{n}^+ \right) \mathrm{d}\mathbf{s} + \int_\gamma (\underline{\sigma}(\mathbf{u})^+ \mathbf{n}^+ + \underline{\sigma}(\mathbf{u})^- \mathbf{n}^-) \cdot (\frac{\mathbf{v}^+ + \mathbf{v}^-}{2}) \, \mathrm{d}\mathbf{s}.$$

Now we can employ a general property of the tensor product:

$$\underline{a} : (\mathbf{b} \otimes \mathbf{c}) = \sum_{i,j=1}^{2} \underline{a}_{ij} (\mathbf{b} \otimes \mathbf{c})_{ij} = \sum_{i,j=1}^{2} \underline{a}_{ij} \mathbf{b}_i \mathbf{c}_j = \sum_{i,j=1}^{2} \underline{a}_{ij} \mathbf{c}_j \mathbf{b}_i = (\underline{a}\mathbf{c}) \cdot \mathbf{b},$$

and modifying accordingly the first integral, we get:

$$\int_\gamma \left(\frac{\underline{\sigma}(\mathbf{u})^+ + \underline{\sigma}(\mathbf{u})^-}{2} \right) \mathbf{n}^+ \cdot (\mathbf{v}^+ - \mathbf{v}^-) \, \mathrm{d}\mathbf{s} + \int_\gamma (\underline{\sigma}(\mathbf{u})^+ \mathbf{n}^+ + \underline{\sigma}(\mathbf{u})^- \mathbf{n}^-) \cdot (\frac{\mathbf{v}^+ + \mathbf{v}^-}{2}) \, \mathrm{d}\mathbf{s} =$$

$$= \int_\gamma \left(\left(\frac{\underline{\sigma}(\mathbf{u})^+ + \underline{\sigma}(\mathbf{u})^-}{2} \right) \mathbf{n}^+ \cdot \mathbf{v}^+ - \left(\frac{\underline{\sigma}(\mathbf{u})^+ + \underline{\sigma}(\mathbf{u})^-}{2} \right) \mathbf{n}^+ \cdot \mathbf{v}^- \right) \mathrm{d}\mathbf{s} +$$

$$+ \int_\gamma (\underline{\sigma}(\mathbf{u})^+ \mathbf{n}^+ + \underline{\sigma}(\mathbf{u})^- \mathbf{n}^-) \cdot (\frac{\mathbf{v}^+ + \mathbf{v}^-}{2}) \, \mathrm{d}\mathbf{s} =$$

$$= \int_\gamma \left(\frac{\underline{\sigma}(\mathbf{u})^+}{2} \mathbf{n}^+ \cdot \mathbf{v}^+ + \frac{\underline{\sigma}(\mathbf{u})^-}{2} \mathbf{n}^+ \cdot \mathbf{v}^+ - \cancel{\frac{\underline{\sigma}(\mathbf{u})^+}{2} \mathbf{n}^+ \cdot \mathbf{v}^-} - \frac{\underline{\sigma}(\mathbf{u})^-}{2} \mathbf{n}^+ \cdot \mathbf{v}^- + \right.$$

$$\left. + \underline{\sigma}(\mathbf{u})^+ \mathbf{n}^+ \cdot \frac{\mathbf{v}^+}{2} + \cancel{\underline{\sigma}(\mathbf{u})^+ \mathbf{n}^+ \cdot \frac{\mathbf{v}^-}{2}} + \underline{\sigma}(\mathbf{u})^- \mathbf{n}^- \cdot \frac{\mathbf{v}^+}{2} + \underline{\sigma}(\mathbf{u})^- \mathbf{n}^- \cdot \frac{\mathbf{v}^-}{2} \right) \mathrm{d}\mathbf{s} =$$

$$= \int_\gamma \left(\frac{\underline{\sigma}(\mathbf{u})^+}{2} \mathbf{n}^+ \cdot \mathbf{v}^+ + \cancel{\frac{\underline{\sigma}(\mathbf{u})^-}{2} \mathbf{n}^+ \cdot \mathbf{v}^+} + \frac{\underline{\sigma}(\mathbf{u})^-}{2} \mathbf{n}^- \cdot \mathbf{v}^- + \underline{\sigma}(\mathbf{u})^+ \mathbf{n}^+ \cdot \frac{\mathbf{v}^+}{2} - \right.$$

$$- \cancel{\underline{\sigma}(\mathbf{u})^{-}\mathbf{n}^{+} \cdot \frac{\mathbf{v}^{+}}{2}} + \underline{\sigma}(\mathbf{u})^{-}\mathbf{n}^{-} \cdot \frac{\mathbf{v}^{-}}{2} \Bigg) \, \mathrm{d}\mathbf{s} =$$

$$= \int_{\gamma} \Bigg((\underline{\sigma}(\mathbf{u})^{+}\mathbf{n}^{+}) \cdot \mathbf{v}^{+} + (\underline{\sigma}(\mathbf{u})^{-}\mathbf{n}^{-}) \cdot \mathbf{v}^{-} \Bigg) \, \mathrm{d}\mathbf{s},$$

that is equal to the *lhs* and the proof is complete. □

1.2.5 Well-posedness and error analysis

In this subsection we are interested in showing the well-posedness of the discrete problem (1.15) and giving a quantitative estimate of the error between the continuous solution of problem (1.5) and the discrete solution solving (1.15).
From now on, we will use the notation $x \lesssim y$ to represent the inequality $x \leq Cy$, where C is a generic positive constant.
We set $\widetilde{\mathbf{V}}_h^r = \mathbf{V}_h^r + \mathbf{H}^2(\mathcal{T}_h)$ and we introduce the following norms:

$$||\mathbf{v}_h||_{DG}^2 = ||\mathbf{D}^{\frac{1}{2}}\underline{\epsilon}(\mathbf{v}_h)||_{\mathcal{L}^2(\mathcal{T}_h)}^2 + ||\eta^{1/2}[\![\mathbf{v}_h]\!]||_{\mathcal{L}^2(\mathcal{F}_I \cup \mathcal{F}_D)}^2 \quad \forall\ \mathbf{v}_h \in \mathbf{V}_h^r,$$

$$|||\mathbf{v}_h|||_{DG}^2 = ||\mathbf{v}_h||_{DG}^2 + ||\eta^{-1/2}\{\underline{\sigma}(\mathbf{v}_h)\}||_{\mathcal{L}^2(\mathcal{F}_I \cup \mathcal{F}_D)}^2 \quad \forall\ \mathbf{v}_h \in \widetilde{\mathbf{V}}_h^r, \tag{1.17}$$

where we have indicated with $\mathbf{D}^{\frac{1}{2}}$ the square root of the 4^{th} order tensor $\mathbf{D}$, i.e. there exists a tensor $\mathbf{T}$ such that $\mathbf{D} = \mathbf{T}^{*}\mathbf{T}$ with $\mathbf{T}^{*}$ the adjoint operator of $\mathbf{T}$ and $\mathbf{T} = \mathbf{D}^{\frac{1}{2}}$.
It can be shown that these two norms are equivalent on $\mathbf{V}_h^r$, meaning that :

$$||\mathbf{v}_h||_{DG} \leq |||\mathbf{v}_h|||_{DG} \lesssim ||\mathbf{v}_h||_{DG} \qquad \forall\ \mathbf{v}_h \in \mathbf{V}_h^r. \tag{1.18}$$

While the first inequality follows directly from the definition of the two norms, the second one is not so trivial (cf. [12]) and is based on a trace-inverse inequality on the polynomial space $\mathbf{V}_h^r$.
Before discussing the error estimates for the method (1.15), we state its well-posedness and some preliminary results.

Lemma 2. *(Well-posedness). Problem* (1.15) *admits a unique solution, provided that the stabilization parameter* α *in* (1.12) *is chosen large enough.*

Proof. We first show that $A(\cdot,\cdot)$ is continuous w.r.t the norm (1.17) in $\widetilde{\mathbf{V}}_h^r$. This implies that the same result holds true using the $||\cdot||_{DG}$ norm with functions in $\mathbf{V}_h^r$, thanks to the equivalence relation of the norms (1.18). Then we will prove that $A(\cdot,\cdot)$ is also coercive w.r.t. the $||\cdot||_{DG}$ norm in $\mathbf{V}_h^r$.

- Continuity on $\widetilde{\mathbf{V}}_h^r$:

$$|A(\mathbf{u},\mathbf{v})| \lesssim |||\mathbf{u}|||_{DG}|||\mathbf{v}|||_{DG} \qquad \forall\ \mathbf{u},\mathbf{v} \in \widetilde{\mathbf{V}}_h^r.$$

Let $\mathbf{u},\mathbf{v} \in \widetilde{\mathbf{V}}_h^r$ then:

$$|A(\mathbf{u},\mathbf{v})| \leq \left|\sum_{\mathcal{K}\in\mathcal{T}_h}\int_{\mathcal{K}} \underline{\sigma}(\mathbf{u}) : \underline{\epsilon}(\mathbf{v})\ \mathrm{d}\mathbf{x}\right| + \left|\sum_{\gamma\in\mathcal{F}_I\cup\mathcal{F}_D}\int_{\gamma}\{\underline{\sigma}(\mathbf{u})\} : [\![\mathbf{v}]\!]\ \mathrm{d}\mathbf{s}\right| +$$

$$+\left|\sum_{\gamma\in\mathcal{F}_I\cup\mathcal{F}_D}\int_{\gamma}[\![\mathbf{u}]\!] : \{\underline{\sigma}(\mathbf{v})\}\ \mathrm{d}\mathbf{s}\right| + \left|\sum_{\gamma\in\mathcal{F}_I\cup\mathcal{F}_D}\int_{\gamma}\eta[\![\mathbf{u}]\!] : [\![\mathbf{v}]\!]\ \mathrm{d}\mathbf{s}\right|.$$

Using the Cauchy-Schwarz inequality and the definition of the $||\cdot||_{DG}$ norm we get:

$$(I) = \left|\sum_{\mathcal{K}\in\mathcal{T}_h}\int_{\mathcal{K}}\sum_{i,j=1}^{2}\sigma_{ij}(\mathbf{u})\epsilon_{ij}(\mathbf{v})\ \mathrm{d}\mathbf{x}\right| = \left|\sum_{\mathcal{K}\in\mathcal{T}_h}\int_{\mathcal{K}}\sum_{i,j=1}^{2}\sum_{k,l=1}^{2}D_{ijkl}\epsilon_{kl}(\mathbf{u})\epsilon_{ij}(\mathbf{v})\ \mathrm{d}\mathbf{x}\right| \leq$$

$$\leq \sum_{\mathcal{K}\in\mathcal{T}_h}\int_{\mathcal{K}}|\mathbf{D}^{\frac{1}{2}}\underline{\epsilon}(\mathbf{u})||\mathbf{D}^{\frac{1}{2}}\underline{\epsilon}(\mathbf{v})|\ \mathrm{d}\mathbf{x} \leq |||\mathbf{u}|||_{DG}\ |||\mathbf{v}|||_{DG}.$$

$$(II) = \left|\sum_{\gamma\in\mathcal{F}_I\cup\mathcal{F}_D}\int_{\gamma}\{\underline{\sigma}(\mathbf{u})\} : [\![\mathbf{v}]\!]\ \mathrm{d}\mathbf{s}\right| = \left|\sum_{\gamma\in\mathcal{F}_I\cup\mathcal{F}_D}\int_{\gamma}\eta^{-1/2}\{\underline{\sigma}(\mathbf{u})\} : \eta^{1/2}[\![\mathbf{v}]\!]\ \mathrm{d}\mathbf{s}\right| \leq$$

$$\leq \left(\sum_{\gamma\in\mathcal{F}_I\cup\mathcal{F}_D}||\eta^{-1/2}\{\underline{\sigma}(\mathbf{u})\}||^2_{\mathcal{L}^2(\gamma)}\right)^{1/2}\left(\sum_{\gamma\in\mathcal{F}_I\cup\mathcal{F}_D}||\eta^{1/2}[\![\mathbf{v}]\!]||^2_{\mathcal{L}^2(\gamma)}\right)^{1/2} =$$

$$= ||\eta^{-1/2}\{\underline{\sigma}(\mathbf{u})\}\ ||_{\mathcal{L}^2(\mathcal{F}_I\cup\mathcal{F}_D)}\ ||\eta^{1/2}[\![\mathbf{v}]\!]\ ||_{\mathcal{L}^2(\mathcal{F}_I\cup\mathcal{F}_D)} \leq |||\mathbf{u}|||_{DG}\ |||\mathbf{v}|||_{DG}.$$

Analogously, for the third term:

$$(III) \leq \left(\sum_{\gamma \in \mathcal{F}_I \cup \mathcal{F}_D} ||\eta^{-1/2} \{\underline{\sigma}(\mathbf{v})\}||^2_{\mathcal{L}^2(\gamma)} \right)^{1/2} \left(\sum_{\gamma \in \mathcal{F}_I \cup \mathcal{F}_D} ||\eta^{1/2} [\![\mathbf{u}]\!]||^2_{\mathcal{L}^2(\gamma)} \right)^{1/2} =$$

$$= ||\eta^{-1/2} \{\underline{\sigma}(\mathbf{v})\}\ ||_{\mathcal{L}^2(\mathcal{F}_I \cup \mathcal{F}_D)}\ ||\eta^{1/2} [\![\mathbf{u}]\!]\ ||_{\mathcal{L}^2(\mathcal{F}_I \cup \mathcal{F}_D)} \leq |||\mathbf{u}|||_{DG}\ |||\mathbf{v}|||_{DG}.$$

Finally, we estimate the fourth term with:

$$(IV) \leq \left(\sum_{\gamma \in \mathcal{F}_I \cup \mathcal{F}_D} ||\eta^{1/2} [\![\mathbf{v}]\!]\ ||^2_{\mathcal{L}^2(\gamma)} \right)^{1/2} \left(\sum_{\gamma \in \mathcal{F}_I \cup \mathcal{F}_D} ||\eta^{1/2} [\![\mathbf{u}]\!]\ ||^2_{\mathcal{L}^2(\gamma)} \right)^{1/2} =$$

$$= ||\eta^{1/2} [\![\mathbf{v}]\!]\ ||_{\mathcal{L}^2(\mathcal{F}_I \cup \mathcal{F}_D)}\ ||\eta^{1/2} [\![\mathbf{u}]\!]\ ||_{\mathcal{L}^2(\mathcal{F}_I \cup \mathcal{F}_D)} \leq |||\mathbf{u}|||_{DG}\ |||\mathbf{v}|||_{DG}.$$

Summing up the four bounds, we get:

$$|A(\mathbf{u}, \mathbf{v})| \lesssim |||\mathbf{u}|||_{DG} |||\mathbf{v}|||_{DG} \qquad \forall\ \mathbf{u}, \mathbf{v} \in \widetilde{\mathbf{V}}^r_h.$$

- **Coercivity on $\mathbf{V}^r_h$:**

$$A(\mathbf{v}_h, \mathbf{v}_h) \gtrsim ||\mathbf{v}_h||^2_{DG} \qquad \forall\ \mathbf{v}_h \in \mathbf{V}^r_h.$$

Recalling the definition of $A(\cdot, \cdot)$, we have:

$$A(\mathbf{v}_h, \mathbf{v}_h) = ||\mathbf{D}^{1/2} \underline{\epsilon}(\mathbf{v}_h)||^2_{\mathcal{L}^2(\mathcal{T}_h)} - 2 \sum_{\gamma \in \mathcal{F}_I \cup \mathcal{F}_D} \int_\gamma \{\underline{\sigma}(\mathbf{v}_h)\} : [\![\mathbf{v}_h]\!] + \sum_{\gamma \in \mathcal{F}_I \cup \mathcal{F}_D} ||\eta^{1/2} [\![\mathbf{v}_h]\!]||^2_{\mathcal{L}^2(\gamma)}.$$

We next estimate the second term on the right hand side:

$$\left| \sum_{\gamma \in \mathcal{F}_I \cup \mathcal{F}_D} \int_\gamma \{\underline{\sigma}(\mathbf{v}_h)\} : [\![\mathbf{v}_h]\!] \right| \leq$$

$$\leq ||\eta^{-1/2} \{\underline{\sigma}(\mathbf{v}_h)\}\ ||_{\mathcal{L}^2(\mathcal{F}_I \cup \mathcal{F}_D)}\ ||\eta^{1/2} [\![\mathbf{v}_h]\!]\ ||_{\mathcal{L}^2(\mathcal{F}_I \cup \mathcal{F}_D)}$$

$$\leq \frac{\delta}{2} ||\eta^{-1/2} \{\underline{\sigma}(\mathbf{v}_h)\}\ ||^2_{\mathcal{L}^2(\mathcal{F}_I \cup \mathcal{F}_D)} + \frac{1}{2\delta} ||\eta^{1/2} [\![\mathbf{v}_h]\!]\ ||^2_{\mathcal{L}^2(\mathcal{F}_I \cup \mathcal{F}_D)},$$

where we have used the Cauchy-Schwarz inequality and the following Young's inequality:

$$ab \leq \frac{\delta}{2} a^2 + \frac{1}{2\delta} b^2 \qquad \text{for a } \delta \in (0, 1).$$

If $\mathbf{w}$ is a piecewise polynomial, we can also use the following trace-inverse estimate:

$$||\mathbf{w}||_{\mathbf{L}^2(\gamma)} \lesssim \frac{r}{h^{1/2}}||\mathbf{w}||_{\mathbf{L}^2(\mathcal{K})} \qquad \forall\ \gamma \in \partial\mathcal{K} \qquad \forall\ \mathbf{w} \in \mathbb{P}^r(\mathcal{K}). \tag{1.19}$$

Using the above estimate, the fact that $\underline{\sigma}(\mathbf{v}_h) \in \mathbf{V}_h^r$ and the definition of the penalization parameter as in (1.12), we obtain:

$$\begin{aligned} ||\eta^{-1/2}\{\underline{\sigma}(\mathbf{v}_h)\}\ ||^2_{\mathcal{L}^2(\mathcal{F}_I\cup\mathcal{F}_D)} &\lesssim \sum_{\gamma\in\mathcal{F}_I\cup\mathcal{F}_D} \frac{h}{\alpha r^2}||\mathbf{D}^{-1/2}\{\underline{\sigma}(\mathbf{v}_h)\}||^2_{\mathcal{L}^2(\gamma)} \\ &\lesssim \frac{h}{\alpha r^2}\frac{r^2}{h}\sum_{\mathcal{K}\in\mathcal{T}_h}||\mathbf{D}^{-1/2}\mathbf{D}\underline{\epsilon}(\mathbf{v}_h)||^2_{\mathcal{L}^2(\mathcal{K}^+\cup\mathcal{K}^-)} \\ &\lesssim \frac{1}{\alpha}||\mathbf{D}^{1/2}\underline{\epsilon}(\mathbf{v}_h)||^2_{\mathcal{L}^2(\mathcal{T}_h)}. \end{aligned}$$

Hence, it follows that:

$$A(\mathbf{v}_h,\mathbf{v}_h) \geq$$

$$||\mathbf{D}^{1/2}\underline{\epsilon}(\mathbf{v}_h)||^2_{\mathcal{L}^2(\mathcal{T}_h)} - \delta\ ||\eta^{-1/2}\{\underline{\sigma}(\mathbf{v}_h)\}\ ||^2_{\mathcal{L}^2(\mathcal{F}_I\cup\mathcal{F}_D)} + (1-\frac{1}{\delta})\ ||\eta^{1/2}[\![\mathbf{v}_h]\!]\ ||^2_{\mathcal{L}^2(\mathcal{F}_I\cup\mathcal{F}_D)}$$

$$\geq (1-\frac{C\delta}{\alpha})\ ||\mathbf{D}^{1/2}\underline{\epsilon}(\mathbf{v}_h)\ ||^2_{\mathcal{L}^2(\mathcal{T}_h)} + (1-\frac{1}{\delta})\ ||\eta^{1/2}[\![\mathbf{v}_h]\!]\ ||^2_{\mathcal{L}^2(\mathcal{F}_I\cup\mathcal{F}_D)},$$

where in the last step we have exploited the arithmetic-geometric inequality, for any $\delta \in (0,1)$.

Finally we can choose δ such that both $(1-\frac{1}{\delta})$ and $(1-\frac{C\delta}{\alpha})$ are positive, bounded away from zero and such that $\alpha \geq 4C$, in order to obtain:

$$A(\mathbf{v}_h,\mathbf{v}_h) \geq \frac{1}{2}\ ||\mathbf{D}^{1/2}\underline{\epsilon}(\mathbf{v}_h)\ ||^2_{\mathcal{L}^2(\mathcal{T}_h)} + \frac{1}{2}\ ||\eta^{1/2}[\![\mathbf{v}_h]\!]\ ||^2_{\mathcal{L}^2(\mathcal{F}_I\cup\mathcal{F}_D)} = \frac{1}{2}||\mathbf{v}_h||^2_{DG}.$$

which shows the coercivity on $\mathbf{V}_h^r$

- **Continuity of the linear functional** $F(\cdot)$ on $\mathbf{V}_h^r$.

$$\begin{aligned} \left|\sum_{\mathcal{K}\in\mathcal{T}_h}\int_{\mathcal{K}}\mathbf{f}\cdot\mathbf{v}\ \mathrm{d}\mathbf{x}\right| &\leq \left(\sum_{\mathcal{K}\in\mathcal{T}_h}||\mathbf{f}||^2_{\mathbf{L}^2(\mathcal{K})}\right)^{1/2}\left(\sum_{\mathcal{K}\in\mathcal{T}_h}||\mathbf{v}||^2_{\mathbf{L}^2(\mathcal{K})}\right)^{1/2} \\ &\lesssim ||\mathbf{f}||_{\mathbf{L}^2(\mathcal{T}_h)}\left(\sum_{\mathcal{K}\in\mathcal{T}_h}||\underline{\epsilon}(\mathbf{v})||^2_{\mathcal{L}^2(\mathcal{K})}\right)^{1/2} \lesssim ||\mathbf{f}||_{\mathbf{L}^2(\mathcal{T}_h)}||\mathbf{v}||_{DG}, \end{aligned}$$

where we have used the Poincaré inequality for piecewise functions in $\mathbf{H}^1$, cf. [32], together with Korn's inequality.

Now, using the Lax-Milgram Lemma (see [23]), the proof is complete.

□

In the following, we present some useful results to prove the error estimates.

Lemma 3. *(Strong consistency). The exact solution $\boldsymbol{u}$ satisfies the discrete problem, i.e.*

$$A(\boldsymbol{u}, \boldsymbol{v}_h) = \int_\Omega \boldsymbol{f} \cdot \boldsymbol{v}_h \qquad \forall\ \boldsymbol{v}_h \in \boldsymbol{V}_h^r. \tag{1.20}$$

Proof. Here we consider $\mathbf{u}$ as the solution of the boundary value problem (1.1) in Ω with homogeneous Dirichlet and Neumann conditions. From the integration by parts and the *Magic Formula* (1.11), we get:

$$\sum_{\mathcal{K}\in\mathcal{T}_h} \int_{\mathcal{K}} \underline{\sigma}(\mathbf{u}) : \underline{\epsilon}(\mathbf{v})\ \mathrm{d}\mathbf{x} = -\sum_{\mathcal{K}\in\mathcal{T}_h} \int_{\mathcal{K}} (\nabla\cdot\underline{\sigma}(\mathbf{u}))\cdot\mathbf{v}\ \mathrm{d}\mathbf{x} + \sum_{\gamma\in\mathcal{F}_I\cup\mathcal{F}_D} \int_\gamma \{\underline{\sigma}(\mathbf{u})\} : [\![\mathbf{v}]\!]\ \mathrm{d}\mathbf{s}$$

$$+ \sum_{\gamma\in\mathcal{F}_I} \int_\gamma [\![\underline{\sigma}(\mathbf{u})]\!] : \{\mathbf{v}\}\ \mathrm{d}\mathbf{s} \qquad \forall\ \mathbf{v}\in\mathbf{H}^1(\mathcal{T}_h).$$

Since $[\![\underline{\sigma}(\mathbf{u})]\!] = 0$ on each interior face and $-(\nabla\cdot\underline{\sigma}(\mathbf{u})) = \mathbf{f}$, the above expression becomes:

$$\sum_{\mathcal{K}\in\mathcal{T}_h} \int_{\mathcal{K}} \underline{\sigma}(\mathbf{u}) : \underline{\epsilon}(\mathbf{v})\ \mathrm{d}\mathbf{x} - \sum_{\gamma\in\mathcal{F}_I\cup\mathcal{F}_D} \int_\gamma \{\underline{\sigma}(\mathbf{u})\} : [\![\mathbf{v}]\!]\ \mathrm{d}\mathbf{s} = \int_\Omega \mathbf{f}\cdot\mathbf{v}\ \mathrm{d}\mathbf{x} \qquad \forall\ \mathbf{v}\in\mathbf{H}^1(\mathcal{T}_h).$$

Notice that $[\![\mathbf{u}]\!] = 0$ on each interior face and $[\![\mathbf{u}]\!] = \mathbf{u} = 0$ on each boundary face contained in Γ_D. Thus, we can also write:

$$\sum_{\mathcal{K}\in\mathcal{T}_h} \int_{\mathcal{K}} \underline{\sigma}(\mathbf{u}) : \underline{\epsilon}(\mathbf{u})\ \mathrm{d}\mathbf{x} - \sum_{\gamma\in\mathcal{F}_I\cup\mathcal{F}_D} \int_\gamma \{\underline{\sigma}(\mathbf{u})\} : [\![\mathbf{v}]\!]\ \mathrm{d}\mathbf{s} - \sum_{\gamma\in\mathcal{F}_I\cup\mathcal{F}_D} \int_\gamma \{\underline{\sigma}(\mathbf{v})\} : [\![\mathbf{u}]\!]\ \mathrm{d}\mathbf{s}$$

$$+ \sum_{\gamma\in\mathcal{F}_I\cup\mathcal{F}_D} \int_\gamma \eta [\![\mathbf{u}]\!]\cdot[\![\mathbf{v}]\!] = \int_\Omega \mathbf{f}\cdot\mathbf{v}\ \mathrm{d}\mathbf{x} \qquad \forall\ \mathbf{v}\in\mathbf{H}^1(\mathcal{T}_h),$$

that is

$$A(\mathbf{u},\mathbf{v}) = F(\mathbf{v}) \qquad \forall\ \mathbf{v}\in\mathbf{H}^1(\mathcal{T}_h).$$

In particular, we obtain (1.20) because $\mathbf{V}_h^r \subset \mathbf{H}^1(\mathcal{T}_h)$. □

From the consistency of the method and by a simple argument of linearity, the following Lemma holds:

Lemma 4. *(Galerkin orthogonality, cf. [33])*

$$A(\boldsymbol{u} - \boldsymbol{u}_h, \boldsymbol{v}_h) = 0 \quad \forall\ \boldsymbol{v}_h \in \boldsymbol{V}_h^r.$$

This property can be interpreted as the orthogonality between the approximation error $\mathbf{u} - \mathbf{u}_h$ and the space $\mathbf{V}_h^r$ with respect to the scalar product $A(\cdot, \cdot)$ in $\mathbf{V}_h^r$. This means that $\mathbf{u}_h$ is the function in $\mathbf{V}_h^r$ that best approximates the exact solution $\mathbf{u}$ in the energy norm.

Before stating the error estimates, we need to provide a bound for $|||\mathbf{u} - \Pi_h^r \mathbf{u}|||_{DG}$ and we will make use of the following *hp*-approximation:

Lemma 5. *(cf. [34] and [35]) Let $\boldsymbol{v} \in \boldsymbol{H}^s(\mathcal{K})$ and $\underline{\tau} \in \mathcal{H}^s(\mathcal{K})$, for some $s > 1$ and for each $\mathcal{K} \in \mathcal{T}_h$. Then, there exists a sequence of operators: $\Pi_h^r \boldsymbol{v} : \boldsymbol{L}^2(\Omega) \to \mathbf{V}_h^r$ and $\mathbf{\Pi}_h^r \underline{\tau} \to \mathcal{V}_h^r$ for $r = 1, 2, ..$ such that:*

$$\begin{aligned}
&||\boldsymbol{v} - \Pi_h^r \boldsymbol{v}||_{\boldsymbol{H}^q(\mathcal{K})} \lesssim \frac{h^{min(r+1,s)-q}}{r^{s-q}} ||\boldsymbol{v}||_{\boldsymbol{H}^s(\mathcal{K})} \qquad 0 \leq q \leq s, \\
&||\boldsymbol{v} - \Pi_h^r \boldsymbol{v}||_{\boldsymbol{L}^2(\partial\mathcal{K})} \lesssim \frac{h^{min(r+1,s)-1/2}}{r^{s-1/2}} ||\boldsymbol{v}||_{\boldsymbol{H}^s(\mathcal{K})}, \\
&||\underline{\tau} - \mathbf{\Pi}_h^r \underline{\tau}||_{\mathcal{H}^q(\mathcal{K})} \lesssim \frac{h^{min(r+1,s)-q}}{r^{s-q}} ||\underline{\tau}||_{\mathcal{H}^s(\mathcal{K})} \qquad 0 \leq q \leq s, \\
&||\underline{\tau} - \mathbf{\Pi}_h^r \underline{\tau}||_{\mathcal{L}^2(\partial\mathcal{K})} \lesssim \frac{h^{min(r+1,s)-1/2}}{r^{s-1/2}} ||\underline{\tau}||_{\mathcal{H}^s(\mathcal{K})}.
\end{aligned}$$

The hidden constant is independent on $\boldsymbol{v}, \underline{\tau}, h, r$ but depends on the shape-regularity of $\mathcal{K}$ and on the material properties.

Let $\mathbf{e} = \mathbf{u} - \Pi_h^r \mathbf{u}$ and recall the definition of the $||\cdot||_{DG}$ norm:

$$|||\mathbf{e}|||_{DG}^2 = ||\mathbf{D}^{\frac{1}{2}} \underline{\epsilon}(\mathbf{e})||_{\mathcal{L}^2(\mathcal{T}_h)}^2 + ||\eta^{1/2} [\![\mathbf{e}]\!]||_{\mathcal{L}^2(\mathcal{F}_I \cup \mathcal{F}_D)}^2 + ||\eta^{-1/2} \{\underline{\sigma}(\mathbf{e})\}||_{\mathcal{L}^2(\mathcal{F}_I \cup \mathcal{F}_D)}^2$$

and define (I), (II), (III) the terms on its right hand side.
We can now estimate the first term with Lemma 5 and we get:

$$(I) \lesssim \frac{h^{2\min(r+1,s)-2}}{r^{2s-2}} ||\mathbf{u}||_{\mathbf{H}^s(\mathcal{T}_h)}^2. \tag{1.21}$$

For the second term, we use again Lemma 5 to obtain:

$$(II) \lesssim \frac{r^2}{h} \sum_{\mathcal{K}\in\mathcal{T}_h} ||\mathbf{e}||^2_{\mathbf{L}^2(\partial\mathcal{K})} \lesssim \frac{r^2}{h} \frac{h^{2\min(r+1,s)-1}}{r^{2s-1}} ||\mathbf{u}||_{\mathbf{H}^s(\mathcal{T}_h)} = \frac{h^{2\min(r+1,s)-2}}{r^{2s-3}} ||\mathbf{u}||_{\mathbf{H}^s(\mathcal{T}_h)}. \quad (1.22)$$

Analogously, for the term (III) we can write:

$$(III) \lesssim \frac{r^2}{h} \sum_{\mathcal{K}\in\mathcal{T}_h} ||\underline{\sigma}(\mathbf{e})||^2_{\mathcal{L}^2(\partial\mathcal{K})} \lesssim \frac{r^2}{h} \frac{h^{2\min(r+1,s)-3}}{r^{2s-3}} ||\mathbf{u}||_{\mathbf{H}^s(\mathcal{T}_h)} = \frac{h^{2\min(r+1,s)-4}}{r^{2s-5}} ||\mathbf{u}||_{\mathbf{H}^s(\mathcal{T}_h)}. \quad (1.23)$$

Summing on the previous bounds, we obtain:

$$|||\mathbf{u} - \Pi^r_h \mathbf{u}|||_{DG} \lesssim \frac{h^{\min(r+1,s)-1}}{r^{s-1/2}} ||\mathbf{u}||_{\mathbf{H}^s(\mathcal{T}_h)}. \quad (1.24)$$

The error analysis of the method shows that the solution $\mathbf{u}_h$ converges to $\mathbf{u}$ when the error is measured in the norm (1.17) or in average. The error estimator for linear elastic analysis can also be showed when any combination of Neumann and Dirichlet boundary conditions are admissible in the formulation, see for instance [36], [37] and [38].
The estimates are contained in the following theorem:

Theorem 2. *Suppose that the exact solution $\boldsymbol{u} \in \boldsymbol{H}^2(\Omega) \cap \boldsymbol{H}^s(\mathcal{T}_h)$, for some $s \geq 2$. If the parameter α appearing in the definition* (1.12) *of the stabilization function is chosen sufficiently large and $\boldsymbol{u}_h$ is the solution obtained with* (1.15)*, it holds:*

$$||\boldsymbol{u} - \boldsymbol{u}_h||_{DG} \lesssim \frac{h^{min(r+1,s)-1}}{r^{s-1/2}} ||\boldsymbol{u}||_{\boldsymbol{H}^s(\mathcal{T}_h)}, \quad (1.25)$$

$$||\boldsymbol{u} - \boldsymbol{u}_h||_{\boldsymbol{L}^2(\Omega)} \lesssim \frac{h^{min(r+1,s)}}{r^{s+1}} ||\boldsymbol{u}||_{\boldsymbol{H}^s(\mathcal{T}_h)}, \quad (1.26)$$

where $r = min_{\mathcal{K}\in\mathcal{T}_h}(r_\mathcal{K})$ and $h = max_{\mathcal{K}\in\mathcal{T}_h}(h_\mathcal{K})$.

Proof. In order to prove Theorem 2, we will assume, for simplicity, that the mesh $\mathcal{T}_h$ is quasi-uniform and that $r_\mathcal{K} = r \ \forall \mathcal{K} \in \mathcal{T}_h$. Let $\Pi^r_h \mathbf{u} \in \mathbf{V}^r_h$ be defined as in Lemma 5. Now using all the previous results, we obtain:

$||\Pi^r_h \mathbf{u} - \mathbf{u}_h||^2_{DG} \lesssim A(\Pi^r_h \mathbf{u} - \mathbf{u}_h, \Pi^r_h \mathbf{u} - \mathbf{u}_h)$ (Coercivity on $\mathbf{V}^r_h$, Lemma 2)

$$\lesssim A(\Pi_h^r\mathbf{u}-\mathbf{u},\Pi_h^r\mathbf{u}-\mathbf{u}_h) \quad \text{(Consistency as in (1.20))}$$

$$\lesssim |||\Pi_h^r\mathbf{u}-\mathbf{u}|||_{DG}\ |||\Pi_h^r\mathbf{u}-\mathbf{u}_h|||_{DG} \quad \text{(Continuity on } \widetilde{\mathbf{V}}_h^r\text{, Lemma 2)}$$

$$\lesssim |||\Pi_h^r\mathbf{u}-\mathbf{u}|||_{DG}\ ||\Pi_h^r\mathbf{u}-\mathbf{u}_h||_{DG} \quad \text{(Norms equivalence on } \mathbf{V}_h^r\text{)}$$

Recalling the triangle inequality:

$$||\mathbf{u}-\mathbf{u}_h||_{DG} \leq ||\mathbf{u}-\Pi_h^r\mathbf{u}||_{DG} + ||\Pi_h^r\mathbf{u}-\mathbf{u}_h||_{DG},$$

we get

$$||\mathbf{u}-\mathbf{u}_h||_{DG} \lesssim |||\mathbf{u}-\Pi_h^r\mathbf{u}|||_{DG}.$$

Now using (1.24) we have:

$$||\mathbf{u}-\mathbf{u}_h||_{DG} \lesssim \frac{h^{\min(r+1,s)-1}}{r^{s-1/2}}||\mathbf{u}||_{\mathbf{H}^s(\mathcal{T}_h)},$$

and the proof of the first estimate is complete. The bound is optimal in h and sub-optimal in r by a factor $r^{1/2}$ (cf. [39]).
The estimate for the $\mathbf{L}^2$-error can be obtained using a duality argument and the elliptic regularity, i.e.

$$||\mathbf{u}||_{\mathbf{H}^2(\Omega)} \lesssim ||\mathbf{f}||_{\mathbf{L}^2(\Omega)}\ \forall\ \mathbf{f}\in\mathbf{L}^2(\Omega).$$

For the sake of simplicity, we will consider the case of homogeneous Dirichlet boundary conditions, i.e. $\Gamma_N=\emptyset$ and $\mathbf{g}_D=\mathbf{0}$. Thus, we denote with $\mathbf{V}$ the space $\mathbf{H}_0^1(\Omega)=\{\mathbf{v}\in\mathbf{H}^1(\Omega):\mathbf{v}=\mathbf{0}\text{ on }\partial\Omega\}$ and with $(\cdot,\cdot)_{\mathbf{L}^2(\Omega)}$ the scalar product in $\mathbf{L}^2(\Omega)$. Let $\mathbf{u}$ be the solution of Problem (1.5), i.e.

$$\text{find } \mathbf{u}\in\mathbf{V} \text{ such that: } B(\mathbf{u},\mathbf{v})=(\mathbf{f},\mathbf{v})_{\mathbf{L}^2(\Omega)} \quad \forall\ \mathbf{v}\in\mathbf{V},$$

and $\mathbf{u}_h$ the DG solution of Problem (1.15):

$$\text{find } \mathbf{u}_h\in\mathbf{V}_h^r \text{ such that: } A(\mathbf{u}_h,\mathbf{v}_h)=(\mathbf{f},\mathbf{v}_h)_{\mathbf{L}^2(\Omega)} \quad \forall\ \mathbf{v}_h\in\mathbf{V}_h^r.$$

Finally, we introduce the so-called *dual problem*: $\forall\ \mathbf{g}\in\mathbf{L}^2(\Omega)$,

$$\text{find } \boldsymbol{\phi}=\boldsymbol{\phi}(\mathbf{g})\in\mathbf{V} \text{ such that: } B(\mathbf{v},\boldsymbol{\phi})=(\mathbf{g},\mathbf{v})_{\mathbf{L}^2(\Omega)} \quad \forall\ \mathbf{v}\in\mathbf{V},$$

and analogously the *discrete dual problem*: $\forall\ \mathbf{g} \in \mathbf{L}^2(\Omega)$,

$$\text{find } \boldsymbol{\phi}_h = \boldsymbol{\phi}_h(\mathbf{g}) \in \mathbf{V}_h^r \text{ such that: } A(\mathbf{v}_h, \boldsymbol{\phi}_h) = (\mathbf{g}, \mathbf{v}_h)_{\mathbf{L}^2(\Omega)} \quad \forall\ \mathbf{v}_h \in \mathbf{V}_h^r.$$

In our case $A(\cdot,\cdot)$ is symmetric and the following *adjoint consistency* property holds:

$$A(\mathbf{v}_h, \boldsymbol{\phi}) = (\mathbf{g}, \mathbf{v}_h) \quad \forall\ \mathbf{v}_h \in \mathbf{V}_h^r. \tag{1.27}$$

It can be proved that a result of elliptic regularity also holds for the solution of the dual problem, i.e.

$$\exists\ C > 0: \quad ||\boldsymbol{\phi}(\mathbf{g})||_{\mathbf{H}^2(\Omega)} \leq C||\mathbf{g}||_{\mathbf{L}^2(\Omega)} \quad \forall\ \mathbf{g} \in \mathbf{L}^2(\Omega).$$

In particular, this is true for a polygonal and convex domain Ω.
We choose now $\mathbf{g} = \mathbf{u} - \mathbf{u}_h = \mathbf{e}_h$ as the approximation error and we denote $\boldsymbol{\phi} = \boldsymbol{\phi}(\mathbf{e}_h)$ to simplify the notation. Moreover, we choose $\mathbf{v}_h = \mathbf{e}_h$ and we use property (1.27) to get:

$$||\mathbf{e}_h||^2_{\mathbf{L}^2(\Omega)} = A(\mathbf{e}_h, \boldsymbol{\phi}).$$

For the elliptic regularity of the dual problem, we also know that $\boldsymbol{\phi} \in \mathbf{H}^2(\Omega)$ and $||\boldsymbol{\phi}||_{\mathbf{H}^2(\Omega)} \leq C||\mathbf{e}_h||_{\mathbf{L}^2(\Omega)}$. Now thanks to the Galerkin orthogonality (cf. Lemma 4), we know that $A(\mathbf{e}_h, \Pi_h^r\boldsymbol{\phi}) = 0$ and we can write:

$$\begin{aligned}
||\mathbf{e}_h||^2_{\mathbf{L}^2(\Omega)} = A(\mathbf{e}_h, \boldsymbol{\phi}) &= A(\mathbf{e}_h, \boldsymbol{\phi} - \Pi_h^r\boldsymbol{\phi}) \\
&\leq C_1|||\mathbf{e}_h|||_{DG}|||\boldsymbol{\phi} - \Pi_h^r\boldsymbol{\phi}|||_{DG} \quad (\text{ Continuity of } A(\cdot,\cdot) \text{ in } \widetilde{\mathbf{V}}_h^r) \\
&\leq C_2|||\mathbf{e}_h|||_{DG}\ \frac{h}{r^{\frac{3}{2}}}||\boldsymbol{\phi}||_{\mathbf{H}^2(\Omega)} \quad (\text{ Estimate (1.24) with } s = 2) \\
\leq C_3|||\mathbf{e}_h|||_{DG}\ \frac{h}{r^{\frac{3}{2}}}||\mathbf{e}_h||_{\mathbf{L}^2(\Omega)} &\quad (\text{ Elliptic regularity of the dual problem }).
\end{aligned}$$

Note that, when applying the estimate (1.24), the broken norm $\mathbf{H}^2(\mathcal{T}_h)$ that is the sum of the norms in each triangle of the mesh, becomes the usual $\mathbf{H}^2$ norm on the whole domain Ω, thanks to the additivity of the integrals. Thus, we get the following bound:

$$||\mathbf{e}_h||_{\mathbf{L}^2(\Omega)} \leq C_3\ \frac{h}{r^{\frac{3}{2}}}|||\mathbf{e}_h|||_{DG},$$

and the thesis follows applying the energy norm error estimate in (1.25). □

1.2.6 Algebraic formulation

Following the usual argument, to ease the notation we assume $r_{\mathcal{K}} = r \geq 1 \; \forall \; \mathcal{K} \in \mathcal{T}_h$ and we partition the domain Ω in M triangles and we multiply this number by the dimension of the space of polynomials of degree r to obtain the total number N of degrees of freedom: $N = M\frac{1}{2}(r+1)(r+2)$, see Figure 1.3.

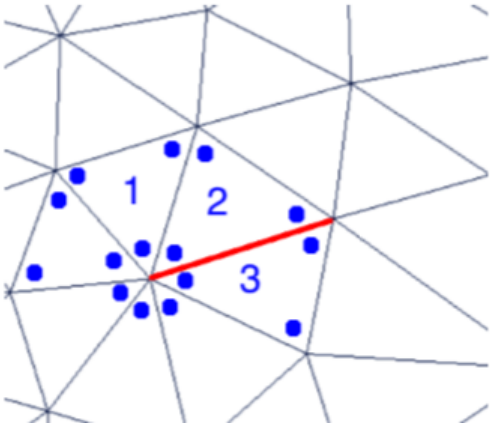

Figure 1.3: Degrees of freedom on a triangular mesh.

We introduce a basis $\{(\Phi_i^1, \Phi_i^2)\}$, $i = 1, ..., N$, for the finite element space $\mathbf{V}_h^r$ and we express the solution $\mathbf{u}_h$ as a linear combination of the shape functions:

$$\mathbf{u}_h(\mathbf{x}) = \sum_{i=1}^{N} (U_i^1 \Phi_i^1(\mathbf{x}) + U_i^2 \Phi_i^2(\mathbf{x})).$$

Here $\mathbf{U} = (U_1^1, U_2^1, ..., U_N^1, U_1^2, U_2^2, ..., U_N^2)$ is the vector of suitable coefficients which constitute the solution of the linear system associated to our problem:

$$A\mathbf{U} = \mathbf{F}. \tag{1.28}$$

This system derives from the variational formulation (1.15), substituting the generic test function $\mathbf{v}_h$ with the basis functions $\{(\Phi_i^1, \Phi_i^2)\} \in \mathbf{V}_h^r$ for $i = 1, ..., N$. It results that the matrix A can be written as the sum of four matrices associated to the four integrals in the bilinear form (1.13), i.e.:

$$A = V - I - I^T + S,$$

with

$$V_{i,j} = \int_\Omega \underline{\sigma}(\Phi_j) : \underline{\epsilon}(\Phi_i) \; \mathrm{d}\mathbf{x}, \qquad \text{for } i, j = 1, ...2N;$$

$$I_{i,j} = \int_{\mathcal{F}_I \cup \mathcal{F}_D} \{\underline{\sigma}(\Phi_j)\} : [\![\Phi_i]\!] \, \mathrm{d}\mathbf{s}, \qquad \text{for } i,j = 1,...2N;$$

$$S_{i,j} = \int_{\mathcal{F}_I \cup \mathcal{F}_D} \eta [\![\Phi_j]\!] : [\![\Phi_i]\!] \, \mathrm{d}\mathbf{s}, \qquad \text{for } i,j = 1,...2N,$$

where $\Phi_j = \Phi_j^1,\ j = 1,...N$ and $\Phi_j = \Phi_j^2,\ j = N+1,...2N$.
Analogously, the vector $\mathbf{F}$ on the right hand side of the system (1.28) arises from the functional (1.14), substituting the test function $\mathbf{v}_h$ with the basis of $\mathbf{V}_h^r$, so that:

$$\mathbf{F}_i = \int_\Omega \mathbf{f} \cdot \Phi_i \mathrm{d}\mathbf{x} - \int_{\mathcal{F}_D} \mathbf{g}_D \cdot (\underline{\sigma}(\Phi_i) \cdot \mathbf{n} - \eta \Phi_i) \, \mathrm{d}\mathbf{s} + \int_{\mathcal{F}_N} \mathbf{g}_N \cdot \Phi_i \, \mathrm{d}\mathbf{s}, \quad \text{for } i = 1,..,2N.$$

Note that we can also write the linear system (1.28) highlighting each component of the solution field, namely:

$$\begin{pmatrix} A^1 & A^2 \\ \\ A^3 & A^4 \end{pmatrix} \begin{pmatrix} \mathbf{U}^1 \\ \\ \mathbf{U}^2 \end{pmatrix} = \begin{pmatrix} \mathbf{F}^1 \\ \\ \mathbf{F}^2 \end{pmatrix} \tag{1.29}$$

where each block of the matrix can be decomposed in the following way:

$$A^l = V^l - I^l - (I^l)^T + S^l, \quad \text{for } l = 1,..,4.$$

Now, let us analyze in details which integral every block matrix represents, in order to describe the implementation of the code for the Discontinuous Galerkin scheme.

As seen before, the integral related to the matrix V is defined as: for $i,j = 1,...,N$

$$V_{i,j}^1 = \int_\Omega \Big((\lambda + 2\mu) \frac{\partial \Phi_j^1}{\partial x} \frac{\partial \Phi_i^1}{\partial x} + \mu \frac{\partial \Phi_j^1}{\partial y} \frac{\partial \Phi_i^1}{\partial y} \Big) \, \mathrm{d}\mathbf{x},$$

$$V_{i,j}^2 = \int_\Omega \Big(\lambda \frac{\partial \Phi_j^2}{\partial y} \frac{\partial \Phi_i^1}{\partial x} + \mu \frac{\partial \Phi_j^2}{\partial x} \frac{\partial \Phi_i^1}{\partial y} \Big) \, \mathrm{d}\mathbf{x},$$

$$V_{i,j}^3 = \int_\Omega \Big(\mu \frac{\partial \Phi_j^1}{\partial y} \frac{\partial \Phi_i^2}{\partial x} + \lambda \frac{\partial \Phi_j^1}{\partial x} \frac{\partial \Phi_i^2}{\partial y} \Big) \, \mathrm{d}\mathbf{x},$$

$$V_{i,j}^4 = \int_\Omega \Big((\lambda + 2\mu) \frac{\partial \Phi_j^2}{\partial y} \frac{\partial \Phi_i^2}{\partial y} + \mu \frac{\partial \Phi_j^2}{\partial x} \frac{\partial \Phi_i^2}{\partial x} \Big) \, \mathrm{d}\mathbf{x}.$$

Observe that, for the matrix I and S, we need a slightly different argument, because we want to discretize integrals over edges. This means that we have to differentiate the integrals according to the fact that we are considering an internal or a border edge.
For $i, j = 1, ..., N$ it holds that:

$$S^1_{i,j} = \sum_{\gamma \in \mathcal{F}_I \cup \mathcal{F}_D} \int_\gamma \Phi^{1,+}_j \Phi^{1,+}_i \, \mathrm{d}\mathbf{s}, \qquad S^2_{i,j} = S^3_{i,j} = 0, \qquad S^4_{i,j} = \sum_{\gamma \in \mathcal{F}_I \cup \mathcal{F}_D} \int_\gamma \Phi^{2,+}_j \Phi^{2,+}_i \, \mathrm{d}\mathbf{s},$$

and

$$I^1_{i,j} = \sum_{\gamma \in \mathcal{F}_I \cup \mathcal{F}_D} \delta_\gamma \Big(\frac{1}{2}(\lambda + 2\mu)\, n^+_1 \int_\gamma \frac{\partial \Phi^{1,+}_j}{\partial x} \Phi^{1,+}_i \, \mathrm{d}\mathbf{s} \; + \; \frac{1}{2}\mu \, n^+_2 \int_\gamma \frac{\partial \Phi^{1,+}_j}{\partial y} \Phi^{1,+}_i \, \mathrm{d}\mathbf{s} \Big),$$

$$I^2_{i,j} = \sum_{\gamma \in \mathcal{F}_I \cup \mathcal{F}_D} \delta_\gamma \Big(\frac{1}{2}\lambda \, n^+_1 \int_\gamma \frac{\partial \Phi^{2,+}_j}{\partial y} \Phi^{1,+}_i \, \mathrm{d}\mathbf{s} \; + \; \frac{1}{2}\mu \, n^+_2 \int_\gamma \frac{\partial \Phi^{2,+}_j}{\partial x} \Phi^{1,+}_i \, \mathrm{d}\mathbf{s} \Big),$$

$$I^3_{i,j} = \sum_{\gamma \in \mathcal{F}_I \cup \mathcal{F}_D} \delta_\gamma \Big(\frac{1}{2}\mu \, n^+_1 \int_\gamma \frac{\partial \Phi^{1,+}_j}{\partial y} \Phi^{2,+}_i \, \mathrm{d}\mathbf{s} \; + \; \frac{1}{2}\lambda \, n^+_2 \int_\gamma \frac{\partial \Phi^{1,+}_j}{\partial x} \Phi^{2,+}_i \, \mathrm{d}\mathbf{s} \Big),$$

$$I^4_{i,j} = \sum_{\gamma \in \mathcal{F}_I \cup \mathcal{F}_D} \delta_\gamma \Big(\frac{1}{2}\mu \, n^+_1 \int_\gamma \frac{\partial \Phi^{2,+}_j}{\partial x} \Phi^{2,+}_i \, \mathrm{d}\mathbf{s} \; + \; \frac{1}{2}(\lambda + 2\mu)\, n^+_2 \int_\gamma \frac{\partial \Phi^{2,+}_j}{\partial y} \Phi^{2,+}_i \, \mathrm{d}\mathbf{s} \Big)$$

where $\delta_\gamma = 1, 2$, depending on whether γ is an interior or boundary edge, respectively, and $\mathbf{n}^+ = (n^+_1, n^+_2)^T$ is the unit outward normal of the element $\mathcal{K}^+$.

Next, we consider the case where γ is an internal edge, meaning that there exists a neighbouring element of $\mathcal{K}^+$ (we can call it $\mathcal{K}^-$) such that $\bar{\gamma} = \partial\overline{\mathcal{K}}^+ \cap \partial\overline{\mathcal{K}}^-$.
For these cases, there are some further contributions to add:

$$S^1_{i,j} = \int_\gamma \Phi^{1,-}_j \Phi^{1,+}_i \, \mathrm{d}\mathbf{s}, \qquad S^2_{i,j} = S^3_{i,j} = 0, \qquad S^4_{i,j} = \int_\gamma \Phi^{2,-}_j \Phi^{2,+}_i \, \mathrm{d}\mathbf{s}$$

and

$$I^1_{i,j} = \; \frac{1}{2}(\lambda + 2\mu)\, n_1 \int_\gamma \frac{\partial \Phi^{1,-}_j}{\partial x} \Phi^{1,+}_i \, \mathrm{d}\mathbf{s} \; + \; \frac{1}{2}\mu \, n_2 \int_\gamma \frac{\partial \Phi^{1,-}_j}{\partial y} \Phi^{1,+}_i \, \mathrm{d}\mathbf{s},$$

$$I^2_{i,j} = \frac{1}{2}\lambda\ n_1 \int_\gamma \frac{\partial \Phi^{2,-}_j}{\partial y}\Phi^{1,+}_i\ \mathrm{ds}\ +\ \frac{1}{2}\mu\ n_2 \int_\gamma \frac{\partial \Phi^{2,-}_j}{\partial x}\Phi^{1,+}_i\ \mathrm{ds},$$

$$I^3_{i,j} = \frac{1}{2}\mu\ n_1 \int_\gamma \frac{\partial \Phi^{1,-}_j}{\partial y}\Phi^{2,+}_i\ \mathrm{ds}\ +\ \frac{1}{2}\lambda\ n_2 \int_\gamma \frac{\partial \Phi^{1,-}_j}{\partial x}\Phi^{2,+}_i\ \mathrm{ds},$$

$$I^4_{i,j} = \frac{1}{2}\mu\ n_1 \int_\gamma \frac{\partial \Phi^{2,-}_j}{\partial x}\Phi^{2,+}_i\ \mathrm{ds}\ +\ \frac{1}{2}(\lambda+2\mu)\ n_2 \int_\gamma \frac{\partial \Phi^{2,-}_j}{\partial y}\Phi^{2,+}_i\ \mathrm{ds}.$$

It is important to notice that all the arguments related to the matrices S and I are not valid for edges on which we impose Neumann boundary conditions, as we can see from the bilinear form (1.13). On such edges, only the matrix V comes into play.

Finally, we remind that for non-homogeneous Dirichlet boundary conditions $\mathbf{g}_D = (g_1, g_2)^T$, we need to impose them weakly by adding extra terms to the vector of external loads as follows:

$$\mathbf{F}^1_i = \sum_{\gamma\in\mathcal{F}_D}\left\{\int_\gamma \eta\Phi^{1,+}_i g_1\ \mathrm{ds}\ -\ 2\left(\ \frac{1}{2}(\lambda+2\mu)\ n_1^+\int_\gamma \frac{\partial\Phi^{1,+}_i}{\partial x}g_1\ \mathrm{ds}\ +\frac{1}{2}\mu\ n_2^+\int_\gamma \frac{\partial\Phi^{1,+}_i}{\partial y}g_1\ \mathrm{ds}\ \right)\right.$$

$$\left.-2\sum_{\gamma\in\mathcal{F}_D}\left\{\left(\ \frac{1}{2}\mu\ n_1^+\int_\gamma \frac{\partial\Phi^{1,+}_i}{\partial y}g_2\ \mathrm{ds}\ +\ \frac{1}{2}\lambda\ n_2^+\int_\gamma \frac{\partial\Phi^{1,+}_i}{\partial x}g_2\ \mathrm{ds}\ \right)\right\},\right.$$

$$\mathbf{F}^2_i = \sum_{\gamma\in\mathcal{F}_D}\left\{\int_{\mathcal{F}_D} \eta\Phi^{2,+}_i g_2\ \mathrm{ds}\ -\ 2\left(\ \frac{1}{2}\lambda\ n_1^+\int_\gamma \frac{\partial\Phi^{2,+}_i}{\partial y}g_1\ \mathrm{ds}\ +\frac{1}{2}\mu\ n_2^+\int_\gamma \frac{\partial\Phi^{2,+}_i}{\partial x}g_1\ \mathrm{ds}\ \right)\right\}$$

$$-2\sum_{\gamma\in\mathcal{F}_D}\left\{\left(\ \frac{1}{2}\mu\ n_1^+\int_\gamma \frac{\partial\Phi^{2,+}_i}{\partial x}g_2\ \mathrm{ds}\ +\ \frac{1}{2}(\lambda+2\mu)\ n_2^+\int_\gamma \frac{\partial\Phi^{2,+}_i}{\partial y}g_2\ \mathrm{ds}\ \right)\right\},$$

for $i = 1, .., N$.

1.3 Numerical results

In this section we illustrate some numerical results for the elastostatic problem with both Dirichlet and Neumann conditions on a square domain $\Omega = (-1, 0) \times (0, 1)$ with uniform and constant Lamé parameters. For each test we report the data of the simulation, the computed errors as well as the computed convergence rates, showing that the optimal accuracy of the error is achieved, according to the theoretical bounds of Theorem 2.

1.3.1 Example 1

In the first test we choose the Lamè coefficients $\lambda = 1$ and $\mu = 0.5$ and the components of the exact solution as:

$$u_1(x, y) = e^x \cos(y),$$

$$u_2(x, y) = \sin(x) \cos(y).$$

Thus, the source term becomes:

$$f_1(x, y) = \frac{3}{2}(\cos(x) \sin(y) - e^x \cos(y)),$$

$$f_2(x, y) = \frac{5}{2} \sin(x) \cos(y) + \frac{3}{2} e^x \sin(y).$$

Notice that the manufactured solution has been chosen in $\mathbf{H}^s(\Omega)$, for any $s \geq 2$. We tested our method on a sequence of meshes with granularity $h = [0.0627, 0.0314, 0.0157]$. For this test, we have set three sides of the square domain as Neumann boundary and the remaining one as Dirichlet boundary, as in Figure 1.4.
Figure 1.6 shows the computed errors in the $\mathbf{L}^2(\Omega)$ and DG norms as a function of the mesh size h (log-log scale). Figure 1.6.a shows that, under h-refinement, the $\mathbf{L}^2(\Omega)$-norm of the error converges to zero at the optimal rate $O(h^{r+1})$, where r is the polynomial degree, here chosen as $r = 1$. Similarly, Figure 1.6.b displays that for the $\mathbf{H}^1(\Omega)$-error, the rate of convergence $O(h^r)$ is achieved.
Finally, Figure 1.5 shows the two components of the computed vector solution using the Discontinuous Galerkin method on a grid of granularity $h = 0.0157$.

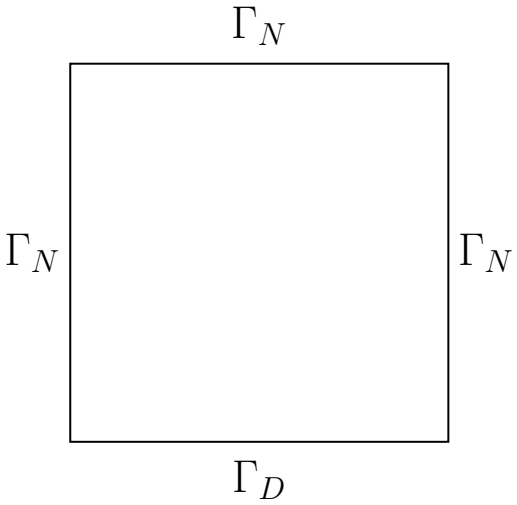

Figure 1.4: Boundary conditions on the computational domain.

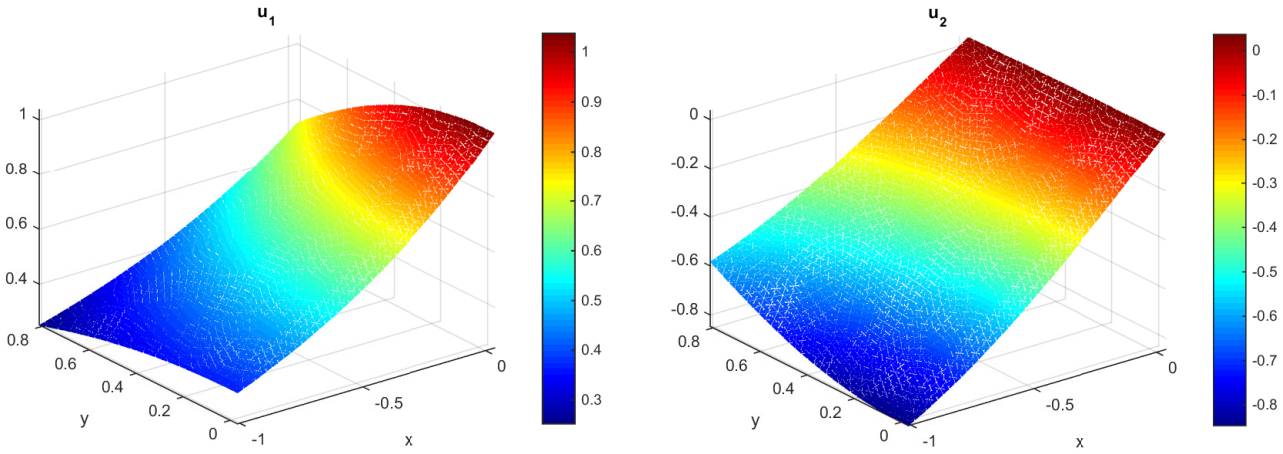

(a) First component of the solution u_1.

(b) Second component of the solution u_2.

Figure 1.5: Example 1. Plot of the computed solution on a grid with granularity $h = 0.0157$ (3 levels of refinement).

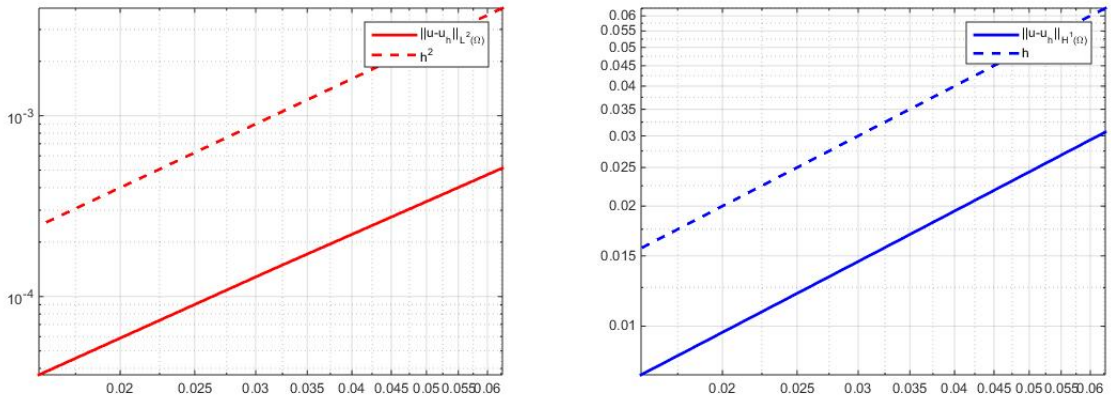

(a) Computed errors in the $\mathbf{L}_2$-norm versus the mesh size h.

(b) Computed errors in the $\mathbf{H}_1$-norm versus the mesh size h.

Figure 1.6: Example 1. Computed errors versus the mesh size h (log-log scale).

1.3.2 Example 2

In the second test we choose the Lamè coefficients $\lambda = 1$ and $\mu = 2$ and the components of the exact solution as:

$$u_1 = e^x \sin(2\pi y),$$

$$u_2 = e^y \sin(2\pi x).$$

Thus, the given source term becomes:

$$f_1 = (8\pi^2 - 5)e^x \sin(2\pi y) - 6\pi e^y \cos(2\pi x),$$

$$f_2 = (8\pi^2 - 5)e^y \sin(2\pi x) - 6\pi e^x \cos(2\pi y).$$

In this test, the exact solution has been chosen in $\mathbf{H}^s(\Omega)$, for any $s \geq 2$ and mixed boundary conditions have been used, as in the previous example. In Figure 1.7 we report the plot of the computed solution with its components, on a grid of granularity $h = 0.0157$. Again, the polynomial degree r is equal to 1, so that we achieve the optimal rate of convergence $O(h^2)$ and $O(h)$ for the $\mathbf{L}^2(\Omega)$ and the DG norm of the errors, respectively, as shown in Figure 1.8.

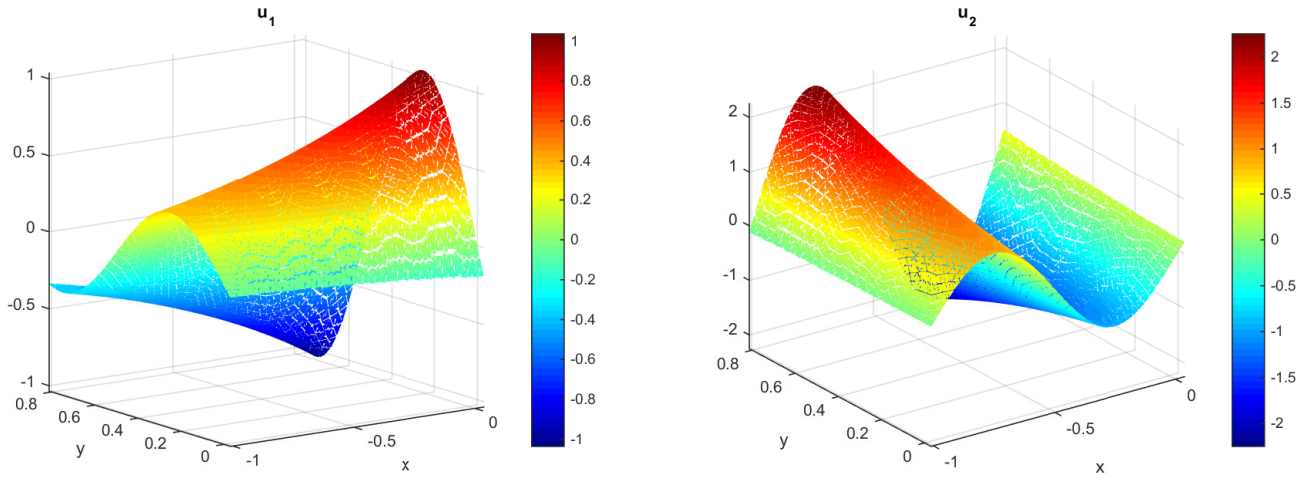

(a) First component u_1 of the solution. **(b)** Second component u_2 of the solution.

Figure 1.7: Example 2. Plot of the computed solution on a grid with granularity $h = 0.0157$ (3 levels of refinement).

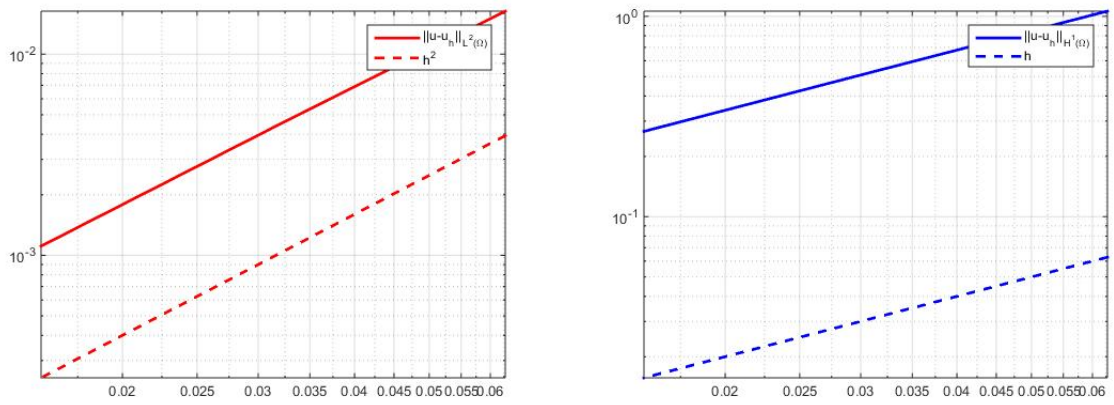

(a) Computed errors in the $\mathbf{L}_2$-norm versus the mesh size h. **(b)** Computed errors in the $\mathbf{H}_1$-norm versus the mesh size h.

Figure 1.8: Example 2. Computed errors versus the mesh size h (log-log scale).

Chapter 2

The elastostatic problem with a fault

2.1 The mathematical model

Now we focus on the case where we have a fault in an elastic medium. We consider an open bounded domain $\Omega \subset \mathbb{R}^2$, with Lipschitz boundary $\partial\Omega$ and outward normal unit vector $\mathbf{n}$. The fracture $\Gamma \subset \Omega$ is considered to be a 1-dimensional $\mathcal{C}^\infty$ manifold, i.e. $\Gamma \subset \mathbb{R}$ with $\mathbf{n}_\Gamma$ the normal unit vector and it is a straight interface. For the sake of the numerical analysis, we will consider the prolongation of Γ until the boundary of the domain, such that it divides Ω into two subdomains Ω_1 and Ω_2, as in Figure 2.1. The boundary is assumed to be composed of two portions: $\Gamma_D \neq \emptyset$, which is closed and where the displacement vector $\mathbf{u}$ is prescribed, and Γ_N where an external load applies.
Our goal is to find the medium displacement $\mathbf{u} : \Omega \to \mathbb{R}^2$ such that:

$$\begin{aligned} -\nabla \cdot \underline{\sigma}(\mathbf{u}) &= \mathbf{f} \quad \text{in } \Omega \setminus \overline{\Gamma}, \\ \underline{\sigma}(\mathbf{u}) - \mathbf{D}\underline{\epsilon}(\mathbf{u}) &= \mathbf{0} \quad \text{in } \Omega \setminus \overline{\Gamma}, \\ \mathbf{u} &= \mathbf{g}_D \quad \text{on } \Gamma_D, \\ \underline{\sigma}(\mathbf{u})\mathbf{n} &= \mathbf{g}_N \quad \text{on } \Gamma_N, \\ [\![\mathbf{u}]\!] &= \mathbf{q}_0 \otimes \mathbf{n}_\Gamma^+ \quad \text{on } \Gamma, \\ [\![\underline{\sigma}(\mathbf{u})]\!] &= \mathbf{q}_1 \quad \text{on } \Gamma, \end{aligned} \tag{2.1}$$

where $\mathbf{f} \in \mathbf{L}^2(\Omega)$ is a given source term, $\mathbf{g}_D \in \mathbf{H}^{\frac{1}{2}}(\Gamma_D)$, $\mathbf{g}_N \in \mathbf{H}^{-\frac{1}{2}}(\Gamma_N)$, $\mathbf{q}_0 \in \mathbf{H}^{\frac{1}{2}}(\Gamma)$ and $\mathbf{q}_1 \in \mathbf{H}^{-\frac{1}{2}}(\Gamma)$. The strain tensor $\underline{\epsilon}$ and the stress tensor $\underline{\sigma}$ are defined as in (1.2) and (1.3)

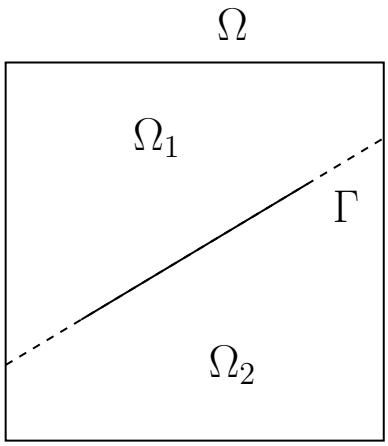

Figure 2.1: The subdomains Ω_1 and Ω_2 separated by the interface Γ.

and we employed the definition of the jump operator as in (1.7).

From an analytical point of view, we have different results of well-posedness based on the regularity of the slip field $\mathbf{q}_0$, as showed in [40] and [41]. In all the cases, it is assumed that the traction is continuous along the fault, i.e. $\mathbf{q}_1 = 0$.

We know by [41] that there exists a unique distributional solution $\mathbf{u} \in \mathbf{H}^{\frac{1}{2}-\epsilon}(\Omega) \cap \mathbf{H}^s(\Omega \setminus \overline{\Gamma})$ of the boundary-value/transmission problem (2.1), for $\epsilon > 0$ and $s < 1$.

The second result is obtained by assuming that the dislocation surface Γ can be extended to a closed Lipschitz, orientable surface S and that $\mathbf{q}_0 \in \mathbf{H}^{\frac{1}{2}}_{00}(\Gamma)$, meaning that $\mathbf{q}_0$ can be extended by zero in $S \setminus \Gamma$ to a function $\tilde{\mathbf{q}}_0 \in \mathbf{H}^{\frac{1}{2}}(S)$:

$$\tilde{\mathbf{q}}_0(\mathbf{x}) = \begin{cases} \mathbf{q}_0(\mathbf{x}), & \text{if } \mathbf{x} \in \Gamma, \\ \mathbf{0}, & \text{if } \mathbf{x} \in S \setminus \Gamma. \end{cases} \tag{2.2}$$

Without loss of generality, we suppose homogeneous Dirichlet boundary condition, i.e. $\mathbf{g}_D = \mathbf{0}$. With all these assumptions, the authors in [42] were able to prove that there exists a unique weak solution $\mathbf{u} \in \mathbf{H}^1_{0,\Gamma_D}(\Omega \setminus \overline{\Gamma})$ to Problem (2.1).

2.2 The Discontinuous Galerkin formulation

In order to derive a DG formulation for the problem with a crack inside the elastic medium, we consider Ω to be a bounded convex polyhedral domain in $\mathbb{R}^2$ and we assume

that $\mathbf{D}$ is symmetric, strictly convex and uniformly bounded over Ω, as in (1.4), and piecewise constant over mesh-elements. Moreover, we require a regular enough slip field $\mathbf{q}_0$ to have the solution $\mathbf{u} \in \mathbf{H}^s(\mathcal{T}_h) \cap \mathbf{H}^2(\Omega \setminus \overline{\Gamma})$, for some $s \geq 2$.
Without loss of generality, we suppose throughout the whole analysis homogeneous Dirichlet and Neumann conditions, i.e. $\mathbf{g}_D = \mathbf{0}$ and $\mathbf{g}_N = \mathbf{0}$. We also assume that the traction is continuous along the fault Γ, i.e. $\mathbf{q}_1 = 0$.
As before, we consider a quasi-uniform triangulation, i.e. $\max_{\mathcal{K}\in\mathcal{T}_h} h_k \lesssim \min_{\mathcal{K}\in\mathcal{T}_h} h_k$, where h_k denotes the diameter of each triangle and we assume that the grid is aligned with Γ. As a result, we can construct a one-dimensional discretization of Γ containing only those vertices of the triangles $\mathcal{K} \in \mathcal{T}_h$ that lie on the interface; the same procedure is applied to generate the discretization of the boundary $\partial\Omega = \Gamma_D \cup \Gamma_N$. Note that, for the analysis of the discrete formulation, we will consider the prolongation of Γ until the boundary of the domain $\partial\Omega$ as in the dashed line of Figure 2.1. We collect the interior faces γ in $\mathcal{F}_I$ and the Dirichlet and Neumann boundaries γ in $\mathcal{F}_\mathcal{D}$ and $\mathcal{F}_N$, respectively, as in Chapter 1. Note that, for the sake of the analysis, we will not consider the faces on Γ belonging to $\mathcal{F}_I$.
Given all the aforementioned assumptions, we can now proceed to formulate a new DG scheme for the interface problem. The aim is to add again null terms in the bilinear form $A(\cdot,\cdot)$, defined in (1.15), but separating the integrals along a generic interior face $\gamma \in \mathcal{F}_I$ and the ones that lay on the crack Γ, on which $(\llbracket \mathbf{u} \rrbracket - \mathbf{q}_0 \otimes \mathbf{n}^+) = 0$.

What results is the following approximate problem: find $\mathbf{u}_h \in \mathbf{V}_h^r$ such that

$$\mathcal{A}(\mathbf{u}_h, \mathbf{v}_h) = \mathcal{F}(\mathbf{v}_h) \qquad \forall\ \mathbf{v}_h \in V_h^r, \tag{2.3}$$

where:

$$\mathcal{A}(\mathbf{u},\mathbf{v}) = \sum_{\mathcal{K}\in\mathcal{T}_h} \int_\mathcal{K} \underline{\sigma}(\mathbf{u}) : \underline{\epsilon}(\mathbf{v})\ \mathrm{d}\mathbf{x} - \sum_{\gamma\in\mathcal{F}_I\cup\mathcal{F}_D\cup\Gamma} \int_\gamma \{\underline{\sigma}(\mathbf{u})\} : \llbracket \mathbf{v} \rrbracket\ \mathrm{d}\mathbf{s}$$
$$- \sum_{\gamma\in\mathcal{F}_I\cup\mathcal{F}_D\cup\Gamma} \int_\gamma \llbracket \mathbf{u} \rrbracket : \{\underline{\sigma}(\mathbf{v})\}\ \mathrm{d}\mathbf{s} + \sum_{\gamma\in\mathcal{F}_I\cup\mathcal{F}_D\cup\Gamma} \int_\gamma \eta \llbracket \mathbf{u} \rrbracket : \llbracket \mathbf{v} \rrbracket\ \mathrm{d}\mathbf{s},$$

$$\mathcal{F}(\mathbf{v}) = \sum_{\mathcal{K}\in\mathcal{T}_h} \int_\mathcal{K} \mathbf{f}\cdot\mathbf{v}\ \mathrm{d}\mathbf{x} - \sum_{\gamma\in\Gamma} \int_\gamma \mathbf{q}_0 \otimes \mathbf{n}^+ : \{\underline{\sigma}(\mathbf{v})\}\ \mathrm{d}\mathbf{s} + \sum_{\gamma\in\Gamma} \int_\gamma \eta\ \mathbf{q}_0 \otimes \mathbf{n}^+ : \llbracket \mathbf{v} \rrbracket\ \mathrm{d}\mathbf{s},$$

and the *penalization* parameter η is defined as in (1.12).
When we have non-homogeneous boundary conditions, the bilinear form does not change

and the linear functional becomes:

$$\mathcal{F}(\mathbf{v}) = \sum_{\mathcal{K}\in\mathcal{T}_h}\int_{\mathcal{K}}\mathbf{f}\cdot\mathbf{v}\ \mathrm{d}\mathbf{x} - \sum_{\gamma\in\mathcal{F}_D}\int_\gamma \mathbf{g}_D\cdot(\underline{\sigma}(\mathbf{v})\cdot\mathbf{n}-\eta\mathbf{v})\ \mathrm{d}\mathbf{s}\ \ + \sum_{\gamma\in\mathcal{F}_N}\langle\mathbf{g}_N,\mathbf{v}\rangle_\gamma$$

$$-\sum_{\gamma\in\Gamma}\int_\gamma \mathbf{q}_0\otimes\mathbf{n}^+ : \{\underline{\sigma}(\mathbf{v})\}\ \mathrm{d}\mathbf{s} + \sum_{\gamma\in\Gamma}\int_\gamma \eta\ \mathbf{q}_0\otimes\mathbf{n}^+ : [\![\mathbf{v}]\!]\ \mathrm{d}\mathbf{s}.$$

Observe that the bilinear form is consistent with (1.15): $\mathcal{A}(\cdot,\cdot) = A(\cdot,\cdot)$ if $\Gamma = \emptyset$, i.e. no interface is present. The interface conditions, that correspond to the last two equations in (2.1), appear in the right-hand side of the new scheme. In particular, the two terms on the *rhs* read as:

$$-\sum_{\gamma\in\Gamma}\int_\gamma \mathbf{q}_0\otimes\mathbf{n}^+ : \{\underline{\sigma}(\mathbf{v})\}\ \mathrm{d}\mathbf{s} + \sum_{\gamma\in\Gamma}\int_\gamma \eta\ \mathbf{q}_0\otimes\mathbf{n}^+ : [\![\mathbf{v}]\!]\ \mathrm{d}\mathbf{s},$$

need to compensate the following terms on the *lhs*:

$$-\sum_{\gamma\in\Gamma}\int_\gamma [\![\mathbf{u}]\!] : \{\underline{\sigma}(\mathbf{v})\}\ \mathrm{d}\mathbf{s} + \sum_{\gamma\in\Gamma}\int_\gamma \eta[\![\mathbf{u}]\!] : [\![\mathbf{v}]\!]\ \mathrm{d}\mathbf{s},$$

which is no longer zero over Γ as in problem (1.1).
At the algebraic level, we will only need to modify the right hand side of the linear system, adding the new terms. Using the notation of Section 1.2.6, we get:

$$\mathbf{F}_i = \int_\Omega \mathbf{f}\cdot\Phi_i \mathrm{d}\mathbf{x} - \int_\Gamma \mathbf{q}_0\cdot(\underline{\sigma}(\Phi_i)\cdot\mathbf{n}-\eta\Phi_i)\ \mathrm{d}\mathbf{s}, \quad \text{for } i = 1,..,2N,$$

or, equivalently, for $\mathbf{q}_0 = (q_{0x}, q_{0y})^T$ and $i = 1,..,N$:

$$\mathbf{F}_i^1 = \sum_{\gamma\in\Gamma}\left\{\int_\gamma \eta\Phi_i^{1,+}q_{0x}\ \mathrm{d}\mathbf{s}\ -\ \left(\ \frac{1}{2}(\lambda+2\mu)\ n_1^+\int_\gamma\frac{\partial\Phi_i^{1,+}}{\partial x}q_{0x}\ \mathrm{d}\mathbf{s}\ +\frac{1}{2}\mu\ n_2^+\int_\gamma\frac{\partial\Phi_i^{1,+}}{\partial y}q_{0x}\ \mathrm{d}\mathbf{s}\ \right)\right\}$$

$$-\sum_{\gamma\in\Gamma}\left\{\left(\ \frac{1}{2}\mu\ n_1^+\int_\gamma\frac{\partial\Phi_i^{1,+}}{\partial y}q_{0y}\ \mathrm{d}\mathbf{s}\ +\ \frac{1}{2}\lambda\ n_2^+\int_\gamma\frac{\partial\Phi_i^{1,+}}{\partial x}q_{0y}\ \mathrm{d}\mathbf{s}\ \right)\right\},$$

$$\mathbf{F}_i^2 = \sum_{\gamma\in\Gamma}\left\{\int_\gamma \eta\Phi_i^{2,+}q_{0y}\ \mathrm{d}\mathbf{s}\ -\ \left(\ \frac{1}{2}\lambda\ n_1^+\int_\gamma\frac{\partial\Phi_i^{2,+}}{\partial y}q_{0x}\ \mathrm{d}\mathbf{s}\ +\frac{1}{2}\mu\ n_2^+\int_\gamma\frac{\partial\Phi_i^{2,+}}{\partial x}q_{0x}\ \mathrm{d}\mathbf{s}\ \right)\right\}$$

$$-\sum_{\gamma\in\Gamma}\left\{\left(\ \frac{1}{2}\mu\ n_1^+\int_\gamma\frac{\partial\Phi_i^{2,+}}{\partial x}q_{0y}\ \mathrm{d}\mathbf{s}\ +\ \frac{1}{2}(\lambda+2\mu)\ n_2^+\int_\gamma\frac{\partial\Phi_i^{2,+}}{\partial y}q_{0y}\ \mathrm{d}\mathbf{s}\ \right)\right\}.$$

2.2.1 Well-posedness and error analysis

For the sake of the analysis, we write Problem (2.3) in the following equivalent form: find $\mathbf{u}_h \in \mathbf{V}_h^r$

$$\tilde{\mathcal{A}}(\mathbf{u}_h, \mathbf{v}_h) = \mathcal{F}(\mathbf{v}_h) \quad \forall\ \mathbf{v}_h \in \mathbf{V}_h^r, \tag{2.4}$$

where

$$\tilde{\mathcal{A}}(\mathbf{u}, \mathbf{v}) = \sum_{\mathcal{K}\in\mathcal{T}_h} \int_{\mathcal{K}} \underline{\sigma}(\mathbf{u}) : \underline{\epsilon}(\mathbf{v})\ \mathrm{d}\mathbf{x} + \int_\Omega \underline{\sigma}(\mathbf{u}) : \mathcal{R}(\llbracket \mathbf{v} \rrbracket)\ \mathrm{d}\mathbf{x}$$

$$+ \int_\Omega \mathcal{R}(\llbracket \mathbf{u} \rrbracket) : \underline{\sigma}(\mathbf{v})\ \mathrm{d}\mathbf{x} + \sum_{\gamma\in\mathcal{F}_I\cup\mathcal{F}_D\cup\Gamma} \int_\gamma \eta \llbracket \mathbf{u} \rrbracket : \llbracket \mathbf{v} \rrbracket\ \mathrm{d}\mathbf{s}, \quad \forall\ \mathbf{u}, \mathbf{v} \in \mathbf{V}_h^r.$$

Here $\mathcal{R}(\cdot) : \mathcal{L}^2(\mathcal{F}_I \cup \mathcal{F}_D) \to \mathcal{V}_h^r$ is the *lifting operator* of the traces of 2×2 symmetric tensors defined as:

$$\int_\Omega \mathcal{R}(\llbracket \mathbf{w} \rrbracket) : \underline{\sigma}(\mathbf{v})\ \mathrm{d}\mathbf{x} = -\sum_{\gamma\in\mathcal{F}_I\cup\mathcal{F}_D\cup\Gamma} \int_\gamma \llbracket \mathbf{w} \rrbracket : \{\underline{\sigma}(\mathbf{v})\}\ \mathrm{d}\mathbf{s} \quad \forall\ \mathbf{v} \in \mathbf{V}_h^r. \tag{2.5}$$

Note that, despite formulations (2.3) and (2.4) are equivalent at the discrete level, formulation (2.4) is not strongly consistent with the continuous problem due to the discrete nature of the lifting operator (2.5).

We define the space $\widetilde{\mathbf{V}}_h^r = \mathbf{V}_h^r + \mathbf{H}^1(\mathcal{T}_h)$ and endow it with the following DG norm:

$$||\mathbf{v}||_{DG} = \sum_{\mathcal{K}\in\mathcal{T}_h} ||\mathbf{D}^{\frac{1}{2}} \underline{\epsilon}(\mathbf{v})||^2_{\mathcal{L}^2(\mathcal{K})} + \sum_{\gamma\in\mathcal{F}_I\cup\mathcal{F}_D\cup\Gamma} ||\eta^{\frac{1}{2}} \llbracket \mathbf{v} \rrbracket||^2_{\mathcal{L}^2(\gamma)} \quad \forall\ \mathbf{v} \in \widetilde{\mathbf{V}}_h^r. \tag{2.6}$$

We next show the following result and refer to [43] for its proof.

Lemma 6. *[43] For any $\boldsymbol{v} \in \widetilde{\boldsymbol{V}}_h^r$ it holds:*

$$||\mathcal{R}(\llbracket \boldsymbol{v} \rrbracket)||^2_{\mathcal{L}^2(\Omega)} \lesssim \frac{1}{\alpha} \sum_{\gamma\in\mathcal{F}_I\cup\mathcal{F}_D\cup\Gamma} ||\eta^{\frac{1}{2}} \llbracket \boldsymbol{v} \rrbracket||^2_{\mathcal{L}^2(\gamma)},$$

where α is the constant appearing in the definition of the penalty function, cf. (1.12).

The well-posedness of the DG formulation (2.4) is established in the following Lemma.

Lemma 7. *(Well-posedness). Problem* (2.4) *admits a unique solution, provided that the stabilization parameter α in* (1.12) *is chosen large enough. Moreover, the semi-discrete*

approximation depends continuously on the data, i.e.

$$||\boldsymbol{u}||_{DG} \lesssim ||\boldsymbol{f}||_{\boldsymbol{L}^2(\Omega)} + ||\boldsymbol{g}_0||_{\boldsymbol{L}^2(\Gamma)}.$$

Proof. Using the standard arguments together with Lemma 6, it can be easily proved that:

$$\tilde{\mathcal{A}}(\mathbf{v},\mathbf{v}) \gtrsim ||\mathbf{v}||^2_{DG},$$

$$\tilde{\mathcal{A}}(\mathbf{v},\mathbf{w}) \lesssim ||\mathbf{v}||_{DG}||\mathbf{w}||_{DG},$$

for all $\mathbf{v},\mathbf{w} \in \widetilde{\mathbf{V}}_h^r$. Thus, the bilinear form $\tilde{\mathcal{A}}$ is continuous and coercive in the space $\widetilde{\mathbf{V}}_h^r$. We are left to show that the functional $\mathcal{F}(\cdot)$ is also continuous in $\widetilde{\mathbf{V}}_h^r$ and then we can employ Lax-Milgram Lemma (see [23]). To this aim by the Cauchy-Schwarz inequality we get:

$$|\mathcal{F}(\mathbf{v})| \leq \left|\sum_{\mathcal{K}\in\mathcal{T}_h}\int_{\mathcal{K}} \mathbf{f}\cdot\mathbf{v}\ \mathrm{d}\mathbf{x}\right| + \left|\sum_{\gamma\in\Gamma}\int_{\gamma} \mathbf{q}_0\otimes\mathbf{n}^+ : \{\underline{\sigma}(\mathbf{v})\}\ \mathrm{d}\mathbf{s}\right| + \left|\sum_{\gamma\in\Gamma}\int_{\gamma} \eta\ \mathbf{q}_0\otimes\mathbf{n}^+ : [\![\mathbf{v}]\!]\ \mathrm{d}\mathbf{s}\right|.$$

We analyze the three terms separately and we use the regularity required for $\mathbf{f}$ and $\mathbf{q}_0$:

$$(I) \leq \left(\sum_{\mathcal{K}\in\mathcal{T}_h} ||\mathbf{f}||^2_{\mathbf{L}^2(\mathcal{K})}\right)^{1/2}\left(\sum_{\mathcal{K}\in\mathcal{T}_h} ||\mathbf{v}||^2_{\mathbf{L}^2(\mathcal{K})}\right)^{1/2} \lesssim ||\mathbf{f}||_{\mathbf{L}^2(\Omega)}\left(\sum_{\mathcal{K}\in\mathcal{T}_h} ||\underline{\epsilon}(\mathbf{v})||^2_{\mathcal{L}^2(\mathcal{K})}\right)^{1/2}$$

$$\lesssim ||\mathbf{f}||_{\mathbf{L}^2(\Omega)}||\mathbf{v}||_{DG},$$

where we have used Poincaré inequality for piecewise functions in $\mathbf{H}^1$, cf. [32], together with Korn's inequality:

For the second term we use the trace inequality (cf. [19]) and we obtain:

$$(II) = \left|\sum_{\gamma\in\Gamma}\int_{\gamma} \mathbf{q}_0\otimes\mathbf{n}^+ : \{\underline{\sigma}(\mathbf{v})\}\ \mathrm{d}\mathbf{s}\ \right| \leq \left(\sum_{\gamma\in\Gamma} ||\mathbf{q}_0\otimes\mathbf{n}^+||^2_{\mathcal{L}^2(\gamma)}\right)^{1/2}\left(\sum_{\gamma\in\Gamma} ||\{\underline{\sigma}(\mathbf{v})\}||^2_{\mathcal{L}^2(\gamma)}\right)^{1/2}$$

$$\leq \left(\sum_{\gamma\in\Gamma} ||\mathbf{q}_0\otimes\mathbf{n}^+||^2_{\mathcal{L}^2(\gamma)}\right)^{1/2}\left(\sum_{\mathcal{K}\in\mathcal{T}_h} ||\mathbf{D}\underline{\epsilon}(\mathbf{v})||^2_{\mathcal{L}^2(\mathcal{K}^+\cup\mathcal{K}^-)}\right)^{1/2}$$

$$\leq ||\mathbf{q}_0\otimes\mathbf{n}^+\ ||_{\mathcal{L}^2(\Gamma)}\ ||\mathbf{D}\underline{\epsilon}(\mathbf{v})\ ||_{\mathcal{L}^2(\mathcal{T}_h)}\ \lesssim ||\mathbf{v}||_{DG}.$$

Finally, we estimate the third term with:

$$(III) \leq \left(\sum_{\gamma \in \Gamma} ||\mathbf{q}_0 \otimes \mathbf{n}^+ ||^2_{\mathcal{L}^2(\gamma)} \right)^{1/2} \left(\sum_{\gamma \in \Gamma} ||\eta^{1/2} [\![\mathbf{v}]\!] ||^2_{\mathcal{L}^2(\gamma)} \right)^{1/2} =$$

$$= ||\mathbf{q}_0 \otimes \mathbf{n}^+ ||_{\mathcal{L}^2(\Gamma)} \, ||\eta^{1/2} [\![\mathbf{v}]\!] ||_{\mathcal{L}^2(\Gamma)} \lesssim ||\mathbf{v}||_{DG}.$$

Summing up over three bounds, the proof is complete.

□

It is easy to see that, since the exact solution $\mathbf{u}$ of Problem (2.1) belongs to $\mathbf{H}^2(\Omega \setminus \overline{\Gamma})$, it satisfies:

$$\mathcal{A}(\mathbf{u}, \mathbf{v}_h) = \mathcal{F}(\mathbf{v}_h) \quad \forall \ \mathbf{v}_h \in \mathbf{V}_h^r,$$

so formulation (2.3) is strongly-consistent. On the other hand, formulation (2.4) is not strongly-consistent, so we have to deal with the consistency error and introduce the residual bilinear form, before stating an error bound, see [44] and [45].

Lemma 8. *Let $R_h(\cdot,\cdot) : \widetilde{\boldsymbol{V}}_h^r \times \boldsymbol{V}_h^r \to \mathbb{R}$ be the residual defined as:*

$$R_h(\boldsymbol{v}, \boldsymbol{w}) = \tilde{\mathcal{A}}(\boldsymbol{v}, \boldsymbol{w}) - \mathcal{A}(\boldsymbol{v}, \boldsymbol{w}) \qquad \forall \ \boldsymbol{v} \in \widetilde{\boldsymbol{V}}_h^r, \forall \ \boldsymbol{w} \in \boldsymbol{V}_h^r. \tag{2.7}$$

Then, for any $\boldsymbol{v}$ such that $\underline{\sigma}(\boldsymbol{v}) \in \mathcal{H}^s(\mathcal{T}_h)$, for some $s \geq 1$, it holds:

$$\sup_{\boldsymbol{w} \in \boldsymbol{V}_h^r, \ \boldsymbol{w} \neq \boldsymbol{0}} \frac{|R_h(\boldsymbol{v}, \boldsymbol{w})|}{||\boldsymbol{w}||_{DG}} \lesssim \frac{h^{min(r+1,s)}}{r^s} ||\underline{\sigma}(\boldsymbol{v})||_{\mathcal{H}^s(\mathcal{T}_h)}, \tag{2.8}$$

Proof. From the definition of the lifting operator $\mathcal{R}$ in (2.5) and denoting by $\Pi_0 : \mathcal{L}^2(\Omega) \to \mathcal{V}_h^r$ the L^2-orthogonal projection onto $\mathcal{V}_h^r$, we can write the residual $\mathcal{R}_h(\cdot,\cdot)$ as:

$$\begin{aligned}
\mathcal{R}_h(\mathbf{v}, \mathbf{w}) &= - \sum_{\gamma \in \mathcal{F}_I \cup \mathcal{F}_D \cup \Gamma} \int_\gamma \{\underline{\sigma}(\mathbf{v})\} : [\![\mathbf{w}]\!] \, \mathrm{d}\mathbf{s} - \int_\Omega \mathcal{R}([\![\mathbf{w}]\!]) : \underline{\sigma}(\mathbf{v}) \, \mathrm{d}\mathbf{x} \\
&= - \sum_{\gamma \in \mathcal{F}_I \cup \mathcal{F}_D \cup \Gamma} \int_\gamma \{\underline{\sigma}(\mathbf{v})\} : [\![\mathbf{w}]\!] \, \mathrm{d}\mathbf{s} - \int_\Omega \mathcal{R}([\![\mathbf{w}]\!]) : \Pi_0(\underline{\sigma}(\mathbf{v})) \, \mathrm{d}\mathbf{x} \\
&= - \sum_{\gamma \in \mathcal{F}_I \cup \mathcal{F}_D \cup \Gamma} \int_\gamma \{\underline{\sigma}(\mathbf{v}) - \Pi_0(\underline{\sigma}(\mathbf{v}))\} : [\![\mathbf{w}]\!] \, \mathrm{d}\mathbf{s}.
\end{aligned}$$

From the Cauchy-Schwarz inequality we have:

$$|\mathcal{R}_h(\mathbf{v}, \mathbf{w})| \leq ||\eta^{\frac{1}{2}} [\![\mathbf{w}]\!]||_{\mathcal{L}^2(\mathcal{F}_I \cup \mathcal{F}_D \cup \Gamma)} \, ||\eta^{-\frac{1}{2}} \{\underline{\sigma}(\mathbf{v}) - \Pi_0(\underline{\sigma}(\mathbf{v}))\}||_{\mathcal{L}^2(\mathcal{F}_I \cup \mathcal{F}_D \cup \Gamma)},$$

where η is the penalty parameter function defined as in (1.12). By adding and subtracting $\{\mathbf{\Pi}_h^r(\underline{\sigma}(\mathbf{v}))\}$, where $\mathbf{\Pi}_h^r$ is defined as in Lemma 5, we obtain:

$$|\mathcal{R}_h(\mathbf{v},\mathbf{w})| \leq ||\eta^{\frac{1}{2}}[\![\mathbf{w}]\!]||_{\mathcal{L}^2(\mathcal{F}_I\cup\mathcal{F}_D\cup\Gamma)} \left(||\eta^{-\frac{1}{2}}\{\underline{\sigma}(\mathbf{v}) - \mathbf{\Pi}_h^r(\underline{\sigma}(\mathbf{v}))\}||^2_{\mathcal{L}^2(\mathcal{F}_I\cup\mathcal{F}_D\cup\Gamma)} + \right.$$

$$\left. + ||\{\mathbf{\Pi}_h^r(\underline{\sigma}(\mathbf{v})) - \Pi_0(\underline{\sigma}(\mathbf{v}))\}||^2_{\mathcal{L}^2(\mathcal{F}_I\cup\mathcal{F}_D\cup\Gamma)} \right)^{\frac{1}{2}}$$

$$= (T_1+T_2)^{\frac{1}{2}} ||\eta^{\frac{1}{2}}[\![\mathbf{w}]\!]||_{\mathcal{L}^2(\mathcal{F}_I\cup\mathcal{F}_D\cup\Gamma)}.$$

The term T_1 can be bounded based on employing the interpolation estimates of Lemma 5:

$$T_1 \lesssim \sum_{K\in\mathcal{T}_h} ||\eta^{-\frac{1}{2}}\{\underline{\sigma}(\mathbf{v}) - \{\mathbf{\Pi}_h^r(\underline{\sigma}(\mathbf{v}))\}||^2_{\mathcal{L}^2(\partial\mathcal{K})} \lesssim \sum_{\mathcal{K}\in\mathcal{T}_h} \frac{h^{2\min(r+1,s)}}{r^{2s+1}} ||\underline{\sigma}(\mathbf{v})||_{\mathcal{H}^s(\mathcal{K})}.$$

For T_2, from the trace inverse inequality (1.19), the definition of the L^2- projection and together with its continuity and interpolation estimates of Lemma 5, we have:

$$T_2 \lesssim \sum_{\mathcal{K}\in\mathcal{T}_h} ||\eta^{-\frac{1}{2}}\{\mathbf{\Pi}_h^r(\underline{\sigma}(\mathbf{v})) - \Pi_0(\underline{\sigma}(\mathbf{v}))\}||^2_{\mathcal{L}^2(\partial\mathcal{K})} \lesssim \frac{1}{\alpha}\sum_{\mathcal{K}\in\mathcal{T}_h} ||\ \{\mathbf{\Pi}_h^r(\underline{\sigma}(\mathbf{v})) - \Pi_0(\underline{\sigma}(\mathbf{v}))\}||^2_{\mathcal{L}^2(\mathcal{K})}$$

$$= \frac{1}{\alpha}\sum_{\mathcal{K}\in\mathcal{T}_h} ||\ \{\Pi_0(\mathbf{\Pi}_h^r(\underline{\sigma}(\mathbf{v})) - \underline{\sigma}(\mathbf{v}))\}||^2_{\mathcal{L}^2(\mathcal{K})} \lesssim \frac{1}{\alpha}\sum_{\mathcal{K}\in\mathcal{T}_h} ||\ \{\Pi_h^r(\underline{\sigma}(\mathbf{v})) - \underline{\sigma}(\mathbf{v})\}||^2_{\mathcal{L}^2(\mathcal{K})}$$

$$\frac{1}{\alpha}\sum_{\mathcal{K}\in\mathcal{T}_h} \frac{h^{2\min(r+1,s)}}{r^{2s}} ||\underline{\sigma}(\mathbf{v})||^2_{\mathcal{H}^s(\mathcal{K})}.$$

Summing up the two contributions, we get:

$$\begin{aligned}
&|\mathcal{R}_h(\mathbf{v},\mathbf{w})| \lesssim \\
&\lesssim ||\eta^{\frac{1}{2}}[\![\mathbf{w}]\!]||_{\mathcal{L}^2(\mathcal{F}_I\cup\mathcal{F}_D\cup\Gamma)} \left(\sum_{\mathcal{K}\in\mathcal{T}_h} \frac{h^{2\min(r+1,s)}}{r^{2s+1}} ||\underline{\sigma}(\mathbf{v})||_{\mathcal{H}^s(\mathcal{K})} + \sum_{\mathcal{K}\in\mathcal{T}_h} \frac{h^{2\min(r+1,s)}}{r^{2s}} ||\underline{\sigma}(\mathbf{v})||^2_{\mathcal{H}^s(\mathcal{K})} \right)^{\frac{1}{2}} \\
&\lesssim ||\eta^{\frac{1}{2}}[\![\mathbf{w}]\!]||_{\mathcal{L}^2(\mathcal{F}_I\cup\mathcal{F}_D\cup\Gamma)} \left(\sum_{\mathcal{K}\in\mathcal{T}_h} \frac{h^{2\min(r+1,s)}}{r^{2s}} ||\underline{\sigma}(\mathbf{v})||^2_{\mathcal{H}^s(\mathcal{K})} \right)^{\frac{1}{2}} \\
&\lesssim ||\mathbf{w}||_{DG} \left(\sum_{\mathcal{K}\in\mathcal{T}_h} \frac{h^{2\min(r+1,s)}}{r^{2s}} ||\underline{\sigma}(\mathbf{v})||^2_{\mathcal{H}^s(\mathcal{K})} \right)^{\frac{1}{2}},
\end{aligned} \tag{2.9}$$

where in the last step we have used the definition of the DG norm in (2.6) and the fact that: $||\eta^{\frac{1}{2}}[\![\mathbf{w}]\!]||_{\mathcal{L}^2(\mathcal{F}_I\cup\mathcal{F}_D\cup\Gamma)} \leq ||\mathbf{w}||_{DG}$.
From (2.9) we can divide everything by $||\mathbf{w}||_{DG}$, $\mathbf{w} \neq \mathbf{0}$, take the supremum over $\mathbf{w} \in \mathbf{V}_h^r, \mathbf{w} \neq \mathbf{0}$ and the proof is complete. □

We will also need the following Strang Lemma for the analysis.

Lemma 9. *(Strang Lemma, cf. [46]). Consider the problem:*

$$find\ u \in V: \quad a(u,v) = F(v) \quad \forall\ v \in V,$$

where V is a Hilbert space with norm $||\cdot||_V$, $F \in V'$ is a bounded, linear functional on V and $a(\cdot,\cdot) : V \times V \to \mathbb{R}$ is a continuous and coercive bilinear form. Suppose also to have an approximation of the before-mentioned problem of the form:

$$find\ u_h \in V_h: \quad a_h(u_h,v_h) = F_h(v_h) \quad \forall\ v \in V_h,$$

where $\{V_h, h > 0\}$ is a family of finite dimensional spaces and $a_h(\cdot,\cdot)$ is a continuos bilinear form on $V_h \times V_h$ and is uniformly coercive on V_h, i.e.

$$a_h(v_h,v_h) \geq \alpha^* ||v_h||_V^2 \quad \forall\ v_h \in V_h, \quad for\ a\ positive\ \alpha^*.$$

Suppose that F_h is a linear and continuous functional on V_h. Then, there exists a unique solution u_h for the approximate problem and

$$||u_h||_V \leq \frac{1}{\alpha^*} \sup_{v_h \in V_h\setminus\{0\}} \frac{F_h(v_h)}{||v_h||_V}.$$

Moreover, the following a-priori error estimate holds:

$$||u-u_h||_V \leq \left(1+\frac{M}{\alpha^*}\right) \inf_{w_h\in V_h} ||u-w_h||_V + \frac{1}{\alpha^*} \sup_{v_h\in V_h\setminus\{0\}} \frac{|f_h(v_h)-a_h(u,v_h)|}{||v_h||_V},$$

where M is the continuity constant of the bilinear form $a(\cdot,\cdot)$.

Now using the well-posedness of problem (2.4) (cf. Lemma 7), the strong consistency of formulation (2.3) and Lemma 9, we obtain the following abstract error bound.

Lemma 10. *Let the penalty parameter α of Problem* (2.4) *be sufficiently large. Then,*

the following estimate holds:

$$||\boldsymbol{u}-\boldsymbol{u}_h||_{DG} \lesssim \inf_{\boldsymbol{v}\in \boldsymbol{V}_h^r} ||\boldsymbol{u}-\boldsymbol{v}||_{DG} + \sup_{\boldsymbol{w}\ \in \boldsymbol{V}_h^r,\ \boldsymbol{w}\neq \boldsymbol{0}} \frac{|R_h(\boldsymbol{u},\boldsymbol{w})|}{||\boldsymbol{w}||_{DG}}, \tag{2.10}$$

where $R_h(\cdot,\cdot)$ is the residual defined in (2.7)*.*

We have now all the technical tools, so we can state the main result for the error analysis.

Theorem 3. *Suppose that the exact solution $\boldsymbol{u}\in \boldsymbol{H}^2(\Omega\setminus\overline{\Gamma})\cap \boldsymbol{H}^s(\mathcal{T}_h)$ and $\underline{\sigma}(\boldsymbol{u})\in \mathcal{H}^s(\mathcal{T}_h)$, for some $s\geq 1$. If the parameter α appearing in the definition* (1.12) *of the stabilization function is chosen sufficiently large and $\boldsymbol{u}_h$ is the solution obtained with* (2.3)*, it holds:*

$$||\boldsymbol{u}-\boldsymbol{u}_h||_{DG} \lesssim \frac{h^{min(r+1,s)-1}}{r^{s-3/2}}||\boldsymbol{u}||_{\boldsymbol{H}^s(\mathcal{T}_h)} + \frac{h^{min(r+1,s)}}{r^s}||\underline{\sigma}(\boldsymbol{u})||_{\mathcal{H}^s(\mathcal{T}_h)}. \tag{2.11}$$

Proof. We recall the abstract bound (2.10) in Lemma (10):

$$||\mathbf{u}-\mathbf{u}_h||_{DG} \lesssim \inf_{\mathbf{v}\in \mathbf{V}_h^r} ||\mathbf{u}-\mathbf{v}||_{DG} + \sup_{\mathbf{w}\ \in \mathbf{V}_h^r,\ \mathbf{w}\neq \mathbf{0}} \frac{|R_h(\mathbf{v},\mathbf{w})|}{||\mathbf{w}||_{DG}},$$

and we start to bound the first term on the right-hand side. Note that we can still exploit Lemma 5 and in particular the estimates (1.21) and (1.22). So we obtain that, for $s\geq 2$:

$$\inf_{\mathbf{v}\in \mathbf{V}_h^r} ||\mathbf{u}-\mathbf{v}||_{DG} \leq ||\mathbf{u}-\Pi_h^r\mathbf{u}||_{DG} \lesssim \frac{h^{\min(r+1,s)-1}}{r^{s-3/2}}||\mathbf{u}||_{\mathbf{H}^s(\mathcal{T}_h)}. \tag{2.12}$$

Finally, the following bound for the second term:

$$\sup_{\mathbf{w}\ \in \mathbf{V}_h^r,\ \mathbf{w}\neq \mathbf{0}} \frac{|R_h(\mathbf{v},\mathbf{w})|}{||\mathbf{w}||_{DG}} \lesssim \frac{h^{\min(r+1,s)}}{r^s}||\underline{\sigma}(\mathbf{v})||_{\mathcal{H}^s(\mathcal{T}_h)}$$

follows directly from the inequality (2.8).
Summing all the previous bounds, the proof of Theorem 3 is complete.

□

To obtain an *a-priori* estimate in the $\mathbf{L}^2(\Omega)$-norm, we need more regularity of the solution, in order to use a duality argument. Therefore, we assume that Ω, $\mathbf{D}$, the fault Γ and the slip field $\mathbf{q}_0$ are sufficiently regular so that $\mathbf{u}\in \mathbf{H}^2(\Omega\setminus\overline{\Gamma})$. The dual problem with the given source $\mathbf{g}\in \mathbf{L}^2(\Omega)$ is also well posed and its unique solution ξ satisfies the following elliptic regularity: $\boldsymbol{\xi}\in \mathbf{H}^2(\Omega\setminus\overline{\Gamma}), \underline{\sigma}(\boldsymbol{\xi})\in \mathcal{H}^1(\Omega\setminus\overline{\Gamma})$, $||\boldsymbol{\xi}||_{\mathbf{H}^2(\Omega\setminus\overline{\Gamma})} \lesssim ||\mathbf{g}||_{\mathbf{L}^2(\Omega)}$ and $||\underline{\sigma}(\boldsymbol{\xi})||_{\mathcal{H}^1(\Omega\setminus\overline{\Gamma})} \lesssim ||\mathbf{g}||_{\mathbf{L}^2(\Omega)}$. The following bound holds.

Theorem 4. *We assume that the grid $\mathcal{T}_h$ is quasi uniform. Let $\boldsymbol{u}_h \in \boldsymbol{V}_h^r$ be the DG solution obtained with a penalty parameter α appearing in* (1.12) *sufficiently large. Then,*

$$||\boldsymbol{u}-\boldsymbol{u}_h||_{\boldsymbol{L}^2(\Omega)} \lesssim \frac{h^{min(r+1,s)}}{r^{s-1}}\left(||\boldsymbol{u}||^2_{\boldsymbol{H}^s(\Omega\setminus\overline{\Gamma})}+\frac{h}{r^2}||\underline{\sigma}(\boldsymbol{u})||_{\mathcal{H}^s(\Omega\setminus\overline{\Gamma})}\right). \tag{2.13}$$

Proof. We solve the dual problem as in (1.27) with $\mathbf{g}=\mathbf{u}-\mathbf{u}_h$ and for any $\boldsymbol{\xi}_h \in \mathbf{V}_h^r$ we obtain:

$$\begin{aligned}||\mathbf{u}-\mathbf{u}_h||^2_{\mathbf{L}^2(\Omega)} &= \mathcal{A}(\boldsymbol{\xi},\mathbf{u}-\mathbf{u}_h)=\mathcal{A}(\boldsymbol{\xi}-\boldsymbol{\xi}_h,\mathbf{u}-\mathbf{u}_h)= \\ &= \tilde{\mathcal{A}}(\boldsymbol{\xi}-\boldsymbol{\xi}_h,\mathbf{u}-\mathbf{u}_h)+\mathcal{R}_h(\boldsymbol{\xi}-\boldsymbol{\xi}_h,\mathbf{u}-\mathbf{u}_h) \\ &\lesssim ||\boldsymbol{\xi}-\boldsymbol{\xi}_h||_{DG}||\mathbf{u}-\mathbf{u}_h||_{DG}+\mathcal{R}_h(\boldsymbol{\xi}-\boldsymbol{\xi}_h,\mathbf{u}-\mathbf{u}_h).\end{aligned}$$

Moreover, thanks to the definition of $\mathcal{R}_h$ in (2.7) and the continuity of $\tilde{\mathcal{A}}(\cdot,\cdot)$ we get:

$$\mathcal{R}_h(\boldsymbol{\xi}-\boldsymbol{\xi}_h,\mathbf{u}-\mathbf{u}_h)=-\mathcal{R}_h(\boldsymbol{\xi}-\boldsymbol{\xi}_h,\mathbf{u})+\mathcal{R}_h(\boldsymbol{\xi},\mathbf{u}-\mathbf{u}_h).$$

Next, using Lemma 8 we have:

$$||\mathbf{u}-\mathbf{u}_h||^2_{\mathbf{L}^2(\Omega)} \lesssim ||\boldsymbol{\xi}-\boldsymbol{\xi}_h||_{DG}||\mathbf{u}-\mathbf{u}_h||_{DG}+\frac{h^{\min(r+1,s)}}{r^s}||\underline{\sigma}(\mathbf{u})||_{\mathcal{H}^s(\Omega\setminus\overline{\Gamma})}||\boldsymbol{\xi}-\boldsymbol{\xi}_h||_{DG}$$

$$+\frac{h}{r}||\underline{\sigma}(\boldsymbol{\xi})||_{\mathcal{H}^1(\Omega\setminus\overline{\Gamma})}||\mathbf{u}-\mathbf{u}_h||_{DG},$$

and by the elliptic regularity of the dual problem:

$$||\mathbf{u}-\mathbf{u}_h||^2_{\mathbf{L}^2(\Omega)} \lesssim ||\boldsymbol{\xi}-\boldsymbol{\xi}_h||_{DG}||\mathbf{u}-\mathbf{u}_h||_{DG}+\frac{h^{\min(r+1,s)}}{r^s}||\underline{\sigma}(\mathbf{u})||_{\mathcal{H}^s(\Omega\setminus\overline{\Gamma})}||\boldsymbol{\xi}-\boldsymbol{\xi}_h||_{DG}+$$

$$+\frac{h}{r}||\mathbf{u}-\mathbf{u}_h||_{\mathbf{L}^2(\Omega)}||\mathbf{u}-\mathbf{u}_h||_{DG}.$$

Choosing $\boldsymbol{\xi}=\Pi_h^r(\boldsymbol{\xi})$ we can use estimate (2.12) with $s=2, r=1$ and the elliptic regularity and we obtain:

$$||\boldsymbol{\xi}-\boldsymbol{\xi}_h||_{DG} \lesssim \frac{h}{r^{\frac{1}{2}}}||\boldsymbol{\xi}||_{\mathbf{H}^2(\Omega\setminus\overline{\Gamma})} \lesssim \frac{h}{r^{\frac{1}{2}}}||\mathbf{u}-\mathbf{u}_h||_{\mathbf{L}^2(\Omega)}.$$

Combining the above bounds, we have:

$$||\mathbf{u}-\mathbf{u}_h||^2_{\mathbf{L}^2(\Omega)} \lesssim \frac{h}{r^{\frac{1}{2}}}||\mathbf{u}-\mathbf{u}_h||_{\mathbf{L}^2(\Omega)}||\mathbf{u}-\mathbf{u}_h||_{DG}+\frac{h^{\min(r+1,s)+1}}{r^{s+1}}||\underline{\sigma}(\mathbf{u})||_{\mathcal{H}^s(\Omega\setminus\overline{\Gamma})}||\mathbf{u}-\mathbf{u}_h||_{\mathbf{L}^2(\Omega)},$$

that is

$$||\mathbf{u}-\mathbf{u}_h||_{\mathbf{L}^2(\Omega)} \lesssim \frac{h}{r^{\frac{1}{2}}}\left(||\mathbf{u}-\mathbf{u}_h||_{DG} + \frac{h^{\min(r+1,s)}}{r^{s+\frac{1}{2}}}||\underline{\sigma}(\mathbf{u})||_{\mathcal{H}^s(\Omega\setminus\overline{\Gamma})}\right).$$

Finally, applying Theorem 3 we obtain the thesis and the proof is complete.

□

2.3 Numerical results

In this section we present some numerical computations to illustrate the performance of the proposed numerical scheme. In each example, we will consider a jump of the elastic displacement through the interface Γ and a discontinuity of the stress tensor.
We will employ two different geometric configurations: a square domain $\Omega = (-1,0)\times(0,1)$ with a horizontal interface $\Gamma = (-1,0)\times\{0.2\}$ and $\Omega = (-0.8,0.8)\times(-0.8,0.8)$ with $\Gamma = [(-0.8;-0.5),(0.8;-0.1)]$. In both cases we choose a sequence of grids aligned with the crack. Figure 2.2 and Figure 2.3 show an example of the computational meshes under 3 levels of successive refinements.

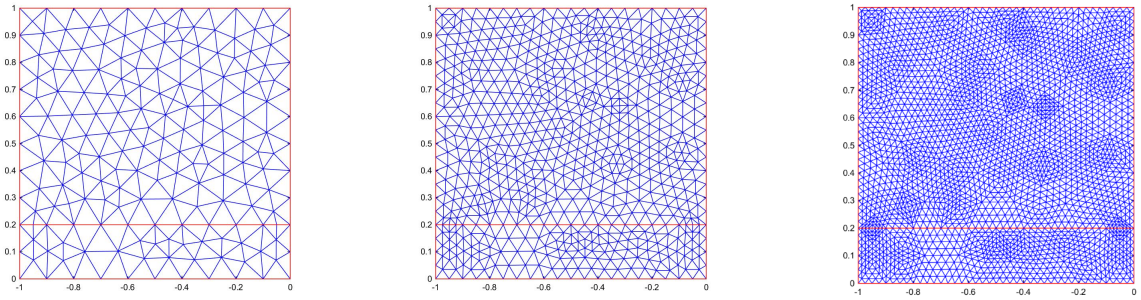

(a) First level of refinement.

(b) Second level of refinement.

(c) Third level of refinement.

Figure 2.2: Example 1: Domain with a horizontal interface $\Gamma = (-1,0)\times\{0.2\}$.

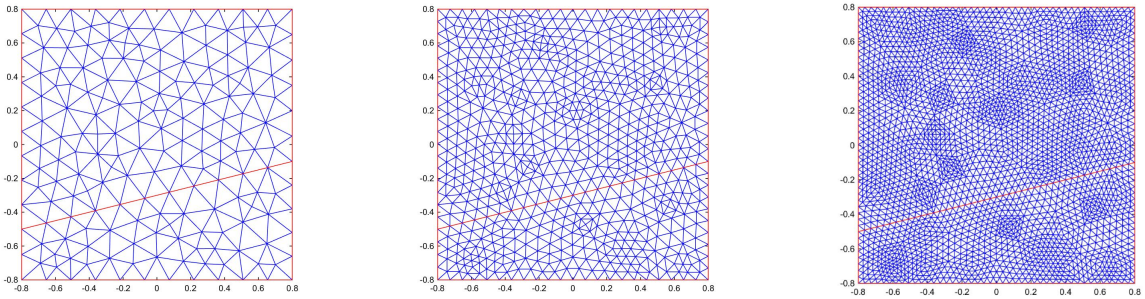

(a) First level of refinement.

(b) Second level of refinement.

(c) Third level of refinement.

Figure 2.3: Example 2: Domain with an oblique interface $\Gamma = [(-0.8; -0.5), (0.8; -0.1)]$.

2.3.1 Example 1

In the first example, we choose the Lamé coefficients $\lambda = 1$ and $\mu = 1$ and the exact solution as:

$$u_1(x, y) = e^x \cos(y) + 1 \cdot (y > y_1 + \frac{(y_0 - y_1)}{(x_0 - x_1)}(x - x_1)),$$

$$u_2(x, y) = x^2 + y^2 + 1 \cdot (y > y_1 + \frac{(y_0 - y_1)}{(x_0 - x_1)}(x - x_1)),$$

where $(x_0, y_0) = (-0.8, -0.5)$ and $(x_1, y_1) = (0.8, 0.1)$ are the coordinates of the intersection of $\Gamma = [(-0.8; -0.5), (0.8; -0.1)]$ with the boundary $\partial\Omega$, cf. Figure 2.3.

The source term is chosen accordingly, i.e.:

$$f_1(x, y) = -2e^x \cos(y),$$

$$f_2(x, y) = 2e^x \sin(y) - 8,$$

as well as the Neumann and the Dirichlet data on $\Gamma_D = (-0.8, 0.8) \times 0.8$ and $\Gamma_N = \partial\Omega \backslash \Gamma_D$. It can be easily shown that in this case the jump through the fault is constant and is given by $\mathbf{q}_0 = [1, 1]^T$, whereas $\mathbf{q}_1 = [0, 0]^T$, meaning that the normal component of the stress is continuous along Γ. Figure 2.4 shows the computed solution on a mesh with approximately 5200 elements ($h = 0.0138$), corresponding to 3 levels of refinement. The computed errors using a polynomial degree $r = 1$ is shown in Figure 2.5 as a function of the mesh size h (log-log scale). We can clearly observe a quadratic (linear respectively) convergence rate when the error is measured in the $\mathbf{L}_2$ ($\mathbf{H}_1$, respectively) norm, as

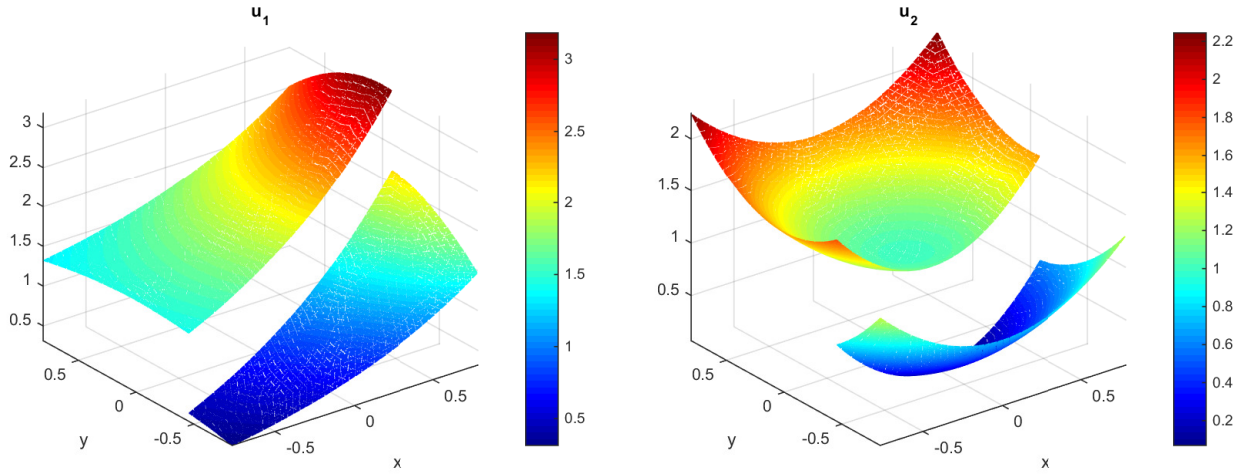

(a) First component of the solution u_1. **(b)** Second component of the solution u_2.

Figure 2.4: Example 1: Plot of the computed solution on a grid with granularity $h = 0.0138$ (3 levels of refinement).

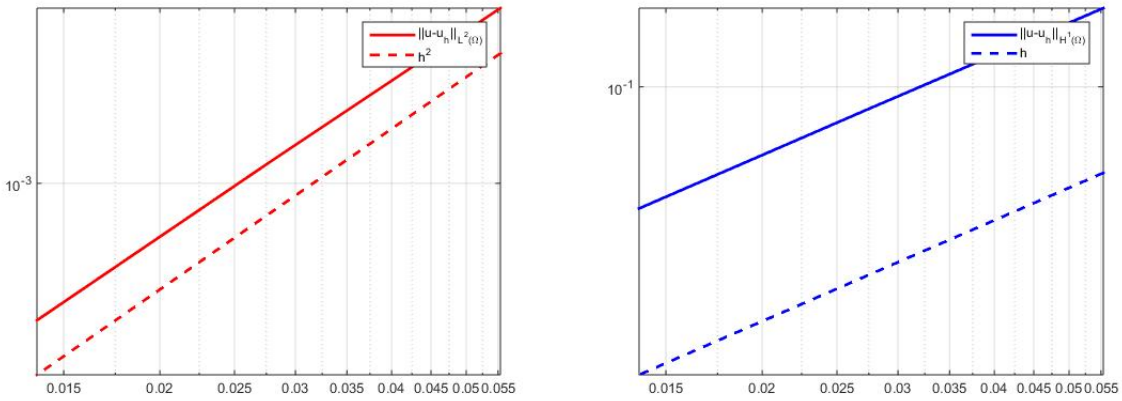

(a) Computed errors in the $\mathbf{L}_2$-norm versus the mesh size h. **(b)** Computed errors in the $\mathbf{H}_1$-norm versus the mesh size h.

Figure 2.5: Example 1: Computed errors versus the mesh size h (log-log scale).

2.3.2 Example 2

In this example we choose uniform Lamé coefficients $\lambda = 1$ and $\mu = 1$ and the components of the exact solution as:

$$u_1(x, y) = \sin(2\pi x) + x^2 \cdot (y > y_0),$$

$$u_2(x, y) = \sin(2\pi y) + x^2 \cdot (y > y_0),$$

where $y_0 = 0.2$ is the y-coordinate of the horizontal interface $\Gamma = (-1, 0) \times \{0.2\}$.
The given source term becomes:

$$f_1(x, y) = 12\pi^2 \sin(2\pi x) - 6 \cdot (y > y_0),$$

$$f_2(x, y) = 12\pi^2 \sin(2\pi y) - 2 \cdot (y > y_0).$$

and the Dirichlet boundary datum is chosen accordingly on $\Gamma_D \equiv \partial\Omega$, cf. Figure 2.2.
For this test, the vector $\mathbf{q}_0 = [x^2, x^2]^T$ is parabolic in the x direction and we have a jump of the stress tensor along Γ: $\mathbf{q}_1 = [-2x, -2x]^T$.
The results in Figure 2.6 show that, as expected, the parabolic discontinuity of the displacement in the x direction along the interface Γ. Figure 2.6 displays both the components of the computed solution on a mesh with granularity $h = 0.0157$ (that corresponds to 3 levels of refinement). In Figure 2.7 we report the computed error in the $\mathbf{L}_2$ and $\mathbf{H}_1$ norm as a function of the mesh size h (log-log scale), obtained with a polynomial degree $r = 1$. We can clearly observe a quadratic (linear respectively) convergence of the error when measured if the $\mathbf{L}_2$ norm ($\mathbf{H}_1$ norm respectively), as predicted by the theory.

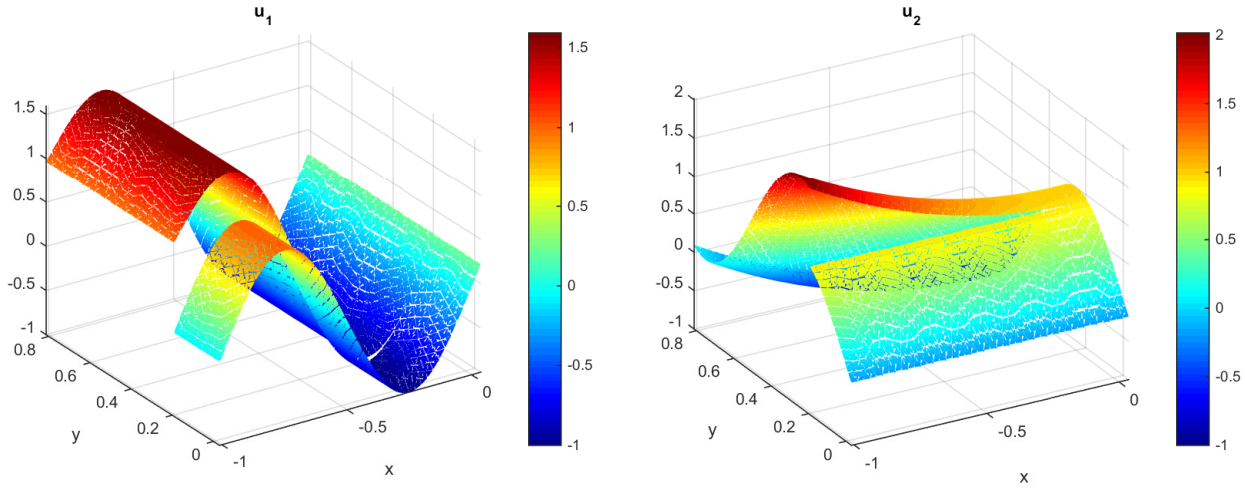

(a) First component of the solution u_1. **(b)** Second component of the solution u_2.

Figure 2.6: Example 2: Plot of the computed solution on a grid with granularity $h = 0.0157$ (3 levels of refinement).

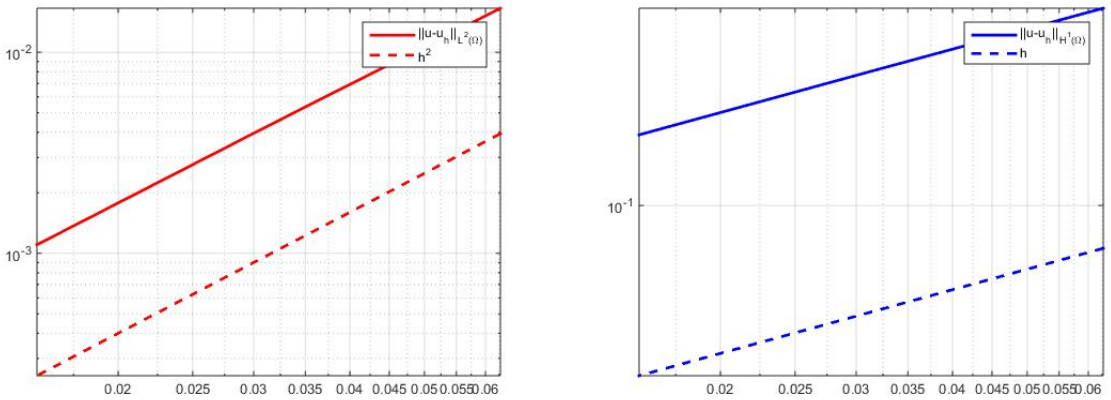

(a) Computed errors in the $\mathbf{L}_2$-norm versus the mesh size h. **(b)** Computed errors in the $\mathbf{H}_1$-norm versus the mesh size h.

Figure 2.7: Example 2: Computed errors versus the mesh size h (log-log scale).

2.3.3 Example 3

In the third example we choose uniform Lamé coefficients $\lambda = 1$ and $\mu = 1$ and the components of the exact solution as:

$$u_1(x, y) = \sin(2\pi x) + \sin(2\pi x) \cdot (y > y_0),$$

$$u_2(x, y) = \sin(2\pi y) + \sin(2\pi y) \cdot (y > y_0),$$

where y_0 is the y-coordinate of the horizontal interface Γ, defined as $\Gamma = (-1, 0) \times \{0.2\}$. The given source term is:

$$f_1(x, y) = 12\pi^2 \sin(2\pi x) + 12\pi^2 \sin(2\pi x) \cdot (y > y_0),$$

$$f_2(x, y) = 12\pi^2 \sin(2\pi y) + 12\pi^2 \sin(2\pi y) \cdot (y > y_0).$$

For this test, the vector $\mathbf{q}_0 = [\sin(2\pi x),\ \sin(2\pi y)]^T$ is a trigonometric function in the x and y directions and we have $\mathbf{q}_1 = [0,\ -6\pi \cos(2\pi y) - 2\pi \cos(2\pi x)\ ]^T$.
Figure 2.8 and Figure 2.9 show the two discontinuous components of the computed solution on a mesh with approximately 4000 elements (granularity $h = 0.0157$, corresponding to 3 levels of refinement) and the computed errors, respectively. We remark that again we observe the convergence rates predicted by the theory.

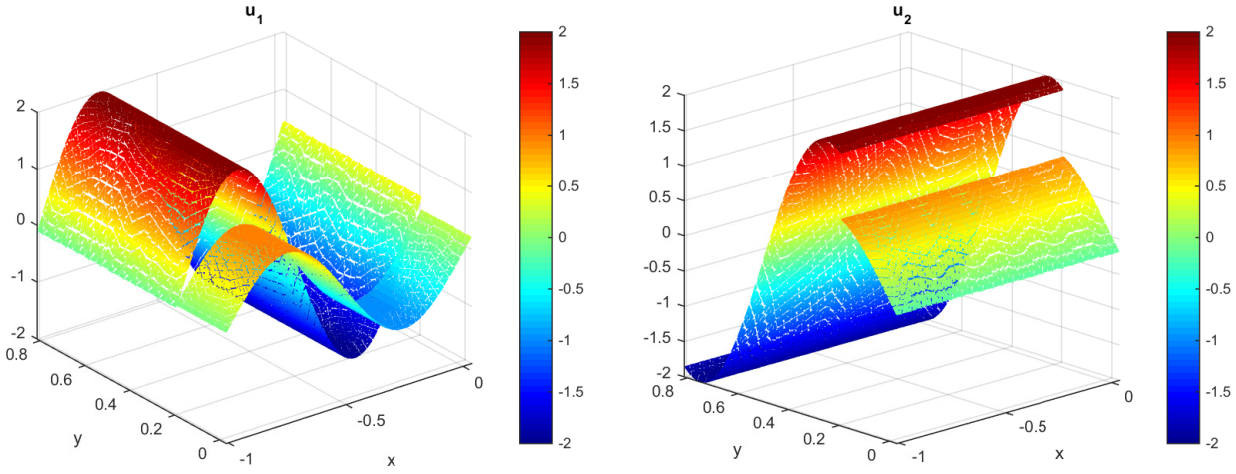

(a) First component of the solution u_1. **(b)** Second component of the solution u_2.

Figure 2.8: Example 3: Plot of the computed solution on a grid with granularity $h = 0.0157$ (3 levels of refinement).

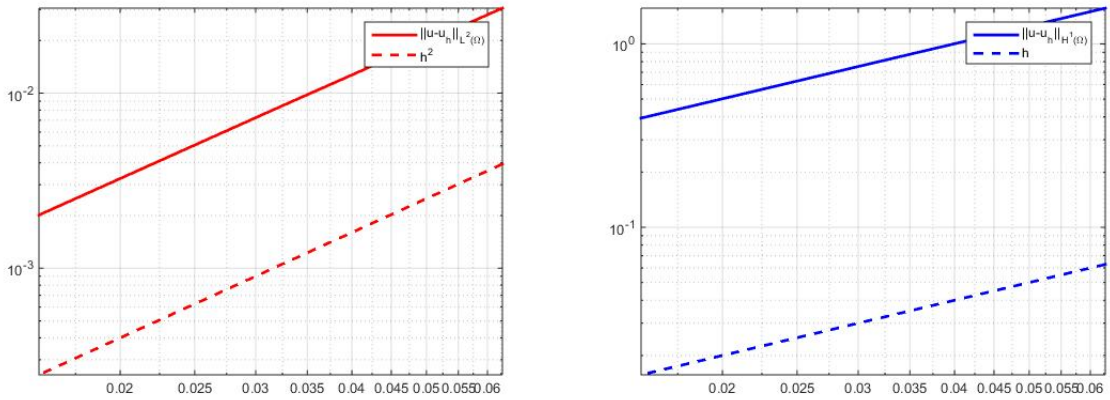

(a) Computed errors in the $\mathbf{L}_2$-norm versus the mesh size h.

(b) Computed errors in the $\mathbf{H}_1$-norm versus the mesh size h.

Figure 2.9: Example 3: Computed errors versus the mesh size h (log-log scale).

2.3.4 Example 4

In the last experiment, we try to combine the problem with discontinuous Lamè parameters across a geometrical interface to the one with a discontinuous solution across a different crack. Thus, we take the unit square domain $\Omega = (0,1) \times (0,1)$ divided by two faults: the horizontal interface $\Gamma_1 = \{0.4\} \times (0,1)$ and the vertical interface $\Gamma_2 = (0,1) \times \{0.5\}$, as shown in Figure 2.10.

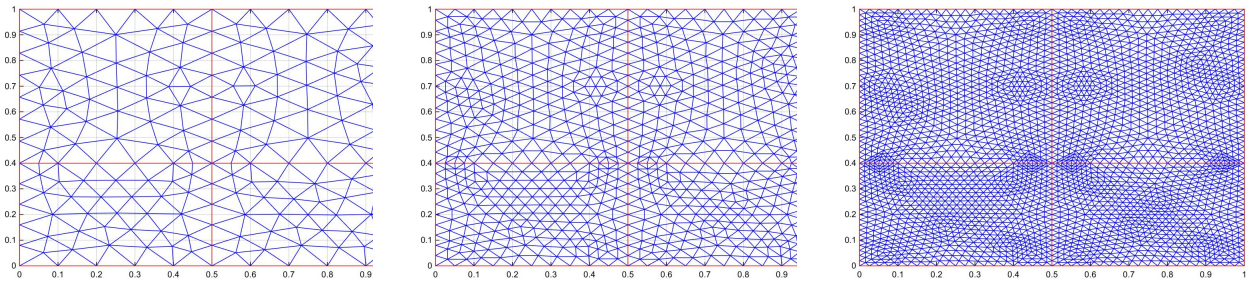

(a) First level of refinement.

(b) Second level of refinement.

(c) Third level of refinement.

Figure 2.10: Example 3: Domain with two interfaces: $\Gamma_1 = \{0.4\} \times (0,1)$ and the vertical $\Gamma_2 = (0,1) \times \{0.5\}$.

We choose:

$$\lambda = \mu = 1, \quad \text{if } x < x_0$$

$$\lambda = \mu = 2, \quad \text{if } x \geq x_0$$

and the components of the exact solution as:

$$u_1(x, y) = \sin(2\pi x) + \sin(2\pi x) \cdot (y > y_0),$$

$$u_2(x, y) = \sin(2\pi y) + \sin(2\pi y) \cdot (y > y_0),$$

where $y_0 = 0.4$ is the y-coordinate of Γ_1 and $x_0 = 0.5$ is the x-coordinate of Γ_2.
The given source term is given by:

$$f_1(x, y) = 12\pi^2 \sin(2\pi x) + 12\pi^2 \sin(2\pi x) \cdot (x \geq x_0) - 6 \cdot (y > y_0) - 6 \cdot (x \geq x_0) \cdot (y > y_0),$$

$$f_2(x, y) = 12\pi^2 \sin(2\pi y) + 12\pi^2 \sin(2\pi y) \cdot (x \geq x_0) - 2 \cdot (y > y_0) - 2 \cdot (x \geq x_0) \cdot (y > y_0).$$

We impose Dirichlet boundary conditions on the whole boundary $\partial\Omega$ and the datum $\mathbf{g}_D$ is chosen accordingly. Figure 2.11 shows the two components of the computed solution on a mesh with granularity $h = 0.0135$, that corresponds to 3 levels of refinement of an initial mesh grid with 342 elements. In Figure 2.12, as before, we report the computed errors in the $\mathbf{L}_2$ norm (left) and $\mathbf{H}_1$ norm (right) as a function of the mesh size h (log-log scale). These results have been obtained base on employing piecewise linear polynomials, i.e. $r = 1$. As expected, we clearly observe a linear convergence of the error when measured in the $\mathbf{H}_1$ norm and a quadratic convergence of the error when measured in the $\mathbf{L}_2$ norm.

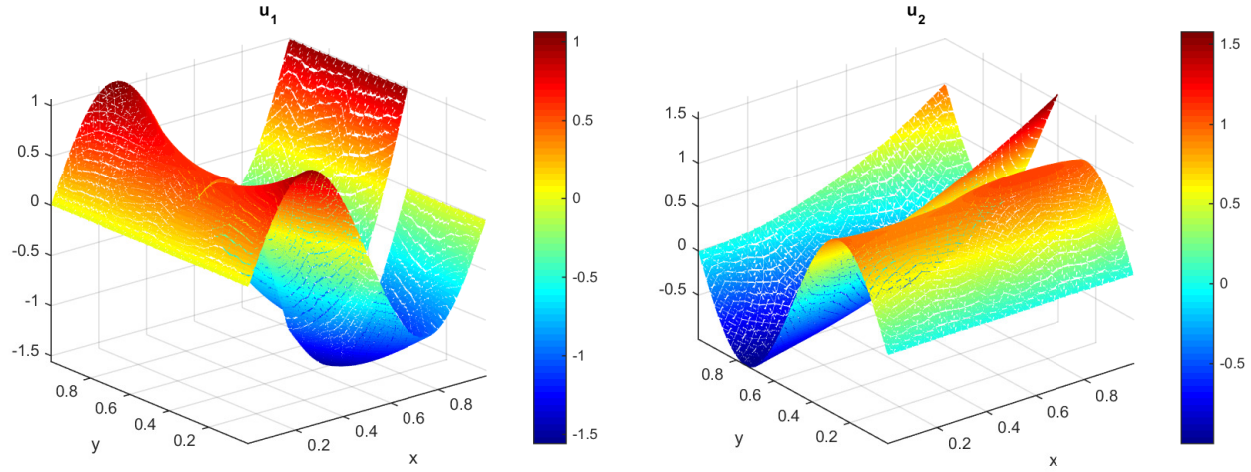

(a) First component of the solution u_1. **(b)** Second component of the solution u_2.

Figure 2.11: Example 4: Plot of the computed solution on a grid with granularity $h = 0.0135$ (3 levels of refinement).

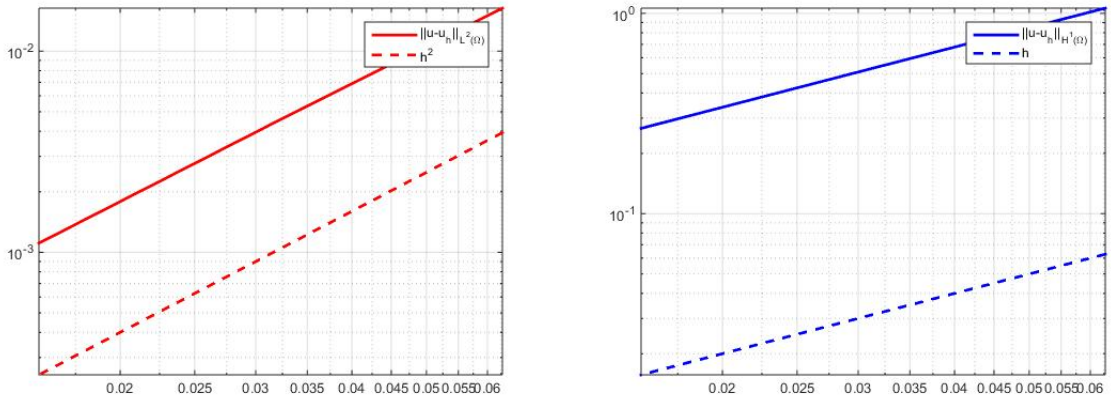

(a) Computed errors in the $\mathbf{L}_2$-norm versus the mesh size h.

(b) Computed errors in the $\mathbf{H}_1$-norm versus the mesh size h.

Figure 2.12: Example 4: Computed errors versus the mesh size h (log-log scale).

Chapter 3

The inverse problem and its numerical approximation

Mathematically, we model the portion of the Earth where the fault is located as an elastic medium Ω in the regime of small oscillations, the slip is represented by the jump of the displacement on the fault. The surface of the earth is traction free, along the fault the traction is continuous and in the part of Ω buried we impose homogeneous Dirichlet boundary conditions. The mathematical model in two dimensions then reads as follows:

$$\begin{aligned} -\nabla \cdot \underline{\sigma}(\mathbf{u}_\Gamma) &= \mathbf{f} \quad \text{in } \Omega, \\ \underline{\sigma}(\mathbf{u}_\Gamma) - \mathbf{D}\underline{\epsilon}(\mathbf{u}_\Gamma) &= \mathbf{0} \quad \text{in } \Omega, \\ \mathbf{u}_\Gamma &= \mathbf{0} \quad \text{on } \Gamma_D, \\ \underline{\sigma}(\mathbf{u}_\Gamma)\mathbf{n} &= \mathbf{0} \quad \text{on } \Gamma_N, \\ [\![\mathbf{u}_\Gamma]\!] &= \mathbf{q}_0 \quad \text{on } \Gamma, \\ [\![\underline{\sigma}(\mathbf{u}_\Gamma)\mathbf{n}]\!] &= \mathbf{0} \quad \text{on } \Gamma, \end{aligned} \tag{3.1}$$

where the fault Γ is an open curve in Ω (see Figure 3.1).

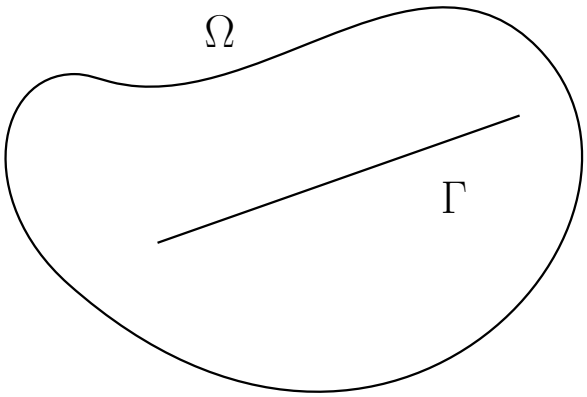

Figure 3.1: Region occupied by the elastic material with a linear inclusion.

As we mentioned above, a-priori assumptions on the unknowns are needed in order to regularize the inverse problem and to implement a reconstruction algorithm:

- **Assumption 1:** the domain Ω is a bounded simply connected and convex domain of $\mathbb{R}^2$ such that $\text{diam}(\Omega) \leq E$, with E a given positive constant, and $\partial\Omega$ is Lipschitz.
- **Assumption 2:** suppose that Γ is a segment of endpoints P, Q such that:

  $$L^{-1} \leq |P - Q| \leq L \quad \text{and} \quad d(\Gamma, \mathbb{R}^2 \setminus \Omega) \geq L^{-1}$$

  for a constant $L \geq 1$.
- **Assumption 3:** assume that Ω is homogeneous and isotropic, being (λ, μ) the Lamé coefficients, i.e. the elastic tensor field $\mathbf{D}$ is defined as in (1.3).
- **Assumption 4:** $\mathbf{D}$ is bounded and strongly convex in Ω, i.e., there exists a positive constant ξ such that:

  $$\mathbf{D}\underline{A} \cdot \underline{A} \geq \xi |\underline{A}|^2$$

  for any symmetric 2×2 matrix $\underline{A} \neq \underline{0}$.
- **Assumption 5:** suppose that the slip field $\mathbf{q}_0$ is piecewise constant and the stress is continuous through Γ. Physically this suggests that the fault Γ is not opening or

self-intersecting, hence only slipping is allowed.

Now let $B_R(\mathbf{0}) \subset \mathbb{R}^2$ be the closed ball of radius R centered in $\mathbf{0}$ and $\Omega_{d_0} = \{\mathbf{x} \in \Omega : \text{dist}(\mathbf{x}, \partial\Omega) \geq d_0\}$.
Given all the stated assumptions, consider the map $T : \Omega_{d_0} \times \Omega_{d_0} \times B_R(0) \to \mathbf{L}^2(\Sigma)$:

$$T(P, Q, \mathbf{q}_0) = \mathbf{u}_\Gamma^{\mathbf{q}_0}|_\Sigma, \tag{3.2}$$

where $\mathbf{u}_\Gamma^{\mathbf{q}_0}|_\Sigma$ is the trace of the displacement $\mathbf{u}_\Gamma$, satisfying (3.1), on some open portion Σ of the Neumann boundary Γ_N.
The *inverse* problem we are interested is to determine the slip field $\mathbf{q}_0$ and the fault $\Gamma = (P, Q)$ simultaneously from the measurements of $\mathbf{u}_\Gamma$ on Σ. Hence, we are interested in studying the properties of the inverse map T^{-1}.
We know from the results obtained in the previous chapters that a unique distributional or weak solution $\mathbf{u}_\Gamma$ of the *forward* problem (3.1) exists, according to the regularity of $\mathbf{q}_0$. It is also easy to show that T is injective because uniqueness for the *inverse* problem holds. In the following theorem we prove, by using unique-continuation properties of solution to the Lamé system, that one surface measurement of the displacement field is sufficient to recover uniquely both the crack and the slip field, assuming all the mentioned hypotheses.

Theorem 5. *(Uniqueness). Let $\Gamma_1, \Gamma_2 \subset \Omega$ be two linear faults satisfying **Assumption 2** and $\boldsymbol{q}_1$, $\boldsymbol{q}_2 \neq \boldsymbol{0}$ two constant vector slip fields. Let $\boldsymbol{u}_1$ and $\boldsymbol{u}_2$ be the unique solution of* (3.1) *corresponding to the constant slip $\boldsymbol{q}_0 = \boldsymbol{q}_i$ and the fault $\Gamma = \Gamma_i$, for $i = 1, 2$. If $\boldsymbol{u}_1|_\Sigma = \boldsymbol{u}_2|_\Sigma$, then $\Gamma_1 = \Gamma_2$ and $\boldsymbol{q}_1 = \boldsymbol{q}_2$.*

Proof. By usual arguments, we define the difference $\mathbf{w} = \mathbf{u}_1 - \mathbf{u}_2$ on $\Omega \setminus \overline{\Gamma_1 \cup \Gamma_2}$. Then

$$\begin{aligned} -\nabla \cdot \mathbf{D}\underline{\epsilon}(\mathbf{w}) = \mathbf{0} \quad &\text{in } \Omega \setminus \overline{\Gamma_1 \cup \Gamma_2}, \\ \mathbf{w} = \mathbf{0} \quad &\text{on } \Gamma_D, \\ \underline{\sigma}(\mathbf{w})\mathbf{n} = \mathbf{0} \quad &\text{on } \Gamma_N, \end{aligned} \tag{3.3}$$

where we have used the homogeneous boundary conditions of (3.1). We also know from the hypothesis of the theorem that $\mathbf{u}_1|_\Sigma = \mathbf{u}_2|_\Sigma$, so it follows:

$$\mathbf{w}|_\Sigma = \mathbf{0}.$$

We can then apply the result in [47] to obtain the unique continuation property for elliptic operators. This means that $\mathbf{w} = \mathbf{0}$ in $\Omega \setminus \overline{\Gamma_1 \cup \Gamma_2}$.
We assume that $\overline{\Gamma}_1 \neq \overline{\Gamma}_2$, and we fix $\mathbf{y} \in \overline{\Gamma}_1$ such that $\mathbf{y} \notin \overline{\Gamma}_2$. Then there exists a ball $B_r(\mathbf{y})$ of radius r and centered in $\mathbf{y}$ that does not intersect $\overline{\Gamma}_2$. Hence,

$$\mathbf{0} = [\![\mathbf{w}]\!]_{B_r(\mathbf{y})\cap\Gamma_1} = [\![\mathbf{u}_1]\!]_{B_r(\mathbf{y})\cap\Gamma_1} = \mathbf{q}_1,$$

and this leads to a contradiction, because $\mathbf{q}_1$ has support on Γ_1.
The same argument can be repeated switching the role of Γ_1 and Γ_2, to conclude that $\overline{\Gamma}_1 = \overline{\Gamma}_2$. Therefore,

$$\mathbf{0} = [\![\mathbf{w}]\!]_{\Gamma_1} = [\![\mathbf{w}]\!]_{\Gamma_2} \to [\![\mathbf{u}_1]\!]_{\Gamma_1} = [\![\mathbf{u}_2]\!]_{\Gamma_2} \to \mathbf{q}_1 = \mathbf{q}_2,$$

and the proof is complete. □

We have proved that the map T is injective. On the other hand, to regularize the *inverse* problem and since measurements are affected by errors we also need to study the continuous dependence of the unknowns from the data. This will be discussed in the next section.

3.1 Lipschitz stability

To prove Lipschitz continuity of T^{-1} we will show that the assumptions of the following general result proved in [48] are satisfied in our setting.

Theorem 6. *Let H be a Banach space, $U \in \mathbb{R}^d$ an open set and $K \subset U$ a convex compact set. Let $T \in C^1(U; H)$ and assume T is injective as well as $DT(y)$, where for each $y \in U$ $DT(y) \in \mathcal{L}(\mathbb{R}^d, H)$ is the Fréchet derivative of T evaluated in $y \in U$. Then, there exists a constant C such that $\forall\ y, y' \in K$,*

$$|y - y'| \leq C||T(y) - T(y')||_H.$$

We will apply Theorem 6 with $H = \mathbf{L}^2(\Sigma)$, $U = \Omega\times\Omega\times\mathbb{R}^2$ and assuming Ω to be a convex set, we choose $K = \Omega_{d_0} \times \Omega_{d_0} \times B_R(0)$. Moreover we will let $T(y) := T(P, Q, \mathbf{q}_0)$ where $T(P, Q, \mathbf{q}_0)$ is defined in (3.2). Thus we are left to show that T is Fréchet-differentiable and that its derivative is injective.

We will first show that T is Gateaux differentiable. We denote by Γ_t the segment $[P_t, Q_t]$ where:

$$P_t = (1-t)P_0 + tP_1, \quad Q_t = (1-t)Q_0 + tQ_1, \quad t \in (0,1),$$

and $\mathbf{q}_t$ the following slip field with support on Γ_t:

$$\mathbf{q}_t = (1-t)\mathbf{q}_0 + t\mathbf{q}_1, \quad t \in (0,1).$$

Now we define: $\mathbf{u}_t = \mathbf{u}_{\Gamma_t}^{\mathbf{q}_t}$ the solution of the model in (3.1) with $\mathbf{q}_0$ replaced by $\mathbf{q}_t$ and Γ by Γ_t. We know by [5] that the map T in (3.2) is Gateaux differentiable and can be explicitly formulated. Let $\mathbf{u}_t' = \frac{d}{dt}\mathbf{u}_t$ be the derivative of the medium displacement with respect to the variable t. We briefly remind the reader the generalization of the concept of directional derivative for a functional between locally convex topological vector spaces, the so-called "Gateaux derivative" (see [49]): suppose that X and Y are locally convex topological vector spaces (for example, Banach spaces), $U \subset X$ is open, and $F : X \to Y$. The Gateaux differential $dF(u;\psi)$ of F at $u \in U$ in the direction $\psi \in X$ is defined as:

$$dF(u;\psi) = \lim_{\tau \to 0} \frac{F(u+\tau\psi) - F(u)}{\tau} = \frac{d}{d\tau} F(u+\tau\psi).$$

If the limit exists for all $\psi \in X$, then one says that F is Gateaux differentiable at u. First of all, we write the elastic displacement $\mathbf{u}_t$ as the sum of two terms, thanks to the linearity of the model:

$$\mathbf{u}_t = \mathbf{v}_t + \widetilde{\mathbf{u}}, \tag{3.4}$$

where $\mathbf{v}_t$ is the solution of:

$$\begin{aligned} -\nabla \cdot \mathbf{D}\underline{\epsilon}(\mathbf{v}_t) &= \mathbf{0} \quad \text{in } \Omega \setminus \overline{\Gamma_t}, \\ \mathbf{v}_t &= \mathbf{0} \quad \text{on } \Gamma_D, \\ \underline{\sigma}(\mathbf{v}_t)\mathbf{n} &= \mathbf{0} \quad \text{on } \Gamma_N, \\ [\![\mathbf{v}_t]\!] &= \mathbf{q}_t \quad \text{on } \Gamma_t, \\ [\![\underline{\sigma}(\mathbf{v}_t)\mathbf{n}_t]\!] &= \mathbf{0} \quad \text{on } \Gamma_t, \end{aligned} \tag{3.5}$$

and $\widetilde{\mathbf{u}}$ satisfies a classic linear elasticity PDEs system with a source $\mathbf{f} \neq \mathbf{0}$:

$$\begin{aligned} -\nabla \cdot \mathbf{D}\underline{\epsilon}(\widetilde{\mathbf{u}}) &= \mathbf{f} \quad \text{in } \Omega, \\ \widetilde{\mathbf{u}} &= \mathbf{0} \quad \text{on } \Gamma_D, \\ \underline{\sigma}(\widetilde{\mathbf{u}})\mathbf{n} &= \mathbf{0} \quad \text{on } \Gamma_N, \\ [\![\widetilde{\mathbf{u}}]\!] &= \mathbf{0} \quad \text{on } \Gamma_t, \\ [\![\underline{\sigma}(\widetilde{\mathbf{u}})\mathbf{n}_t]\!] &= \mathbf{0} \quad \text{on } \Gamma_t, \end{aligned} \tag{3.6}$$

Now we know that the displacement $\mathbf{v}_t$ can be written in a form of a double layer potential, as in [5] and [50]: for any $\mathbf{y} \in \partial\Omega$

$$\mathbf{v}_t(\mathbf{y}) = \int_{\Gamma_t} \mathbf{D}\underline{\epsilon}(\mathbf{N}(\mathbf{x}, \mathbf{y}))\mathbf{n}_t \cdot \mathbf{q}_t \, \mathrm{d}\sigma(\mathbf{x}) =$$

$$= \int_0^1 \mathbf{D}\underline{\epsilon}(\mathbf{N}((1-s)P_t + sQ_t, \mathbf{y}))\mathbf{n}_t \cdot \mathbf{q}_t \, |Q_t - P_t| \mathrm{d}s, \tag{3.7}$$

where $\mathbf{N}(\cdot, \mathbf{y})$ is the Neumann function related to the elastic problem (3.5) with homogeneous mixed boundary conditions. We also define $\boldsymbol{\tau}_t = \frac{Q_t - P_t}{|Q_t - P_t|}$ as the unit tangent vector field to the segment Γ_t and $\mathbf{n}_t = \boldsymbol{\tau}_t^{\perp}$ as the unit normal vector field.
On the other hand, $\widetilde{\mathbf{u}}$ is the solution of a linear elasticity problem with classic transmission conditions. Hence, $\widetilde{\mathbf{u}} \in \mathbf{H}^1(\Omega)$ and it does not depend neither on Γ_t nor on $\mathbf{q}_t$:

$$\frac{d}{dt}\widetilde{\mathbf{u}} = 0.$$

This implies that:

$$\mathbf{u}_t' = \frac{d}{dt}\mathbf{v}_t,$$

whose explicit form is provided in the following Lemma.

Lemma 11. *For any* $\boldsymbol{y} \in \partial\Omega$

$$\begin{aligned} \boldsymbol{u}_t'(\boldsymbol{y}) = &+ \int_0^1 \boldsymbol{D}\underline{\epsilon}(\boldsymbol{N}((1-s)P_t + sQ_t, \boldsymbol{y}))\boldsymbol{n}_t \cdot (\boldsymbol{q}_1 - \boldsymbol{q}_0)(|Q_t - P_t|)ds \\ &+ \boldsymbol{D}\underline{\epsilon}(\boldsymbol{N}(Q_t, \boldsymbol{y})) \; (\; ((Q_1 - Q_0) \cdot \boldsymbol{\tau}_t)\boldsymbol{n}_t - \; ((Q_1 - Q_0) \cdot \boldsymbol{n}_t)\boldsymbol{\tau}_t \;) \cdot \boldsymbol{q}_t \\ &- \boldsymbol{D}\underline{\epsilon}(\boldsymbol{N}(P_t, \boldsymbol{y})) \; (\; ((P_1 - P_0) \cdot \boldsymbol{\tau}_t)\boldsymbol{n}_t - ((P_1 - P_0) \cdot \boldsymbol{n}_t)\boldsymbol{\tau}_t \;) \cdot \boldsymbol{q}_t. \end{aligned} \tag{3.8}$$

Proof. Taking the derivative of $\mathbf{v}_t$ defined in (3.7), we have:

$$\begin{aligned}\mathbf{u}_t'(\mathbf{y}) = &\int_0^1 \Big(\frac{d}{dt}\mathbf{D}\underline{\epsilon}(\mathbf{N}((1-s)P_t+sQ_t,\mathbf{y}))\Big)\mathbf{n}_t\cdot\mathbf{q}_t|Q_t-P_t|\ \mathrm{d}s\\ &+\int_0^1 \mathbf{D}\underline{\epsilon}(\mathbf{N}((1-s)P_t+sQ_t,\mathbf{y}))\mathbf{n}_t\cdot\frac{d}{dt}(\mathbf{q}_t|Q_t-P_t|)ds\\ &+\int_0^1 \mathbf{D}\underline{\epsilon}(\mathbf{N}((1-s)P_t+sQ_t,\mathbf{y}))\Big(\frac{d\mathbf{n}_t}{dt}\Big)\cdot\mathbf{q}_t|Q_t-P_t|\mathrm{d}s\\ &:= I_1+I_2+I_3. \end{aligned}\tag{3.9}$$

Following the proof in [5], we obtain:

$$\begin{aligned}I_1 = &\mathbf{D}\underline{\epsilon}(\mathbf{N}(Q_t,\mathbf{y}))(A_t(1)\mathbf{n}_t-B_t(1)\boldsymbol{\tau}_t)\cdot\mathbf{q}_t\\ &-\mathbf{D}\underline{\epsilon}(\mathbf{N}(P_t,\mathbf{y}))(A_t(0)\mathbf{n}_t-B_t(0)\boldsymbol{\tau}_t)\cdot\mathbf{q}_t\\ &-\int_0^1\mathbf{D}\underline{\epsilon}(\mathbf{N}((1-s)P_t+sQ_t,\mathbf{y}))\frac{d}{ds}(A_t(s)\mathbf{n}_t\cdot\mathbf{q}_t-B_t(s)\boldsymbol{\tau}_t\cdot\mathbf{q}_t)\mathrm{d}s,\end{aligned}\tag{3.10}$$

where

$$A_t(1)=(Q_1-Q_0)\cdot\boldsymbol{\tau}_t,\quad A_t(0)=(P_1-P_0)\cdot\boldsymbol{\tau}_t,$$

$$B_t(1)=(Q_1-Q_0)\cdot\mathbf{n}_t,\quad B_t(0)=(P_1-P_0)\cdot\mathbf{n}_t,$$

$$\frac{d}{ds}(A_t(s)\mathbf{n}_t\cdot\mathbf{q}_t-B_t(s)\boldsymbol{\tau}_t\cdot\mathbf{q}_t)=\Big(((Q_1-Q_0)-(P_1-P_0))\cdot\boldsymbol{\tau}_t)\mathbf{n}_t-((Q_1-Q_0)-(P_1-P_0))\cdot\mathbf{n}_t)\boldsymbol{\tau}_t\Big)\cdot\mathbf{q}_t.$$

For the term I_2, note that

$$\int_0^1\mathbf{D}\underline{\epsilon}(\mathbf{N}((1-s)P_t+sQ_t,y))\mathbf{n}_t\cdot\frac{d}{dt}(\mathbf{q}_t|Q_t-P_t|)\mathrm{d}s=$$

$$=\int_0^1\mathbf{D}\underline{\epsilon}(\mathbf{N}((1-s)P_t+sQ_t,y))\mathbf{n}_t\cdot\frac{d}{dt}((t\mathbf{q}_1+(1-t)\mathbf{q}_0)|Q_t-P_t|)\mathrm{d}s=$$

$$=\int_0^1\mathbf{D}\underline{\epsilon}(\mathbf{N}((1-s)P_t+sQ_t,\mathbf{y}))\mathbf{n}_t\cdot\Big(\mathbf{q}_t\frac{d}{dt}(|Q_t-P_t|)+(\mathbf{q}_1-\mathbf{q}_0)(|Q_t-P_t|)\Big)\mathrm{d}s=$$

$$=\int_0^1\mathbf{D}\underline{\epsilon}(\mathbf{N}((1-s)P_t+sQ_t,\mathbf{y}))\mathbf{n}_t\cdot\Big(\mathbf{q}_t(((Q_1-Q_0)-(P_1-P_0))\cdot\boldsymbol{\tau}_t)+(\mathbf{q}_1-\mathbf{q}_0)(|Q_t-P_t|)\Big)\mathrm{d}s.$$

Finally, it is easy to show that

$$\frac{d\mathbf{n}_t}{dt}=-\Big(\frac{(Q_1-Q_0)-(P_1-P_0)}{|Q_t-P_t|}\cdot\mathbf{n}_t\Big)\boldsymbol{\tau}_t,$$

and we get:

$$I_3 = -\int_0^1 \mathbf{D}\underline{\epsilon}(\mathbf{N}((1-s)P_t + sQ_t, \mathbf{y}))\boldsymbol{\tau}_t \cdot \mathbf{q}_t\Big((Q_1 - Q_0) - (P_1 - P_0)\Big) \cdot \mathbf{n}_t \, \mathrm{d}s.$$

Summing up all the results for I_1, I_2 and I_3, the proof is complete.

□

Now we have to show that the Gateaux derivative in Lemma 11 is continuous, so that it coincides with the Fréchet derivative (cf [51] and [52]) which will be continuous as well. If we next prove that this derivative is also injective, then we can apply Theorem 6.

Lemma 12. *For a fixed $\boldsymbol{y}$ on $\partial\Omega$, the map F: $(P_t, Q_t, \boldsymbol{q}_t) \to \boldsymbol{u}'_t(\boldsymbol{y})$, as defined in Lemma 11, is continuous.*

Proof. The proof is trivial because we can exploit the result of local regularity for the Neumann function. By fixing $\mathbf{y}$ on $\partial\Omega$, $\mathbf{N}(\cdot, \mathbf{y})$ is the weak solution of a homogeneous elliptic problem with constant coefficients and mixed boundary conditions, i.e.:

$$\begin{aligned} -\nabla \cdot \mathbf{D}\underline{\epsilon}(\mathbf{N}(\cdot, \mathbf{y})) &= \mathbf{0} \quad \text{in } \Omega, \\ \mathbf{N}(\cdot, \mathbf{y}) &= \mathbf{0} \quad \text{on } \Gamma_D, \\ \underline{\sigma}(\mathbf{N}(\cdot, \mathbf{y}))\mathbf{n} &= \mathbf{0} \quad \text{on } \Gamma_N, \end{aligned} \tag{3.11}$$

and so it is locally C^∞. We perturb the position of the fault and of the constant slip field and we use the linearity of the integrals in the slip and the regularity of the Neumann function to obtain the continuity of $\mathbf{u}'_t(\mathbf{y})$. This means that small perturbations of both the slip field and the fault correspond to small variation of $\mathbf{u}'_t(\mathbf{y})$, i.e.:
$\forall\ \epsilon > 0\ \exists\ \delta P_t, \delta Q_t, \delta \mathbf{q}_t$ such that

$$|F(P_t + \delta P_t, Q_t + \delta Q_t, \mathbf{q}_t + \delta \mathbf{q}_t) - F(P_t, Q_t, \mathbf{q}_t)| < \epsilon.$$

□

We are left to show that the Frèchet derivative is injective.

Lemma 13. *(Uniqueness). For a fixed $\boldsymbol{y}$ on $\partial\Omega$ and a fixed configuration for $t = t_0 \in (0, 1)$, the map $F : (P_{t_0}, Q_{t_0}, \boldsymbol{q}_{t_0}) \to \boldsymbol{u}'_t(\boldsymbol{y})|_{t=t_0}$ is injective.*

Proof. Let us define $\mathbf{V} = (\mathbf{V}_1, \mathbf{V}_2, \mathbf{V}_3)$ with $\mathbf{V}_1 = P_1 - P_0, \mathbf{V}_2 = Q_1 - Q_0, \mathbf{V}_3 = \mathbf{q}_1 - \mathbf{q}_0$ the directions of the Frèchet derivative, so that $F(P_{t_0}, Q_{t_0}, \mathbf{q}_{t_0})[\mathbf{V}] = \mathbf{u}'_t(\mathbf{y})|_{t=t_0}$. We can

exploit the linearity of the Frèchet derivative, so that it is sufficient to prove that $F[\mathbf{V}]= \mathbf{0} \Rightarrow \mathbf{V} = \mathbf{0}$ in order to obtain the injectivity property. This means that if $\mathbf{u}'_t(\mathbf{y})|_{t=t_0} = \mathbf{0}$ for some $\mathbf{y}$ on $\partial\Omega$, we want to show that $P_1 = P_0, Q_1 = Q_0$ and $\mathbf{q}_1 = \mathbf{q}_0$. On the other hand, we also derive from the representation of $\mathbf{u}'_t$ and the properties of $\mathbf{N}$ that the derivative of the elastic displacement satisfies the problem:

$$-\nabla \cdot \mathbf{D}\underline{\epsilon}(\mathbf{u}'_t) = \mathbf{0} \quad \text{in } \Omega \setminus \overline{\Gamma_t},$$

$$\underline{\sigma}(\mathbf{u}'_t(\mathbf{y}))\mathbf{n} = \mathbf{0} \quad \text{on}\Gamma_N,$$

which implies by the unique continuation property for elliptic operators:

$$\mathbf{u}'_t = \mathbf{0} \quad \text{in } \Omega \setminus \overline{\Gamma}_t.$$

This means that, for all $\mathbf{y} \in \Omega \setminus \overline{\Gamma}_t$

$$\begin{aligned}\mathbf{u}'_t(\mathbf{y}) = &+ \int_0^1 \mathbf{D}\underline{\epsilon}(\mathbf{N}((1-s)P_t + sQ_t, \mathbf{y}))\mathbf{n}_t \cdot (\mathbf{q}_1 - \mathbf{q}_0)(|Q_t - P_t|)\mathrm{d}s \\ &+ \mathbf{D}\underline{\epsilon}(\mathbf{N}(Q_t, \mathbf{y}))\ (\ ((Q_1 - Q_0)\cdot\boldsymbol{\tau}_t)\mathbf{n}_t - \ ((Q_1 - Q_0)\cdot\mathbf{n}_t)\boldsymbol{\tau}_t\ )\cdot\mathbf{q}_t \\ &- \mathbf{D}\underline{\epsilon}(\mathbf{N}(P_t, \mathbf{y}))\ (\ ((P_1 - P_0)\cdot\boldsymbol{\tau}_t)\mathbf{n}_t - ((P_1 - P_0)\cdot\mathbf{n}_t)\boldsymbol{\tau}_t\ )\cdot\mathbf{q}_t. \\ &= I_1 + I_2 + I_3 = \mathbf{0}. \end{aligned} \tag{3.12}$$

We know that for the second and the third term it has to be $Q_1 = Q_0$ and $P_1 = P_0$, otherwise we will get confliction since these terms would blow up, while the derivative must be zero. Therefore, we get $I_2 = I_3 = \mathbf{0}$.
Note that but by the well-know regularity results for elliptic systems (cf. [47]), we have

$$\mathbf{N}(\mathbf{x}, \mathbf{y}) = \boldsymbol{\Gamma}(\mathbf{x}, \mathbf{y}) + \boldsymbol{\omega}(\mathbf{x}, \mathbf{y}),$$

where $\boldsymbol{\omega}$ is a smooth function and $\boldsymbol{\Gamma}(\mathbf{x}, \mathbf{y})$ is the fundamental free space solution of $\nabla \cdot (\mathbf{D}\underline{\epsilon}(\cdot))$. Now, exploiting the fact that $(\mathbf{q}_1, \mathbf{q}_0)$ and $|Q_t - P_t|$ are constant quantities along Γ_t, we can write I_1 as:

$$\int_0^1 \mathbf{D}\underline{\epsilon}(\mathbf{N}((1-s)P_t + sQ_t, \mathbf{y}))\mathbf{n}_t \cdot (\mathbf{q}_1 - \mathbf{q}_0)(|Q_t - P_t|)\mathrm{d}s =$$

$$\left(\int_0^1 \mathbf{D}\underline{\epsilon}(\boldsymbol{\Gamma}((1-s)P_t + sQ_t, \mathbf{y}) - \boldsymbol{\omega}((1-s)P_t + sQ_t, \mathbf{y}))\mathbf{n}_t \mathrm{d}s \right) \cdot (\mathbf{q}_1 - \mathbf{q}_0)(|Q_t - P_t|)$$

The fundamental solution is known and the integral of its traction along Γ_t can be

explicitly calculated, using symbolic computing software (e.g. Mathematica by Wolfram). One can see that logarithmic singularities at the tips of the segment appear, so again the only way the Frèchet derivative to be zero is to require $Q_1 = Q_0, P_1 = P_0$ and $\mathbf{q}_1 = \mathbf{q}_0$. □

Summarizing the results, we have showed that all the hypotheses of Theorem 6 are satisfied in our setting. Thus we can state a theorem for the Lipschitz stability applied in our context.

Theorem 7. *(Lipschitz stability). Let Γ_1 and Γ_2 be two segments satisfying **Assumption 2** and suppose that **Assumptions 1, 3, 4, 5** are verified. Let $\boldsymbol{u}_{\Gamma_1}^{\boldsymbol{q}_1}$ and $\boldsymbol{u}_{\Gamma_2}^{\boldsymbol{q}_2}$ be the functions satisfying (3.1), where Γ is replaced by Γ_1 and Γ_2, respectively, and $\boldsymbol{q}_0$ by $\boldsymbol{q}_1$ and $\boldsymbol{q}_2$. Then there exists a constant C such that:*

$$d_{\mathcal{H}}(\Gamma_1, \Gamma_2) + |\boldsymbol{q}_1 - \boldsymbol{q}_2| \leq C||\boldsymbol{u}_{\Gamma_1}^{\boldsymbol{q}_1} - \boldsymbol{u}_{\Gamma_2}^{\boldsymbol{q}_2}||_{L^2(\Sigma)},$$

where Σ is an open subset of Γ_N.
Here $\delta_{\mathcal{H}}$ denotes the Hausdorff distance:

$$d_{\mathcal{H}}(\Gamma_1, \Gamma_2) = \min\{\max\{|P_1 - P_2|, |Q_1 - Q_2|\}, \max\{|P_1 - Q_2|, |Q_1 - P_2|\}\},$$

where P_1, Q_1 and P_2, Q_2 are the endpoints of Γ_1 and Γ_2 respectively.

All the properties of the map T allow us to regularize the problem and make it well-posed. We are now ready to construct an algorithm to solve the *inverse* map T^{-1}, being sure that the result will be physical relevant and will not cause oscillations.

3.2 Numerical approximation of the inverse problem

A possible way to solve the *inverse* problem would be to write the solution $\mathbf{u}_\Gamma$ of the problem in (3.1) explicitly as a function of the slip field and the fault Γ in a similar way to the decomposition in (3.4):

$$\mathbf{u}_\Gamma = \mathbf{u}_0 + \mathbf{w}. \tag{3.13}$$

The displacement $\mathbf{u}_0$ in (3.13) is defined as a double layer potential on Γ, through the Neumann function associated to the elasticity tensor in the free space, so that it satisfies:

$[\![\mathbf{u}_0]\!]_{|\Gamma} = \mathbf{q}_0$ and $[\![\underline{\sigma}(\mathbf{u}_0)\mathbf{n}]\!]_{|\Gamma} = \mathbf{0}$. The function $\mathbf{w}$ in (3.13) would be a regular correction term to take into account the given source $\mathbf{f}$ and the mixed boundary conditions in (3.1).

However, this approach would lead us to a highly complicated system of integral equations to determine the slip field and the position of the fault.
We will implement instead a Tikhonov-type algorithm to generate a numerical reconstruction of the fault geometry and slip field from a finite number of surface measurements. The key idea behind the Tikhonov method (see cf. [53] and [54]), that is a common method of regularization for ill-posed problems, is to directly incorporate *a-priori* information penalizing the misfit functional with an additional term. In particular, the Tikhonov regularized estimate is defined as the solution to the following minimization problem:

$$\mathcal{F}_{TIK}(\beta) = \text{argmin}_{\mathbf{u}} ||\widetilde{\mathbf{u}} - \mathbf{u}||_2^2 + \beta^2 ||R\mathbf{u}||_2^2, \tag{3.14}$$

where in our case $\mathbf{u}$ is the elastic displacement solving (3.1) and $\widetilde{\mathbf{u}}$ are the available measurements on Σ, i.e. $\widetilde{\mathbf{u}} = \mathbf{u}|_\Sigma$. The first term in (3.14) is the same $\mathbf{L}^2$ residual norm appearing in the least-squares approach and ensures fidelity to data, becuase it minimizes the distance in average between the measured datum and the real solution. The operator R of the second term in (3.14) is called the "regularizer" or "side constraint" and captures *a-priori* knowledge about the expected behavior of $\mathbf{u}$ through an additional penalty term. If no additional regularity is assumed (that is, if β or R is zero) then we can minimize $\mathcal{F}_{TIK}$ to zero easily, but then the solution is highly oscillatory, locally very large and usually has no physical relevance, because of the instability of the inverse problem. Common choices for the regularizing operator R include discrete approximations of the surface gradient or Laplacian operators, forcing solutions with limited high-frequency energy and thus capturing *a-priori* belief that solution should be smooth. The parameter α acts like a Lagrangian multiplier and controls the trade-off between the two terms, see for instance [55].
However, in our context, we have already regularized the ill-posed *inverse* problem, restricting the set of unknowns to a finite dimensional set and proving a Lipschitz stability. Therefore, the functional to be minimized is the following:

$$F = \min \int_\Sigma |\widetilde{\mathbf{u}} - \mathbf{u}(\Gamma, \mathbf{q}_0)|^2 \, \mathrm{d}\mathbf{s}, \tag{3.15}$$

where Γ and $\mathbf{q}_0$ are the fault and the slip field we want to determine, respectively, with the constraint that Γ is a segment and $\mathbf{q}_0$ is constant.
Before discussing the numerical scheme that we will employ to solve the optimization

problem in (3.15), it will be necessary to discretize the data we are provided with, following some hints from the algorithm presented in [56], [57] and [58].

3.3 Parameterization and discretization of the data

First, let us consider a square domain $\Omega \subset \mathbb{R}^2$, where we define the bottom edge as a Dirichlet boundary Γ_D and the Neumann boundary as the union of the remaining faces, i.e. $\Gamma_N = \partial\Omega \setminus \Gamma_D$. Let us denote by $\mathbf{P}_j, j = 1, ...N$ the points, as in Figure 3.2, that belong to the surface $\Sigma \subset \Gamma_N$, where displacement measurements $\tilde{\mathbf{u}}_j$ on the points $\mathbf{P}_j$ are available. Assume that Γ is a linear crack, dividing the domain Ω into two sub-regions. To uniquely determine the position of the fault, we define two parameters:
1: d is the distance between the intersection of the fault with the left side of the domain and the bottom edge Γ_D, as shown in Figure 3.2;
2: θ is the angle of the inclination of the fault, measured with respect to the direction of Γ_D, represented by the dashed line in Figure 3.2.

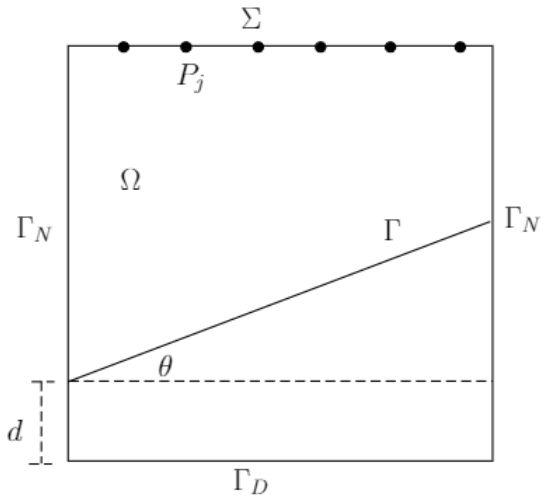

Figure 3.2: Parameterization of the fault position and displacement measurements on the boundary Σ.

Now, for a fixed fault Γ defined through the pair (d, θ), we introduce the functional:

$$F_{d,\theta}(\mathbf{q}_0) = (\sum_{j=1}^{N} |\tilde{\mathbf{u}}_j - \ \mathbf{u}(P_j)|^2)/(\sum_{j=1}^{N} |\tilde{\mathbf{u}}_j|^2), \tag{3.16}$$

that is the discrete analogue of (3.15). Next we define $\mathcal{C}$ the set of admissible slip fields, namely all the functions $\mathbf{q}_0$ piecewise constant or piecewise linear, i.e.

$$\mathbf{q}_0 = (a_{11}x + a_{12}y + b_1, a_{21}x + a_{22}y + b_2)^T = A\mathbf{x} + \mathbf{b}, \tag{3.17}$$

where we have used the following definition:

$$A = \begin{pmatrix} a_{11} & a_{12} \\ a_{21} & a_{22} \end{pmatrix}, \qquad \mathbf{x} = \begin{pmatrix} x \\ y \end{pmatrix}, \qquad \mathbf{b} = \begin{pmatrix} b_1 \\ b_2 \end{pmatrix}.$$

In both cases, we assume that the slip field is null on the endpoints of Γ. Note that we did not prove rigorously the Lipschtiz stability for the case of piecewise linear slip fields, but we expect that it holds true also in this case.
Now we have all the discrete data and the ingredients to define a reconstruction algorithm.

3.4 Reconstruction and genetic algorithms

The idea is to use an iterative algorithm that first, given a linear crack, minimizes the functional $F_{d,\theta}$ on all the possible slip fields $\mathbf{q}_0$ of the admissible configurations $\mathcal{C}$.
Then, given the new coefficients for the linear slip field A and $\mathbf{b}$, we minimize the same functional over the fault and we update the values of d and θ. The algorithm is iterative and it ends when the value of the objective function is less or equal than a tolerance, cf. Algorithm 1.

Note that in Step 1 and 3 of Algorithm 1, we have introduced the class of "genetic algorithms", that are methods for solving approximately both constrained and unconstrained optimization problems and are based on natural selection, i.e. the process that drives biological evolution. Genetic algorithms repeatedly modify a population of individual solutions. At each step, the method select *individuals* at random from the current population to be *parents* and uses them to produce the *children* for the next generation. Over successive generations, the population "evolves" toward an optimal solution. Genetic

Algorithm 1: Inverse problem

Result: Determine the slip field $\mathbf{q}_0$ and the position of the fault Γ.
Start from some initial guess for d, θ;
while $F_{d,\theta}(\mathbf{q}_0) > tol$ **do**
1. *Compute*

$$f(d,\theta) = inf_{\mathbf{q}_0 \in C} F_{d,\theta}(\mathbf{q}_0),$$

using a genetic algorithm;
2. *update the slip field* $\boldsymbol{q}_0$ *with* $A, \boldsymbol{b}$*;*
3. *compute*

$$inf_{d,\theta} f(d,\theta)$$

using a genetic algorithm;
4. *update* d, θ*;*

end

algorithms differ from a classical, derivative-based, optimization algorithms because they generate a population of points instead of a single point at each iteration such that the best point in the population approaches an optimal solution.

Before reporting some computational tests of Algorithm 1, we briefly explain how this class of algorithms works in practice. We call *fitness function* the function that has to be minimized and an *individual* any point to which you can apply the fitness function. The algorithm begins by creating a random initial *population*, which is an array of individuals, as shown in the Figure 3.3.

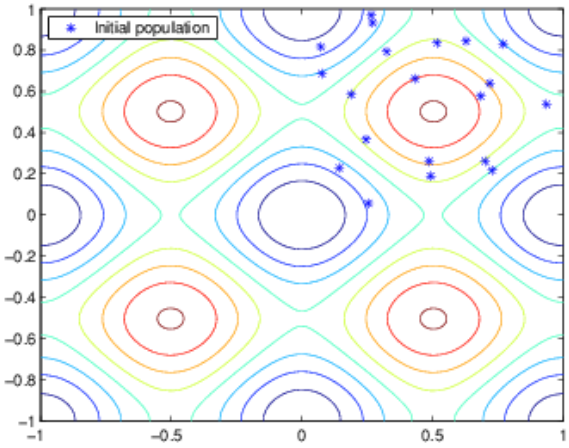

Figure 3.3: Random Initial Population. Example taken from [59].

Then at each iteration, the genetic algorithm performs a series of computations on the current population, called *parents*, and uses them to create individuals in the next generation, called *children*. Typically, there are three main types of rules that are used to create the next generation from the current population:

- *Elite* are the individuals in the current generation with the best fitness values. These individuals automatically survive to the next generation.

- *Crossover* are created by combining the vectors of a pair of parents.

- *Mutation* children are created by introducing random changes, or mutations, to a single parent.

The schematic diagram in Figure 3.4 illustrates the three types of children.

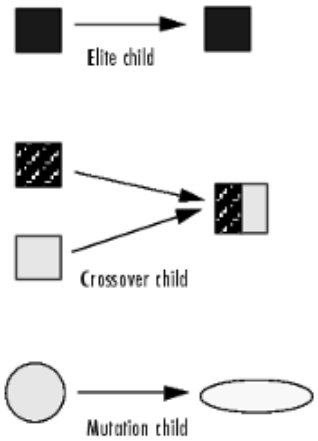

Figure 3.4: Types of children in genetic algorithms. Image taken from [59].

The algorithm creates *crossover* children by combining pairs of parents in the current population. At each coordinate of the child vector, the default crossover function randomly selects an entry, or *gene*, at the same coordinate from one of the two parents and assigns it to the child. The algorithm creates *mutation* children by randomly changing the *genes* of individual parents. Both processes are essential to the genetic algorithm. Crossover enables the algorithm to extract the best genes from different individuals and recombine them into potentially superior children. Mutation increases the diversity of a population and thereby the likelihood that the algorithm will generate individuals with better fitness values. Figure 3.5 shows the populations at iterations 60, 80, 95, and 100.

As the number of generations increases, the individuals in the population get closer together and approach the minimum point $(0, 0)$. Finally, there are several stopping criteria for the genetic algorithms which will be discussed in the next section, when presenting the numerical results.

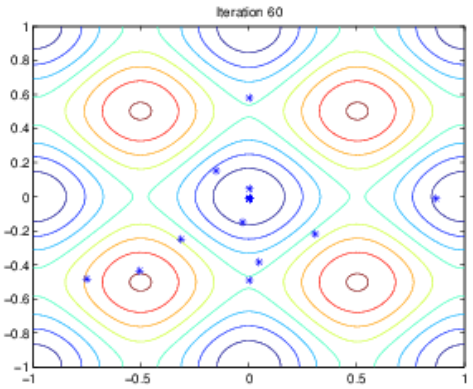

(a) Population after 60 iterations

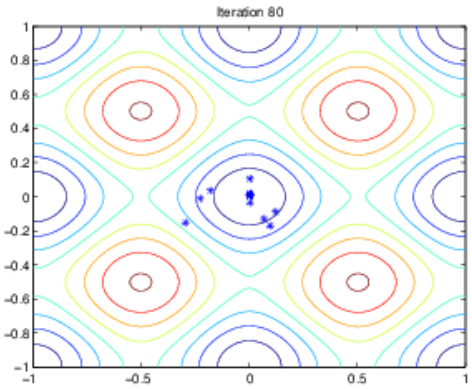

(b) Population after 80 iterations

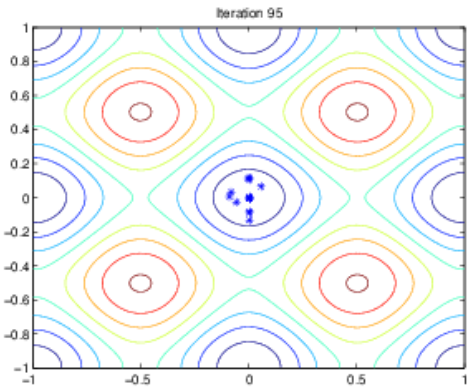

(c) Population after 95 iterations

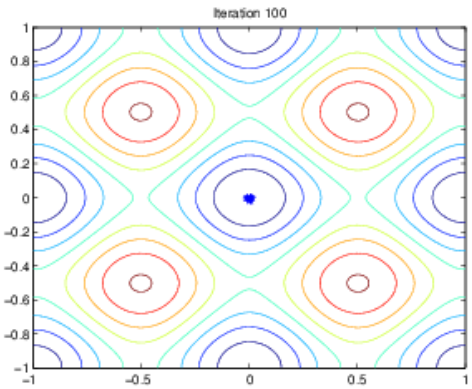

(d) Population after 100 iterations

Figure 3.5: Iterations of a genetic algorithm. Example taken from [59].

3.5 Numerical results

This last section is devoted to the presentation of some computational results with the aim of testing the performance of the proposed approach for the numerical discretization of the inverse problem.

In each example we will suppose to have a square domain $\Omega = (-1, 0) \times (0, 1)$, the crack Γ completely internal to the domain and $\Sigma = \{(x, y) \in \partial\Omega : y = 1\}$, that is the portion of the boundary where the measurements are available, as in Figure 3.2.

For the sake of simplicity, we will select slip fields that are linear only in the x-direction and we will always consider an horizontal fault, meaning that the inclination θ is equal to zero (cf. Figure 3.2). Considering the aforementioned assumptions and the fact that the problem is two dimensional, we will obtain five numbers for each example: (a_1, b_1, a_2, b_2, d), where a_1, b_1, a_2, b_2 are the coefficients of the slip field $(a_1x + b_1, a_2x + b_2)^T$

and d is the distance between the intersection of the fault with the left side of the domain and the bottom edge .

3.5.1 Example 1

In the first example we do not use the tool of the $forward\ problem$ for the data formation process, but we choose a manufactured solution in order to test the performance of the algorithm. We suppose that both the first and the second component of the elastic displacement are sinusoidal with a constant jump on the interface $\mathbf{q}_0 = (1, 3)^T$, null on the endpoints of Γ, and the fault located in $d = 0.7$.
In this thesis we employ the genetic algorithm available in the Matlab *optimization toolbox*. The algorithm terminates as soon as any one of these conditions is satisfied:
- *Generations*: the algorithm stops when the number of generations reaches a maximum value (user dependent).
- *Time limit*: the algorithm terminates whenever the computational time exceed a given value (user dependent).
-*Fitness limit*: the algorithm stops when the value of the fitness function for the best point in the current population is less than or equal to *Fitness limit* (user dependent).
Since the minimum value of the objective function is zero, we set the *Fitness limit* to $1e$-30 and we test the algorithm three times with an increasing number of generations as stopping criterion. In the first test we have used 100 as the maximum number of generations for the genetic algorithm with d as variable and 400 for the genetic algorithm with (a_1, b_1, a_2, b_2) as variables. In the second test we have chosen 150 and 700 generations as stopping criterion, respectively; finally we have analyzed the results with 300 and 1000 generations in the third test, as showed in Table 3.1.

	Max. Nr. of Generations for $f_{d,\theta}$	Max. Nr. of Generations for $F(\mathbf{q}_0)$
Test 1	100	400
Test 2	150	700
Test 3	300	1000

Table 3.1: Set-up of the stopping criterion.

The result it is showed in Table 3.2 and is very close with what we would expect.

Variables	Exact values	Test 1	Test 2	Test 3
a_1	0	0.003	0.001	0
b_1	1	0.997	0.999	1
a_2	0	0.009	0.003	0.001
b_2	3	3.009	3.008	3
d	0.7	0.699	0.702	0.7

Table 3.2: Example 1. Comparison between the exact parameters and the values computed with Algorithm 1.

In Figure 3.6, 3.7 and 3.8 we have an example of the performance of the genetic algorithm with the slip field as variable for the cost functional. The figures show the trend of the *best* and the *mean* fitness values as the number of generations increases. *Best* fitness refers to the fitness of the best individual in the current population. On the other hand, the *average* or the *mean* fitness is simply the mean of the fitness values across the entire population. At each generation the population changes and we get a new average population fitness. What we can clearly see in the plots is that *best* fitness tends to get better as the iterations proceed. This happens quickly at first and then slowing down as the algorithm finds better and better solutions that are harder to improve upon. The *mean* fitness is always less than (or equal to) the best fitness, and the difference between the two goes on decreasing over time.
In conclusion, it is evident the minimum value reached by the functional in the 3 different tests decreases considerably ($4e$-$4, 2.18e$-$7, 7.19e$-12) when we modify the stopping criterion *Generations*. This will allow us to have a better reconstruction.

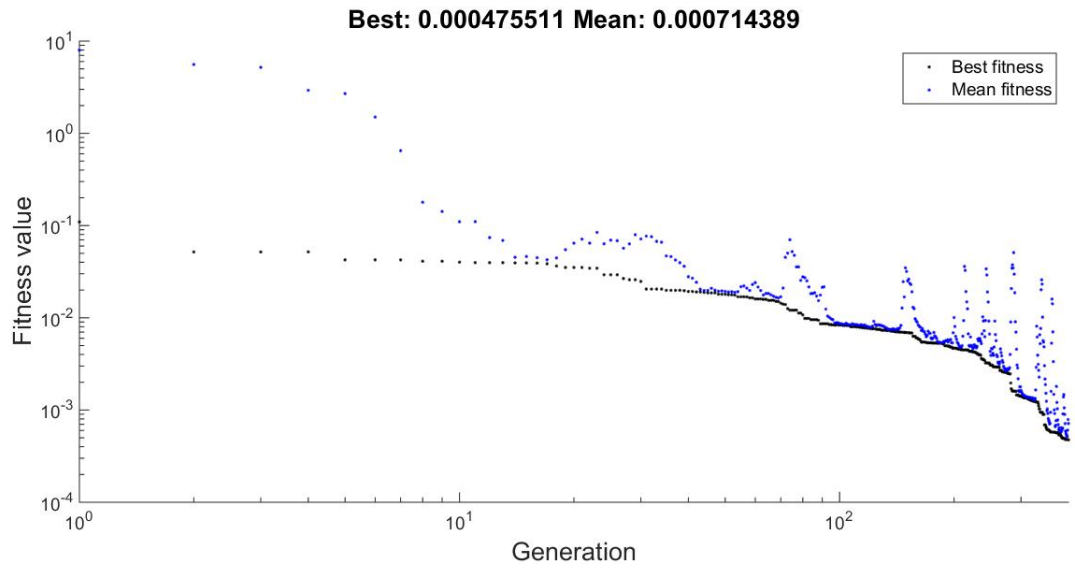

Figure 3.6: Example 1, Test 1: Fitness value versus generation (log-log scale).

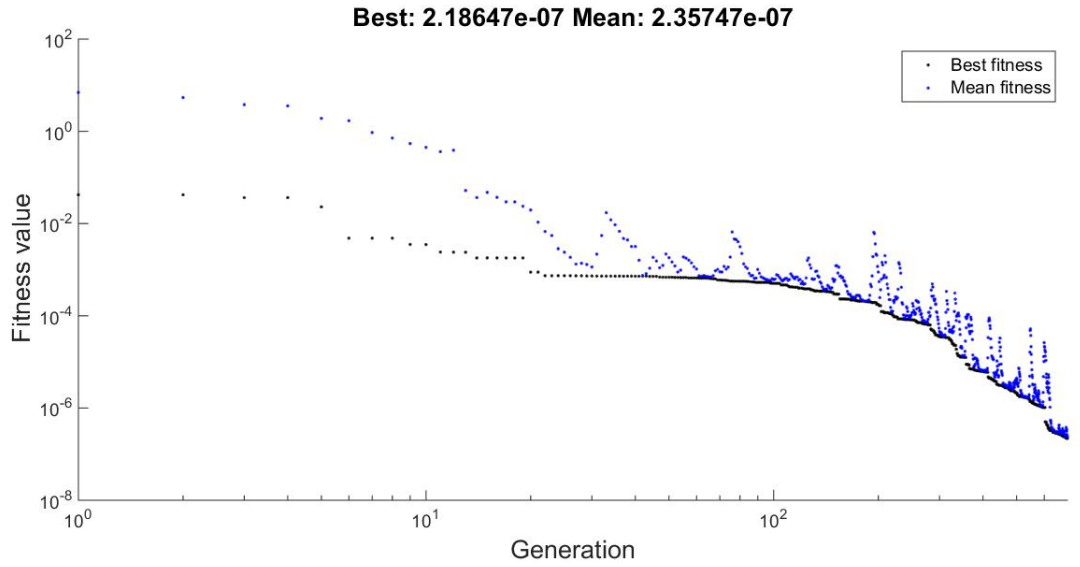

Figure 3.7: Example 1, Test 2: Fitness value versus generation (log-log scale).

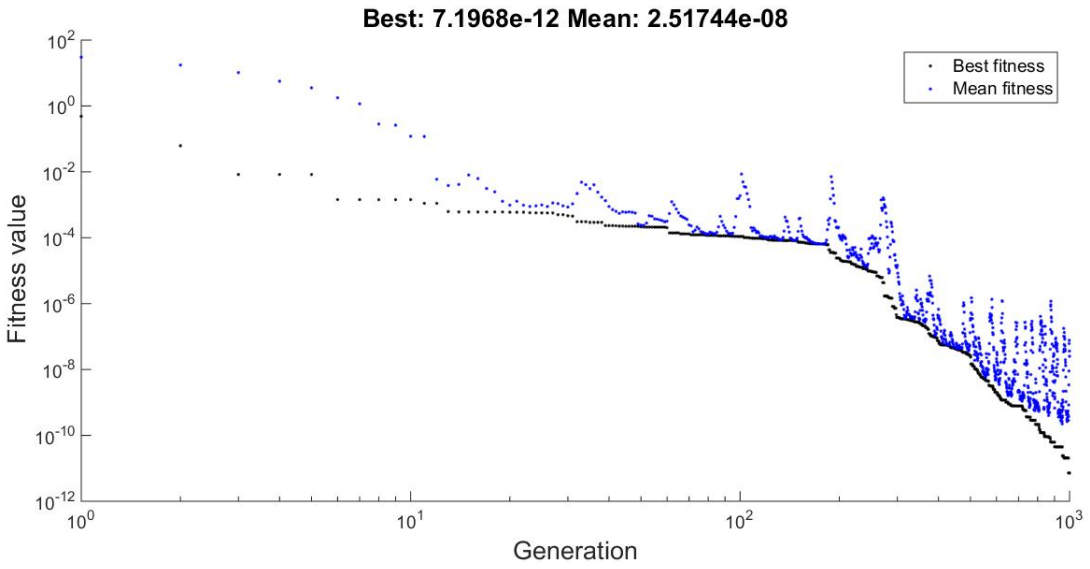

Figure 3.8: Example 1, Test 3: Fitness value versus generation (log-log scale).

We remind the reader that we employ a genetic algorithm twice in a single iteration of Algorithm 1, in order to find both the slip field and the position of the fault.
Thus, increasing the number of possible generations when performing a genetic algorithm does not lead to a growth of the number of iterations for Algorithm 1 as well. It is more likely that increasing the number of generations allows to have a higher precision and consequently, the tolerance is reached by the functional faster and Algorithm 1 stops earlier. Note that the results reported in the Table 3.2 and in Figure 3.6, 3.7 and 3.8 refer to the last iteration of Algorithm 1.

3.5.2 Example 2

In the second example, we still choose a manufactured solution but with a linear slip field $\mathbf{q}_0 = (2x + 1, 3x + 5)^T$, null on the endpoints of Γ, and the fault located in $d = 0.5$. We test the algorithm, for three different set-up of the maximum number of generations, cf. Table 3.3. The computed values of the parameters a_1, b_1, a_2, b_2, d are shown in Table 3.4. In Figure 3.9, 3.10 and 3.11 we report the trend of the *best* and *mean* fitness values as a function of the generations number. Again it is evident that we achieve a better value of the objective function as we increase the stopping criterion of *Generations*: the best values found are: $4.17e\text{-}08, 3.5e\text{-}10, 4.95e\text{-}13$ which correspond to a different maximum number of generations in the three tests: $400, 700, 900$.

	Max. Nr. of Generations for $f_{d,\theta}$	Max. Nr. of Generations for $F(\mathbf{q}_0)$
Test 1	50	400
Test 2	100	700
Test 3	300	900

Table 3.3: Set-up of the stopping criterion.

Variables	Exact values	Test 1	Test 2	Test 3
a_1	2	2.242	2.005	2
b_1	1	0.844	0.996	1
a_2	3	2.899	2.997	3
b_2	5	4.981	5.002	5
d	0.5	0.499	0.5	0.5

Table 3.4: Example 2. Comparison between the exact parameters and the values computed with Algorithm 1.

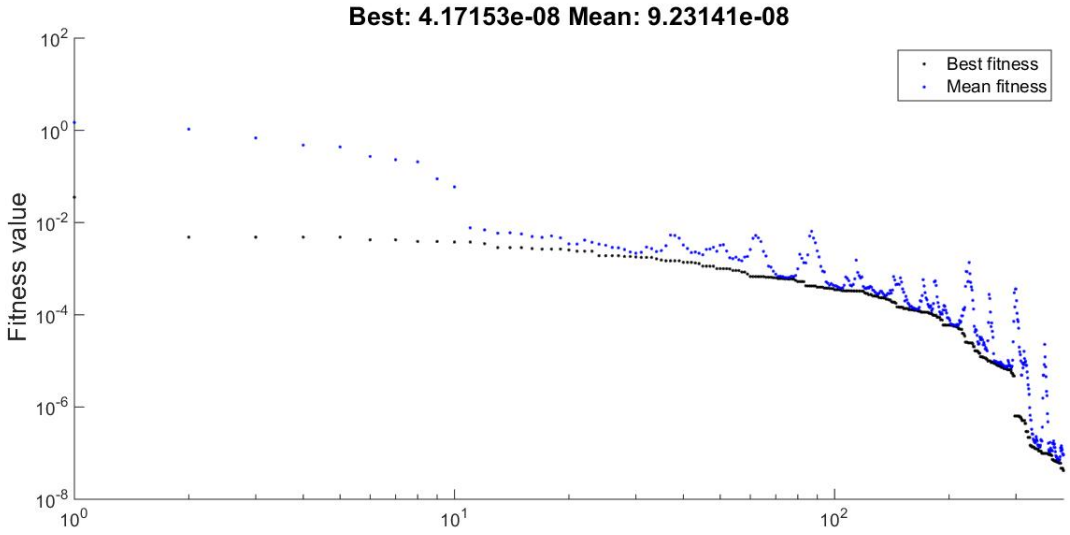

Figure 3.9: Example 2, Test 1: Fitness value versus generation (log-log scale).

3.5.3 Example 3

Finally, in the third example, we use the data coming from the resolution of the *forward problem*. Suppose that we are provided with an external load $\mathbf{f}$ and that we have homogeneous Dirichlet and Neumann boundary conditions, a piecewise constant slip field on Γ, e.g. $\mathbf{q}_0 = (3, 7)^T$ and null on the endpoints of Γ, and the crack position,

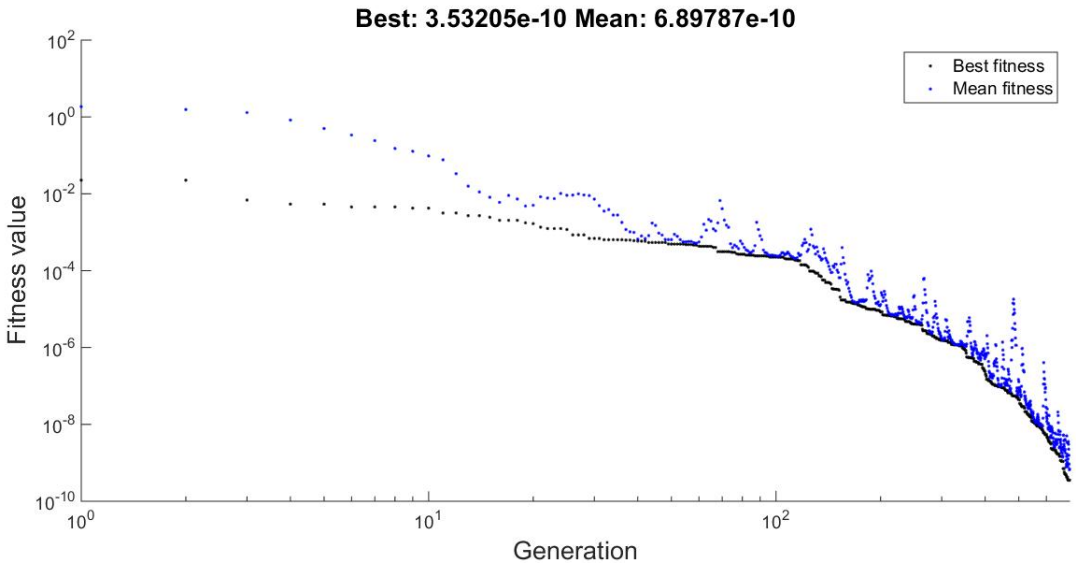

Figure 3.10: Example 2, Test 2: Fitness value versus generation (log-log scale).

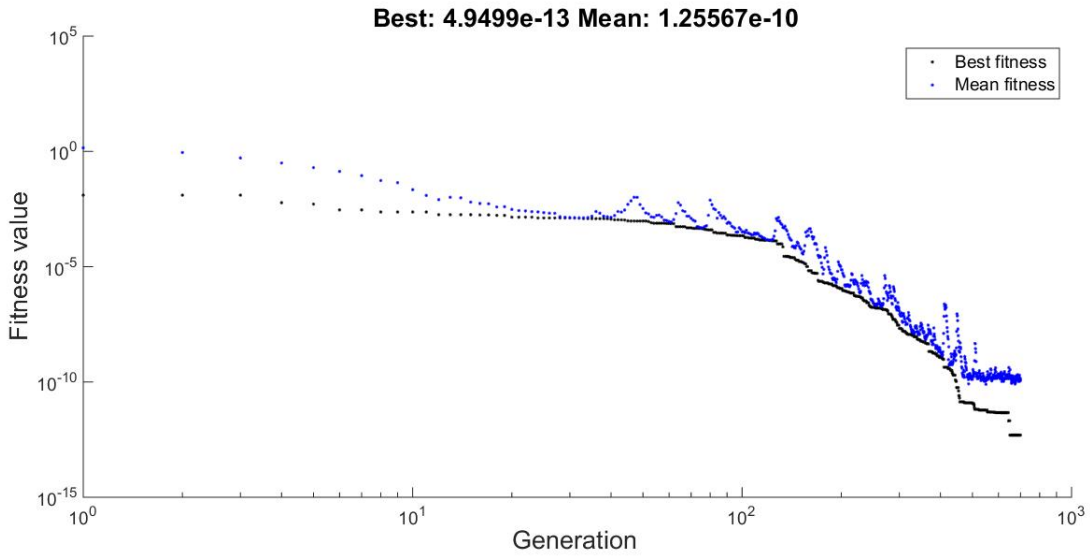

Figure 3.11: Example 2, Test 3: Fitness value versus generation (log-log scale).

e.g. $d = 0.2$. We do not know the analytical expression of the true solution, but we let the Discontinuous Galerkin algorithm solve the Lamè system in order to obtain the first and the second component of the numerical displacement, as showed in Figure 3.12.

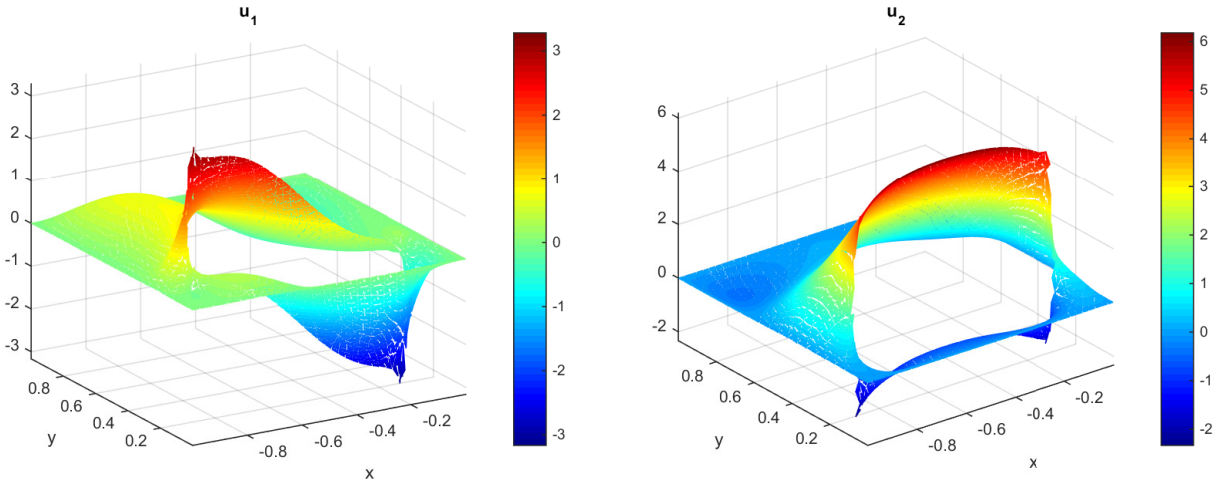

(a) First component of the solution u_1. **(b)** Second component of the solution u_2.

Figure 3.12: Example 3. Plot of the computed solution on a grid with granularity $h = 0.0135$ (3 levels of refinement).

Now we are able to select the values of the elastic displacement on Σ from the vector solution but on a coarser, as we were taking measurements on a portion of the Earth's crust. Then, we use the data of the *forward problem* in the reconstruction Algorithm 1 with a set-up of the generations as in Table 3.5. The result that we obtain is quite accurate and is reported in Table 3.6.

	Max. Nr. of Generations for $f_{d,\theta}$	Max. Nr. of Generations for $F(\mathbf{q}_0)$
Test 1	200	400
Test 2	300	800
Test 3	400	1200

Table 3.5: Set-up of the stopping criterion.

Variables	Exact values	Test 1	Test 2	Test 3
a_1	0	0.003	0.001	0
b_1	3	2.887	3.999	3
a_2	0	0.118	0.001	0
b_2	7	7.189	7.001	7
d	0.2	0.199	0.2	0.2

Table 3.6: Example 3. Comparison between the exact parameters and the values computed with Algorithm 1.

Chapter 4

Conclusions

In the first part of this work, we investigated the elastostatic equations in a two dimensional setting. The PDEs sytem is applied to Lipschitiz and bounded domains that can be either homogeneous and without cracks or heterogeneous (i.e. Lamè coefficient are not necessarily uniform inside the body) and can present a fault, where interface conditions are applied. On one hand, we supposed suitable hypotheses on the regularity of the data, i.e. the source term, the Cauchy stress tensor, the boundary conditions and the slip field for the interface problem, and we analyzed the well-posedness of both the models from an analytical point of view. On the other hand, from a numerical point of view, we proposed and studied a discontinuous Galerkin finite element method, that is the most natural choice when dealing with cracks phenomena. We proved the well-posedness of the resulting schemes and an *a-priori* error estimate that take into account the local regularity of the exact solution. In both cases we were able to recover an optimal bound in the mesh size of the computational domain and a sub-optimal bound in the local approximation degree, when the error is measured in a suitable energy norm. The sharpness of our theoretical analysis has been confirmed by the numerical experiments carried on simplified test cases with manufactured solutions. However, the two methods seem to be robust and stable and can be employed in cases of practical interest, such as in the earthquake modeling and in the analysis of the slip conditions between subduction zones.

To the same aim of simulating seismic scenarios, the second part of the thesis is devoted to an accurate study of the inverse problem, that is the determination of the fault position and the slip on the fault from surface measurements of the elastic displacement in a homogeneous body. In particular, we established uniqueness and we mitigated the

ill-posedness of the inverse problem, by supposing the fault to be a segment inside the medium and the slip to be a constant field. These *a-priori* assumptions allowed us to prove a Lipschitz stability starting from a theorem of functional analysis. As a result, we were able to develop an iterative Tikhonov algorithm for the reconstruction of the unknown parameters, being sure that the result would have been physically relevant and not oscillatory. Indeed, this was confirmed by our numerical experiments.

Concerning the future works, the natural continuation of this thesis is the extension of the forward elastostatic problem in a three dimensional setting and the study of numerical schemes for the dynamic linear elasticity model with cracks.
Moreover, it would be interesting to study the inverse problem exploiting the possibility of rewriting the elastic displacement as a double layer potential on the fault and analyze in detail the resulting system of integral equations and the case of a fault in an heterogeneous medium.
Finally, in order to recover the unknown parameters, the iterative method that we proposed could be substituted by an algorithm based on the shape derivative of the functional to be minimized. This scheme is obviously much more complicated to construct but probably more effective and useful in the geophysical applications.

Bibliography

[1] J. Hadamard. "Sur les problèmes aux dérivées partielles et leur signification physique". In: *Princeton University Bulletin* (1902), 49–52.

[2] Y. Okada. "Surface deformation due to shear and tensile faults in a half-space". In: *Bulletin of the Seismological Society of America* 75.4 (1985).

[3] Y. Okada. *Internal deformation due to shear and tensile faults in a half-space*. 1992.

[4] J.P. Hirth and J. Lothe. *Theory of dislocations*. Krieger Pub. Co., 4th edition, 1982.

[5] E. Beretta, E. Francini, and S. Vessella. "Determination of a linear crack in an elastic body from boundary measurements-Lipschitz stability." In: *SIAM Journal on Mathematical Analysis* 40.3 (2008), pp. 984–1002.

[6] F. Triki and D. Volkov. "Stability estimates for the fault inverse problem". In: *Inverse Problems* 35 (2019).

[7] H. Ammari, E. Beretta, and E. Francini. "Reconstruction of Thin Conductivity Imperfections". In: *Applicable Analysis* 83.1 (2004), pp. 63–76.

[8] URL: http://speed.mox.polimi.it.

[9] A. Quarteroni and A. Valli. *Domain Decomposition Methods for Partial Differential Equations*. Claredon Press, 1999.

[10] A. Toselli and O. Widlund. *Domain Decomposition Methods - Algorithms and Theory*. Springer-Verlag, Berlin Heidelberg, 2005.

[11] F. Rapetti et al. "Non-conforming high order approximations of the elastodynamics equation". In: *Computer Methods in Applied Mathematics and Engineering* 209 (2012), pp. 212–238.

[12] B. Rivière. *Discontinuous Galerkin methods for solving elliptic and parabolic equations: theory and implementation*. Society for Industrial and Applied Mathematics, 2008.

[13] J.S. Hesthaven and T. Warburton. *Nodal Discontinuous Galerkin methods: Algorithms, Analysis, and Applications*. Springer, 2010.

[14] J. Nitsche. "Über ein variationsprinzip zur lösung von dirichletproblemen bei verwendung von teilräumen, die keinen randbedingungen unterworfen sind". In: *Abhandlungen aus dem mathematischen Seminar der Universität Hamburg* 36 (1971), pp. 199–2389–15.

[15] I. Babuška. "The finite element method with penalty." In: *Mathematics of computation*. 27.122 (1973), pp. 221–228.

[16] D. A. Di Pietro and A. Ern. *Mathematics aspects of discontinuous Galerkin methods*. Springer Science & Business Media, 2011.

[17] D. N. Arnold. "An interior penalty finite element method with discontinuous elements". In: *SIAM Journal on Numerical Analysis* 19.4 (1982), pp. 742–760.

[18] G.J. van Zwieten et al. "Discontinuities without discontinuity: The Weakly-enforce Slip Method". In: *Comput. Methods Appl. Mech. Engrg* 271 (2013), pp. 144–166.

[19] R.A. Adams and J.J.F. Fournier. *Sobolev Spaces, Volume 140 of Pure and Applied Mathematics, 2nd edn.* Elsevier, Amsterdam, 2003.

[20] L. C. Evans. *Partial differential equations*. 1999.

[21] B. Lautrup. *Physics of Continuous Matter: Exotic and Everyday Phenomena in the Macroscopic World*. CRC Press, 2004.

[22] S. Salsa. *Equazioni a derivate parziali: Metodi, modelli e applicazioni*. Springer Science & Business Media, 2010.

[23] P.A. Raviart and J.M. Thomas. *Introduction à l'analyse numérique des équations aux dérivées partielles*. Masson, 1983.

[24] S. C. Brenner and R. Scott. *The mathematical theory of finite element methods*. Springer Science & Business Media, 2008.

[25] W. Rudin. *Principi di analisi matematica*. Milano, McGraw-Hill, 1991.

[26] J. L. Lions and E. Magenes. *Non-Homogeneous Boundary Value Problems and Applications*. Springer-Verlag, Berlin, 1972.

[27] P.F. Antonietti et al. "Stability Analysis of Discontinuous Galerkin Approximations to the Elastodynamics Problem". In: *Mathematical Problems in Engineering* 68 (2013), pp. 143–170.

[28] B. Rivière et al. “Discontinuous Galerkin finite element methods for linear elasticity and quasistatic linear viscoelasticity”. In: *Numer. Math.* 95 (2003), pp. 347–376.

[29] P.F. Antonietti et al. “High order discontinuous Galerkin methods on simplicial elements for the elastodynamics equation”. In: *Numer. Algorithms* 71.1 (2016), 181–206.

[30] Y. Chen et al. “On the Local Discontinuous Galerkin Method for Linear Elasticity”. In: *Mathematical Problems in Engineering* (2010).

[31] P. F. Antonietti et al. “Discontinuous Galerkin approximation of flows in fractured porous media on polytopic grids”. In: *SIAM Journal on Scientific Computing* 41.1 (2019), A109–A138.

[32] S. C. Brenner. “Poincaré–Friedrichs inequalities for piecewise H^1 functions”. In: *SIAM J. Numer. Anal.* 41 (2003), 306–324.

[33] A. Quarteroni. *Numerical models for partial differential equations*. Springer Science & Business Media, 2010.

[34] I. Babuška and M. Suri. “The *hp* version of the finite element method with quasiuniform meshes”. In: *RAIRO-Modélisation mathématique et analyse numérique* 21.2 (1987), pp. 199–238.

[35] I. Babuška and M. Suri. “The optimal convergence rate of the p-version of the finite element method”. In: *SIAM Journal on Numerical Analysis* 24.4 (1987), pp. 750–776.

[36] R. E. Bird, W. M. Coombs, and S. Giani. “A posteriori discontinuous Galerkin error estimator for linear elasticity”. In: *Applied Mathematics and Computation* 344-345 (2019), pp. 78–96.

[37] B. Rivière and M. F. Wheeler. “A posteriori error estimates for a discontinuous Galerkin method applied to elliptic problems”. In: *Comput. Math. Appl.* 46 (2003), pp. 141–163.

[38] Z. Cai, X. Ye, and S. Zhang. “Discontinuous Galerkin Finite Element Methods for Interface Problems: A Priori and A Posteriori Error Estimates”. In: *SIAM Journal on Numerical Analysis* 49.5 (2011), pp. 1761–1787.

[39] B. Rivière, M. F. Wheeler, and V. Girault. “Improved energy estimates for interior penalty, constrained and discontinuous Galerkin methods for elliptic problems”. In: *Computational Geoscience* 3 (1999), 337–360.

[40] A. L. Mazzucato and V. Nistor. "Well-posedness and Regularity for the Elasticity Equation with Mixed Boundary Conditions on Polyhedral Domains and Domains with Cracks". In: *Archive for Rational Mechanics and Analysis* ().

[41] A. Aspri et al. "Analysis of a Model of Elastic Dislocations in Geophysics". In: *Arch. Rational Mech. Anal.* ().

[42] A. Aspri, E. Beretta, and A. L. Mazzucato. "Dislocations in a layered elastic medium with applications to fault detection". In:

[43] P.F. Antonietti and I. Mazzieri. "High-order Discontinuous Galerkin methods for the elastodynamics equation on polygonal and polyedhral meshe". In: *Comput. Methods Appl. Mech. Engrg* 342 (2018), pp. 414–437.

[44] I. Perugia and D. Schotzau. "An *hp*-Analysis of the Local Discontinuous Galerkin Method for Diffusion Problems". In: *Journal of Scientific Computing* 17 (2002).

[45] D. Arnold et al. "Unified analysis of discontinuous Galerkin methods for elliptic problems". In: *SIAM J. Numer. Anal.* 39 (2002), pp. 1749–1779.

[46] G. Strang and G. J. Fix. *An analysis of the Finite Element Method*. Wellesley-Cambridge Press, 1973.

[47] I. N. Aronszajn. "A unique continuation theorem for solutions of elliptic partial differential equations or inequalities of second order". In: *J. Math. Pures Appl* 36.9 (1957), pp. 235–249.

[48] L. Bourgeois. "A remark on Lipschitz stability for inverse problems". In: *Comptes Rendus Mathematique* 351.5-6 (2013), 187–190.

[49] R. Gateaux. "Sur les fonctionnelles continues et les fonctionnelles analytiques". In: *Comptes rendus hebdomadaires des séances de l'Académie des sciences, Paris* 157 (1913), pp. 325–327.

[50] E. Beretta and E. Francini. In: *SIAM J. Math. Anal.* 38 (2006), 1249–61.

[51] H. Cartan. *Calcul différentiel*. Paris: Hermann, 1967.

[52] A. Kolmogorov and S. Fomin. *Elements of the Theory of Functions and Functional Analysis*. V.M. Tikhominov, Nauka-Moscow, 1989.

[53] A. N. Tikhonov. "On the stability of the functional optimization problem". In: *USSR Comp. Math. Math. Phys.* 6.4 (1996), pp. 28–33.

[54] A. N. Tikhonov and V. Y. Arsenin. *Solutions of ill-Posed Problems*. New York: Winston, 1977.

[55] A. Neubauer. "An a-posteriori parameter choice for Tikhonov regularization in Hilbert scales leading to optimal convergence rates". In: *SIAM J. Numer. Anal.* 25 (1988), pp. 1313–1326.

[56] D. Volkov, C. Voisin, and I. R. Ionescu. "Reconstruction of faults in elastic half space from measurements." In: *Inverse Problem* 33.5 (2017).

[57] D. Volkov, C. Voisin, and I. R. Ionescu. "Determing Fault Geometries From Surface Displacements". In: *Pure Appl. Geophys.* 174 (2017), pp. 1659–1678.

[58] E. Beretta et al. "Algorithm for the determination of a linear crack in an elastic body from boundary measurements". In: *Inverse Problems* 26.8 (2010).

[59] URL: https://it.mathworks.com/help/gads/how-the-genetic-algorithm-works.html.